University of Dhaka

Gyrotactic Microorganisms modeling of free forced Convective Boundary Layer flow

A dissertation submitted for the degree of
Doctor of Philosophy

By

Nayema Islam Nima

Registration No: 70/2015-16 & 25/2020-21(Re-Reg)

Department of Applied Mathematics

University of Dhaka

Dhaka, Bangladesh

July, 2023

Certificate

This is to certify that the thesis entitled "Gyrotactic Microorganisms modeling of free forced Convective Boundary Layer flow" submitted by **Nayema Islam Nima** as partial fulfillment of the criteria for the degree of **Doctor of Philosophy** in Applied Mathematics. The entire thesis or a portion of it has not been submitted for the award of any other Degree, Diploma, Associateship or Fellowship, whatsoever, of any other University or Institution.

Professor Dr. Mohammad Ferdows
Supervisor
Department of Applied Mathematics
University of Dhaka
Dhaka-1000, Bangladesh

Abstract

The study of microorganisms has attracted the focus of researchers for observing the emergence of microorganisms in bioconvection. Due to their intermixing traits and capacity in order to enhance mass transit, major applications of biological convection phenomena have been observed in numerous biotechnology and biological systems. Some exemplary applications exist in the biomedical fields (nanodrug administration and cancer treatment) and bio-microsystems (the use of enzyme biosensors in technology). Owing to their numerous industrial applications, including heat exchange in low-velocity environments, wind-exposed solar collectors, atmospheric boundary layer flows, and emergency cooling of nuclear reactors, combined (free and forced) or mixed convection problems with gyrotactic microorganisms have attracted considerable attention in recent years.

This dissertation analyses the behaviour of gyrotactic microorganisms in free-forced convective flow over a variety of surface geometries (vertical plates, horizontal plates, cylinders, cones, and spheres). For physical consideration, significant quantities including the melting effect, isothermal and non-isothermal processes, internal heat generation, variable fluid characteristics, and dispersion effects are considered. The first objective of this study is to examine and establish the mathematical formulation for the considered problems. Different emerging laws of physics accustomed to model the partial differential equations system. Then, the second objective is to impose finite difference method, MAPLE algorithm, and MATLAB bvp4c scheme to solve a set of ordinary differential equations. To do numerical calculations, the controlling partial differential equations for energy, momentum, mass conservation, and mobile microorganism conservation balances were initially transformed by similarity transformations into a collection of interconnected nonlinear ordinary differential equations. The last objective is to analyze the effect of governing parameters on different flow fields (velocity, temperature, concentration and microorganism) and also on heat, mass and motile microorganism transfer rate profiles. Motivated by the exploration of the fuel cells with bio-inspired design use phenomenon involving near-wall transport, we first quantitatively and analytically examined the free-forced, steady boundary layer flow from a solid vertical flat plate that is immersed in a porous material with Darcian pores that is home to gyrotactic microorganisms. Subsequently, in our second problem, we analysed the mass, heat, and bioconvective flow, including moving microorganisms

on a porous material-covered a vertical surface with varying porosity. Various fluid characteristics are presumptively porosity-dependent due to the varying porosity. The Darcy model was used to examine bioconvection through porous and impermeable surfaces in the case of uniform and varied permeability, and the consequences of heat generation were considered. Then, in third problem, the work on variable fluid characteristics was expanded to include non-Newtonian fluids with melting influences harbouring gyrotactic microorganisms throughout a vertical plate that is immersed in an enriched non-Darcy porous media, where all flow profiles are observed for fluids that are dilatant, Newtonian, and pseudo-plastic. The fourth problem considered the dispersion effects and the impact on flow in a horizontal cone with mixed convection in a non-Darcy porous media. In order to address the phenomena of heat, mass, and motile microbe transport, several convective boundary conditions were used. This study incorporated the dispersion impact of gyrotactic microorganisms for applications in biology and the environment. The fifth study aims to determine whether an inclined, non-isothermal permeable cylinder containing a mixed, free, and forced convective flow with gyrotactic microorganisms has a stable or unstable solution. Few researches have been conducted on dual solutions for mixed convection with gyrotactic microorganisms, despite the fact that they have many engineering applications and have been studied extensively along a vertical cylinder. Finally, in the last problem, the consistent boundary layer flow of mixed convection approaching a solid sphere's bottom stagnation point with constant heat, mass, and motile microorganism flux containing gyrotactic microorganisms was analysed in the scenario of aiding and opposing flow, and dual solution phenomena were also observed with regard to a particular set of mixed convection characteristics.

Throughout this study, the numerical solution acquired for the profiles of molecular motion, temperature, concentration, and density was plotted for various physical parameter choices. The numerical values representing the Nusselt, Sherwood, and motile microbe density have also been presented and analysed through tables. By contrasting the current study's findings with those of earlier studies, the research leads to a conclusion that upholds the validity of the computational algorithm results. Based on this thesis, we observed significant parametric effects on the flow boundaries. The results show that, in the forced convection regime, the influences of the physical parameters such as buoyancy parameters, Lewis parameter, bioconvection Lewis number, bioconvection Peclet number, dispersions parameter, Biot numbers are more prominent

than in the pure free convection regime. Mixed convection parameter has a significant impact on heat mass and the pace at which motile microorganisms transfer when permeability is changeable with a porous surface especially for pseudo-plastic fluids. The temperature increases for the mixed-convection parameter and plunges for the melting parameter. On the other hand, the concentration slows for a high melting effect. Lewis parameter, bioconvection Lewis number, bioconvection Peclet number have pronounced effects on concentration and microorganism profiles. The results further demonstrate that flow through non-isothermal inclined cylinder where free convection is dominant could distinct flow profiles exist as dual solutions. Only vertical and inclined cylinders exhibit the dual solution phenomenon, and a study on a horizontal cylinder only shows a unique solution. Notably, at the lower stagnation flow of solid sphere dual solutions exist for opposing flows for a particular range of mixed convection parameters, where a stable solution is indicated by the first solution, and an unstable one by the second.

List of publications

1. Ferdows, M., **Nima, N. I.**, & Shit, G. C. (2023). Chemical reactions and heat generation influence on mixed convection flow with gyrotactic microorganisms over a non-isothermal horizontal surface. *International Journal for Computational Methods in Engineering Science and Mechanics*, *24*(4), 296-306.

2. **Nima, N. I.**, & Ferdows, M. (2022). A sustainable computational modeling on gyrotactic free forced bioconvective flow with various slip effects. *Journal of Interdisciplinary Mathematics*, *25*(7), 1989-1997. (SCOPUS).

3. Ferdows, M., Alshuraiaan, B., & **Nima, N. I.** (2022). Effects of non-Darcy mixed convection over a horizontal cone with different convective boundary conditions incorporating gyrotactic microorganisms on dispersion. *Scientific Reports*, *12*(1), 1-14. (Impact factor: 4.996).

4. **Nima, N. I.**, & Ferdows, M. (2021). Dual Solutions in Mixed Convection Flow Along Non-Isothermal Inclined Cylinder Containing Gyrotactic Microorganism. *Journal of Advanced Research in Fluid Mechanics and Thermal Sciences*, *87*(3), 51-63. (SCOPUS).

5. **Nima, N. I.**, Ferdows, M., Adesanya, S. O., & Alzahrani, F. (2021). Double-diffusivity heat generation effects on bioconvection process embedded in a vertical porous surface with variable fluid properties. *Journal of Thermal Analysis and Calorimetry*, *145*(5), 2571-2580. (Impact factor: 4.755).

6. **Nima, N. I.**, Salawu, S. O., Ferdows, M., Shamshuddin, M. D., Alsenafi, A., & Nakayama, A. (2020). Melting effect on non-Newtonian fluid flow in gyrotactic microorganism saturated non-darcy porous media with variable fluid properties. *Applied Nanoscience*, *10*(10), 3911-3924. (Impact factor: 3.674).

7. **Nima, N. I.**, Ferdows, M., & Ardekani, M. M. (2020). Effects of cross diffusion and radiation on magneto mixed convective stagnation flow from a vertical surface in porous media with gyrotactic microorganisms: Similarity and numerical analysis. *Special Topics & Reviews in Porous Media: An International Journal*, *11*(3), 203-219. (Impact factor: 1.44).

8. **Nima, N. I.**, Ferdows, M., Anwar Bég, O., Kuharat, S., & Alzahrani, F. (2020). Biomathematical model for gyrotactic free-forced bioconvection with oxygen diffusion in near-wall transport within a porous medium fuel cell. *International Journal of Biomathematics*, *13*(04), 2050026. (Impact factor: 2.129).

Conference presentations

1. **Nima, N. I.**, & Ferdows, M. (2022, November 11-12). Assisting and opposing mixed convective flow with gyrotactic microorganism at the lower stagnation point of a solid sphere. *The 1st International Conference on Frontier in Sciences (ICFS-2022),* BUET, Dhaka, Bangladesh.

2. **Nima, N. I.**, & Ferdows, M. (2022, August 04-07). A sustainable computational modeling on gyrotactic free forced bioconvective flow with various slip effects. *The 4th International Conference on Sustainable Computing and Management,* IUBAT, Dhaka, Bangladesh.

3. **Nima, N. I.**, & Ferdows, M. (2022, May 16-18). Numerical analysis of free forced convective flow with multiple slip effects through vertical cone containing gyrotactic microorganism. *7th Thermal and Fluids Engineering Conference (ASTFE),* Las Vegas, NV, USA.

4. **Nima, N. I.**, & Ferdows, M. (2021, March 27-28). Dual solution for mixed convection flow through non-isothermal inclined cylinder containing gyrotactic microorganism. *Proceedings of the 4th World Virtual Conference on Applied Sciences and Engineering Applications In conjunction with the 6th International Symposium on Fluid Mechanics and Thermal Sciences,* Malaysia.

5. **Nima, N. I.**, & Ferdows, M. (2019, December 6-8). Melting effect on non-Newtonian fluid flow in a gyrotactic microorganism saturated non –Darcy Porous Media with variable fluid properties. *Proceedings of 21st International Mathematics Conference*, Dhaka, Bangladesh.

Table of contents

List of figures

List of Tables

Nomenclature

A	Microorganism concentration difference parameter
a_1	Co-efficient of thermal dispersion
b_1	Co-efficient of solutal dispersion
c_1	Co-efficient of microorganism dispersion
b	Chemo taxis constant
B_i	Biot number
$B_{i,m}$	Biot number of mass transfer
$B_{i,n}$	Biot number of microorganism transfer
C	Volume fraction of oxygen species
C_w	Wall volume fraction of oxygen species
C_∞	Ambient volume fraction of oxygen species
c_f	Forchheimer empirical constant
C_p	Specific heat at constant pressure
D_c	Effective solutal diffusivity
D_m	Mass diffusivity of the porous medium
D_n	Diffusivity of gyrotactic motile microorganisms
E_c	Eckert number
F	Non-Darcy parameter
g	Acceleration due to gravity
$h_f(x)$	Variable heat coefficient
$h_m(x)$	Variable mass coefficient
$h_n(x)$	Variable motile microorganism coefficient

k	Thermal conductivity
K	Permeability of the porous medium
k_0	Constant permeability
$k(y)$	Variable permeability of porous medium
kp	Porous parameter
kp^*	Permeability parameter
Lb	Bioconvection Lewis number
Le	Lewis number
M	Melting parameter
m	Power law exponent
N_1	Buoyancy ratio parameter
N_2	Buoyancy ratio parameter
Nu_x	Local Nusselt number
n	Volume fraction of gyrotactic motile microorganisms
n_∞	Ambient concentration of motile microorganism
Nn_x	Local density number of gyrotactic motile microorganisms
Pe	Bioconvection Peclet number
Pe_d	Modified Peclet number
Pr	Prandtl number
q_r	Radiative heat flux
q_w	Wall heat flux
q_m	Wall mass flux
q_n	Wall motile microorganism flux
q'''	Exponent term of internal heat generation
Ra	Rayleigh number for the porous medium
Ra_x	Local Rayleigh number for the porous medium
Rb	Bioconvection Rayleigh number

Re	Intertia co-efficient dependent Reynold number
Sh_x	Local Sherwood number
T	Temperature
T_w	Wall temperature
T_m	Melting tempetaure
T_0	Liquid phase temperature
T_∞	Ambient temperature
W_c	Maximum cell swimming speed
u, v	Velocity components along x & y axes
x, y	Cartesian coordinates (x - axis is aligned along the horizontal surface and y - axis is normal to it)

Greek Symbols

α_0	Constant thermal conductivity
α	Thermal diffusivity of the porous medium
α_e	Effective thermal diffusivity
α^*	The ratio of solid thermal conductivity to fluid conductivity
$\alpha(\eta)$	Variable effective thermal diffussivity
β_T	Buoyancy parameter due to temperature
β_C	Buoyancy parameter due to concentration
β_n	Buoyancy parameter due to motile microorganism
$\phi(\eta)$	Dimensionless oxygen species concentration distribution
η	Similarity variable
λ	Mixed convection parameter
γ_n	Average volume of a microorganism
γ	Curvature parameter

γ_0	Constant microorganism diffussivity
$\gamma(\eta)$	Variable effective diffusivity of microorganisms
γ^*	The ratio of thermal diffusivity of the microorganism to the conductivity of the fluid
$\theta(\eta)$	Dimensionless temperature
μ	Dynamic viscosity of fluid
ν	Kinematic viscosity of fluid
ρ	Fluid density
$\chi(\eta)$	Dimensionless density of gyrotactic motile microorganisms
ψ	Stream function
σ_0	Constant solute diffusivity
$\sigma(\eta)$	Variable effective solute diffussivity
σ^*	The ratio of solid thermal diffusivity to fluid diffusivity
ε_0	Constant porosity
$\varepsilon(\eta)$	Variable porosity

Chapter 1

Introduction

This chapter provides a summary of the 2D laminar boundary layer flow of heat and mass transport for the combined free-forced convection of Non-Newtonian and Newtonian fluids in the presence of gyrotactic microorganisms over various geometries. In addition, a thorough literature review based on the issues covered in subsequent chapters is included. The identification of the problem, goals of the study, importance of the research, and chapter layout are all covered within the chapters.

1.1 Literature review

Mixed convection is an amalgamation of forced and free convection, which is the combination of internal volumetric forces and the external forcing system (thermal, species buoyancy, etc.). The study of combined convection boundary layer flow is of considerable interest in modern technology owing to its diverse and ever-growing applications in nuclear reactor transport, transpiration cooling, material processing, fire spread, and fuel cells. The boundary layer theory is particularly useful for evaluating near-wall fluid mechanics, heat transport, and mass transfer characteristics. Porous media is also found in various systems, including geothermal reservoirs, insulation, biomechanics, foams, combustion, and petrochemical filtration. Many researchers have investigated both free and forced convection heat and mass transfer in porous media in external boundary-layer flows from vertical surfaces. Many studies in this regard have been reported considering different multiphysical effects. Lai *et al.* (1991) analysed thermo-solutal convection in a porous medium, showing that the buoyancy ratio and Lewis number have a significant impact on the flow behaviour from the asymptotic free convection limit to the forced convection limit. Beg *et al.* (2008) used a network electrothermal numerical code to study the natural convection flow in a thermally stratified nonlinear permeable regime. Tsai and Huang (2009) considered the cross-diffusion effects in a non-isothermal free-convection boundary-layer flow. Srinivasachary and Reddy (2015) considered non-Newtonian

mixed convection in medium with pores that exhibit the Soret and Dufour diffusion effects. Several studies have been done by numerous researchers on mixed convection flow through porous medium (Bachok *et al.* (2013); Rahman *et al*. (2015); Rana *et al*. (2012); Aman and Ishak (2012); Ahmad and Pop (2010)). Beg *et al.* (2011) employed the finite difference technique to simulate mixed thermal convection nanofluid boundary layer flow in porous media using Buongiorno's nanoscale model. Further studies include Srinivasachary and Surender (2015) (on convection with mixed nanofluids and twofold stratification in porous media), Bhargava *et al.* (2007) investigate the analysis of pulsing heat and flow in porous biomaterials using finite elements, Bansod (2003) observed the movement of heat and mass in isotropic porous medium, Beg *et al.* (2008) studied unsteady rotating Couette flow in Darcy-Forchheimer porous media, Beg *et al.* (2009) observed transient radiative-convective flow in a Darcian porous medium, Postelnicu (2007) analysed chemically reactive thermo-solutal free convection in porous media with cross-diffusion, and Beg (2016) observed orthotropic porous media on mixed thermal convection from a spinning cone. Recently, combined convection with heat generation through porous materials has been analysed in several studies (Mondal (2020); Abu-Hamdeh *et al*. (2020); Maleque (2010)). Gangadhar *et al*. (2020) studied the flow of the mixed convection boundary layer for casson fluid, Zhao (2021) investigated the convection for viscoelastic fluids, and Bakar and Roslan (2020) studied heat generation and mixed convection in a hollow driven by the lid.

Transport processes through a porous medium have recently proved challenging to research due to their wide-ranging application areas include thermal insulation and geothermal activities, food processing as well as other petrochemical uses. Many of these studies have facilitated our understanding of the mechanics of the porous matrix. In most of these studies, the classical Darcy model was employed, which holds true for transport that is viscous and low-speed. Darcy's model relates effective flow velocity to the pressure drop across a porous medium. It accurately approximates many diverse fluid dynamics applications including energy systems. Complete reviews of heat transfer via convection in porous media were published by Nield and Bejan (2013) and Pop and Ingham (2001). Srinivasachary and Reddy (2012; 2015) discovered power-law fluids for spontaneous and mixed convection in Darcy porous medium, whereas Lai *et al.* (1991) utilised the Darcy model to spot mixed convection in porous medium. Merkin (1969; 1972) reported forced convective flow. Subsequently, Chen and Minkowyez

(1977) presented a theoretical framework for the convective flow in porous media. Chen (1977) examined the convective thermal structure along an inclined wall, whereas Kumari and Gorla (1997) analysed the convection problem in the boundary layer region. (Ranganathann (1984); Hseih (1993); Aldoss *et al.* (1995); and Sheikholeslami *et al.* (2017)) investigated several areas of convective flow problems in porous media under different scenarios. Mathur (2017) studied free convection's response in a constrained medium, whereas Mohammed and Abdou (2017) investigated free convection with a nonuniform plate temperature. Porous media are frequently exploited in renewable thermal energy installations, including geothermic ones, and have been studied by (Marpu and Satymurty (1989); Beg *et al*. (2016); and Huang (1985)). Nakayama and Koyama (1987) suggested a similarity transformation for forced, mixed, and pure convection in porous media with and without Darcian symmetry. Kumari *et al.* (1997) extended the Cheng-Minkowyez formulation to rheological power-law fluids. Beg *et al*. (2009) used the Nakayama-Koyama Darcy formulation to investigate magnetohydrodynamic thermo-solutal mixed convection dynamics from an extending sheet in porous media with cross-diffusion. Further studies include Tripathi and Beg (2012), who employed a generalised Darcy model for studying the peristaltic pumping of non-Newtonian Maxwell viscous fluids passing over a porous media, and Beg *et al.* (2013), who deployed the Cheng-Minkowyez Darcy formulation to simulate fluid–particle transport in dialysis filtration systems.

In the last few decades, several studies on heat and mass transfer through mixed convection employing non-Darcian porous media have been published. Non-Darcian models are Darcy formulations that include vorticity diffusion, inertial drag, and mixtures of these factors according to Srinivasachary and Surender (2014). Various models for assessing the Brinkman-extended Darcy, the Forchheimer-extended Darcy, and other non-Darcian flows in porous mediumand generalised stream models, have been published in the literature (Srinivasachary and Surender (2014); Ibrahim *et al*. (2000); Kumari *et al.* (2019); Wang and Qin (2019); Hayat *et al*. (2020)). The non-Darcy model discussed in this study is a continuation of the classical Darcian formulation achieved by including a squared velocity factor to account for inertial effects in the momentum equation. The study by Pranitha *et al*. (2015) addressed the double diffusivity issues related to power-law fluid in non-Darcian environment. Amanulla *et al*. (2019) considered non-Darcy porous medium to observe MHD Prandtl fluid flow. Gibanov *et al.* (2017) studied mixed diffusivity in a triangular saturated porous matrix, whereas Golafshan and Asghar (2019)

investigated effects of radiation on mixed convection containing MHD third grade nanofluid. In addition, Esfe *et al*. (2019) observed mixed convection inside lid-driven cavities containing nanofluids.

All the aforementioned studies have been done conducted depending on the Darcy law assumption, which disregards the impact of the variable porosity of a porous medium. However, in many factual applications involving impervious boundaries in packed beds and fixed beds experienced in several chemical engineering and material processes, the uniform porosity assumptions fail; therefore, it is imperative to incorporate this critical effect. Several important effects, such as uneven flow distribution, particularly at the solid boundary, have been established (Schwartz and smith (1953); Tiemey *et al*. (1958); Benenati and Brosilow (1962)) when variable porosity is factored into the momentum equation. In view of this established fact, porosity-dependent flows have been an area of rigorous study in recent times because of their usefulness in many industrial areas such as rocket engines, cooling of nuclear reactors, gas transport, and microwave heating, which have variable properties and additional forces. For example, some studies (Choi (1982); Lai and Kulacki (1990); and Pop (1992)) are devoted to such effects in the boundary layer region. Chandrasekhar (1979; 1984; and 1985) studied the permeability changes in mixed convection flows and observed a significant effect of variation in porosity on velocity distribution and heat transfer. Ibrahim and Hassanie (2000) studied variable permeability Patokratoras (2005; 2007) discussed variable viscosity for forced and mixed convection. Darbhasayanam (2016) investigated the variable oscillatory convective flow with thermophoresis. Ahmed *et al*. (2019) studied the MHD nanofluid flow with variable thermo-physical properties. Related studies on convective flow with variable properties are not limited to Singh (2012); Nalinakshi *et al*. (2013); Dinesh *et al*. (2015); Rajput *et al*. (2018); Qasim *et al*. (2019) and the cited references. Recently, researchers have shown massive interest in internal heat generation in exothermic reacting fluids owing to the heat emission from chemical reactions. A short review of the literature showed that (Magyari (2007); Merkin *et al*. (2008); as well as Mealey and Merkin (2008)) examined how internal heat generation affects the flow of free convective boundary layers. A nonuniform heat source or heat flux for a permeable surface was observed by Abd El-Aziz *et al.* (2019) and Prasad *et al*. (2019). In addition, Tashtoush and Duwair (2005) analysed the transient convective flow of reactions with varying wall temperatures. Saleem and Abd El-Aziz (2019) studied Entropy production and convective heat

transfer for fluids with non-Newtonian power laws. (Crepeau and Clarksean (1997); Ferdows and Liu (2017); Olanrewaju (2012); and Makinde (2011)) documented several influences on internal heat generation within a moving fluid under various geometries. Selimefendigil and Hakan (2017) and Ahmed *et al*. (2019) studied the internal heat generation for mixed convection in nanofluid flow, whereas Sobamowo and Akinshilo (2017) reported differential-type pipe flow when internal heat creation occurs. Other studies on heat generation can be found in (Vajravelu (1980); Suresh *et al*. (2016); as well as Girinath and Dinesh (2018)).

In all the aforementioned studies, the thermal dispersion effects were ignored. Many researchers (Plumb (1983); El-Amin (2004); Kairi (2011); Nusser and Duwairi (2016); Khashi'ie *et al*. (2020); Aghbari *et al*. (2019); Meena (2021)) have examined convective heat transfer through porous medium and thermal dispersion in various situations. Plumb (1983) stated that when inertial effects are dominant, thermal dispersion effects in porous media become important. Thermal dispersion's effects on convection in non-Darcy porous medium are studied by El-Amin (2004) and Kairi (2011). The impacts of thermal dispersion for mixed convection flow with a nanofluid through vertical surfaces were observed in (Khashi'ie *et al*. (2020); Aghbari *et al*. (2019); and Meena (2021)). A key and pertinent factor in the gas turbine, nuclear reactor, and heat exchanger sectors is the analysis of mass and heat fluxes employing a convective boundary condition. Through a boundary surface with a limited heat capacity, heat is transferred to the convecting fluid in this manner, resulting in a convective heat transfer coefficient. (i.e. the Biot number). Given the nature of these applications, Hady *et al.* (2016) studied non-Darcy natural convection with convective boundary conditions containing microorganisms. In recent years, mixed convection flow through vertical surfaces was studied by (Rosali *et al.* (2016); Patil *et al.* (2014); RamReddy *et al*. (2018); and Zainal *et al.* (2020)) when convective boundary conditions are present, Mahat *et al.* (2019) observed boundary layer flow with mixed convection via a horizontal circular cylinder.

From the perspective of technology and industrial usage, non-Newtonian fluids like glues, tars, biological solutions, and polymers are essential when compared to traditional liquids such as oil, water, and glycol ethylene compounds. Non-Newtonian liquids are considered strong for heat transfer (Ogunseye *et al.* (2019); Krishnamurthy *et al.* (2016); Salawu and Ogunseye (2020)). With the melting effect, the flow of chemical reactions non-Newtonian liquids accompanied by heat dispersion in gyrotactic microorganism nonlinear porous media is often

used in energy storage systems, permafrost melting, and magma solidification. Without the melting effect, Salawu and Dada (2018) reported the pressure-driven flow of hydromagnetic fluid in Darcy-Forchheimer media with Dufour and Soret impacts. The non-Darcy term weakens the flow momentum and species dispersion in the medium. However, the importance of the melting effect on the fluid concentration cannot be overemphasised. Merkin *et al*. (2015) examined the influence of melting in a vertical plate of liquid flow with permeable media and boundary-layer mixed convection. Ahmad and Pop (2014) considered a vertical boundary layer surface to be a consequence of the melting effect on opposing flows with mixed convection. This study shows the existence of a dual result for the mixed-convection term. Shoba *et al*. (2010) and Kameswaran *et al*. (2016) investigated the thermal dispersion fluid species in non-Darcy median with mixed convection. Reportedly, for both opposing and aiding flows, the melting and temperature dispersion in the boundary layer increased the flow velocity. Non-Newtonian bioconvective driven flow in permeable media has several applications in electrochemistry (Salawu *et al.* (2019)); gyrotatic microorganisms (Mabood *et al.* (2014)); rheology and lubricity of drilling fluids (Beg *et al*. (2018); melting heat transfer characteristics (Khan *et al*. (2019)); and bioconvection aspects in second-grade nanofluids (Waqas *et al*. (2020)).

Convection in porous fluid-saturated media from axisymmetric bodies (e.g., cones, cylinders, and spheres) has attracted numerous researchers owing to its numerous engineering applications and geophysics, such as thermal insulation, geophysical flows, cooling of electronic systems, hydrology of ground water, filtration techniques, ceramic processes, petroleum reservoirs, chemical catalytic reactors, and ground water pollution. Flow over vertical cylinders has piqued the interest of authors due of the variety of uses it has in the insulation of vertical porous pipes, gas/oil pipeline connections, and subsurface electricity transmission lines, the elimination of radioactive waste, polymer processes, and the heating or cooling of sheets or films. Loganathan and Eswari (2017) observed natural convection flow for cylindrical surfaces. Sewucipto and Yuwono (2021) observed the influence of an upstream installation on a cylindrical surface. Rashidi *et al.* (2012) and Dhanai *et al.* (2016) studied combined free and forced or mixed convective nanofluid flows over inclined surfaces, and Rihan (2020) and Mkhatshwa *et al*. (2020) examined the flow of mixed convection across a vertical cylinder. Power-law wall temperature distribution in convection has been studied by several authors (Ali (1995), Ferdows *et al.* (2019)). Ferdows *et al.* (2019) investigated wall temperature variations for

natural convection along a vertical plate, and Munoz-Cobo *et al.* (2003) and Kim *et al.* (2014) investigated cylindrical surfaces. Studies on solid spheres have piqued the interest of authors because of their wide range of engineering applications (Jafarpur (1992); Aklasasbeh *et al.* (2014)) in stacked beds of spherical bodies in spherical storage tanks. Several studies ((Chaing (1964); Wang and Kleinstreuer (1988); Nazar *et al.* (2002); Aklasasbeh *et al.* (2014)) were conducted on mixed, free, and forced convection flow over solid spheres in the early years. Subsequently, Gaffar *et al.* (2015) investigated double-diffusive convection for an isothermal sphere; Fauzi *et al.* (2014) studied mixed convective flow at the lower stagnation point of the sphere for a constant heat flux; Aziz *et al.* (2019) and Swalmeh *et al.* (2019) studied mixed convection for micropolar fluid from a solid sphere; and Tham *et al.* (2013) observed mixed convection over solid spheres for nanofluids containing gyrotactic microorganisms. In all the aforementioned studies, either prescribed wall temperature or prescribed heat flux were considered in the boundary conditions.

In convective heat transfer to solve highly complex nonlinear problems, we obtain multiple (dual) solutions. In many cases, computing both unstable and stable states is important because stable solutions and unstable solutions frequently interact, resulting in anomalous occurrences. According to the study by Subhashini and Sumathi (2014), engineering applications could be viewed differently if mixed convective boundary layer flows have dual solutions. Ridha and Curie (1996) were the first to find a dual solution for opposing flows. Subhashini *et al*. (2013) extended this research to assist the flow. For a mixed-convection boundary layer, two solutions were initially looked into by Ingham (1986) and Merkin (1986). Rostami *et al*. (2018) and Salleh *et al*. (2018) explored a nanofluid's mixed convection. Recently, Khan *et al*. (2020) also provided a silica-alumina hybrid nanofluid dual solution for mixed convection on curved surfaces.

In the field of biological fluid dynamics, engineers utilise self-moving microorganisms, such as mobile species of bacteria and algae, in motion. Bioconvection is a common feature of microorganism propulsion. Bioconvection patterns are observed swimming microbe cultures, which, in response to environmental cues like gravity, light, magnetic fields, and chemical gradients, tend to move towards the top surface of their environment despite being heavier than water (Vadasz (2008)). These control mechanisms are known as taxes, and the corresponding

microorganisms may be gravitactic, phototactic, magneto-tactic, chemo-tactic, etc. These microbes use rotating flagella to swim automated by commutative molecular motors embedded in the cell wall, as studied by Berg (1975). According to Kuznetsov (2006), due to the density gradient brought about by swimming microorganisms, bioconvection can be categorized as macroscopic fluid motion, which intensifies the density of water in a specific direction that generates the bioconvection flow. Self-driving mobile microorganisms prefer to rise in volume of water in the system by producing a bioconvective stream in one direction, according to (Alloui *et al.* (2007); Avramenko and Kuznetsov (2010); Khan *et al.* (2013); Kuznetsov (2006); and Kuznetsov (2011)). Chemical or oxytactical properties, gyrotactic properties, and negative gravitational characteristics were used to classify motile microorganisms. The bottom-heavy microbe with gyrotaxis was the most frequent. Kuznetsov *et al*. (2010) proposed encapsulating motile microorganisms in nanofluid. The addition of motile microbes to the solution provides several benefits, including improved mass transfer, microscale mixing, and fluid stability. ((Latiff *et al.* (2017); Zaib *et al.* (2018); Rashad and Nabway (2019); Khan *et al.* (2019); Saleem *et al.* (2019); Sudhagar *et al.* (2019); Mahday and Nabway (2020); Mahdy (2021)) provided significant research in relation to bioconvection to systems for bioengineering, including thermobioconvection, microbial enhancement, biomicrosystems, and biofuels. Gyrotactic microorganism flow and convective boundary conditions in mixed convection was observed in refs. (Latiff *et al.* (2017); Zaib *et al.* (2018); Rashad and Nabway (2019)) and mixed convection phenomena with gyrotactic microorganisms over cones was observed by Khan *et al.* (2019) and Saleem *et al.* (2019). Waqas *et al.* (2021) observed microorganisms that swim and move about in a magneto-Burgers nanofluid flow, and Hussian and Malik (2021) studied MHD nanofluid flow with convective boundary conditions containing gyrotactic microorganisms.

Bioconvection has prospective usage in bio-microsystems owing to its species-mixing transport and boosting, which are significant factors in various microsystems (Tsai *et al.* (2009); Shitanda *et al.* (2007)). Recently, initiatives towards green technologies have been the primary motivation for using the mechanisms of microorganism bioconvection in developing ecological engineering systems. The study by Wager (1911) provides detailed insight into the bioconvection of microorganisms. In their studies, Han *et al.* (2019) and Zhang *et al.* (2019) considered digital microfluidic for diluter-based microalgal biosensor motion and fluorimetric senor, respectively. Nield and Bejan (2006) defined bioconvection as "the pattern creation in suspensions of

microorganisms such as bacteria and algae due to the microorganisms' up-swimming." In still water, gyrotactic organisms like Cnivalis swim upward because their centre of mass is behind their center of buoyancy. They respond to the torque dynamics as taxis. In recent years, many studies have been conducted on near-wall boundary layer free/forced/mixed bioconvection flows, which have featured many different computational approaches owing to the inherent nonlinearity in bioconvection boundary value problems. These include Uddin *et al.* (2017) (bioconvection nanofluid slip flow from undulating walls using finite elements and Maple quadrature); Latiff *et al.* (2016) (microstructural forced bioconvection slip nanofluid flow from extending/contracting elastic sheets using finite difference schemes); Basir *et al.* (2016) (coating flow of a stretching cylinder with nano-bioconvection boundary layers using shooting methods); and Beg *et al.* (2018) (Jeffery-Hamel nozzle and swirling disk nanofluid bioconvection flows, which employed a domain decomposition method). Khan and Makinde (2014) investigated the magnetic nano-bioconvection boundary layer flow using a convective boundary condition and shooting method. Raees *et al.* (2015) studied a mixed gyrotactic bioconvection nanofluid flow using the homotopy analysis method. Xu and Pop (2014) studied gyrotactic bioconvection nanofluid flows in a horizontal channel by using homotopy analysis and a passively controlled nanofluid model. Beg *et al.* (2013) used the Keller box finite difference implicit method and Nakamura tridiagonal method to analyse free and forced Newtonian nanofluid oxytactic bioconvection in Darcian porous media, describing the key influences of the Rayleigh and Lewis numbers on the heat, mass, and momentum transfer characteristics.

The active reaction of motile Microorganisms to stimuli, such as chemical reactions, light, or gravity, has contributed to their momentous effectiveness. Studies related to thermo-bioconvection in non-Newtonian diluted microorganism gyrotactic fluids are significantly beneficial to bio-microsystems. Kuznetsov and Avramenko (2004) studied the nanoparticle bioconvection suspension phenomenon on a vertical plate. It was observed that the nanoparticle concentration of the nanofluid bioconvection was small, without a significant impact on the base fluid viscosity. Shaw *et al.* (2014) investigated gyrotactic microorganism nanofluids in drenched absorbent media with Soret and hydromagnetic effects on bioconvection and reported that for a high Peclet number; the thermal and species rates diminish with the Lewis number. The effect of the mixture on the dilation rheology of a sphaltene–laden interface was examined by Liu (2017). The dynamic interfacial tension and dilatational rheology were effectively captured by a

computational application of a binary diffusion model using the same parameters. Niu *et al.* (2012) examined the energy transport and flow slip of a nanofluid non-Newtonian on an infinitely flat surface. The dimensionless formulated problem was numerically solved, and it was observed that the bioconvection terms have a considerable impact on the motile microorganisms and species in the system. Uddin *et al.* (2013) and Mozaffari (2019) considered non-Newtonian motile microorganism nanofluids with free convection in permeable medium. Shamshuddin *et al.* (2019) studied the Von Karman swirling bioconvection nanofluid flow in a rotating disk. Kohno *et al.* (2000) analysed the reaction of biological microorganisms, such as Staphylococcus aurous, Escherichia coli, and Streptococcus mutants, to the ferrite magnetic effect. This study was extended by (Strasak *et al.* (2002); Fojt *et al.* (2004); and Shamshuddin *et al.* (2019)), in which the low frequency of the magnetic field was examined for some biological microorganisms. Chowdary *et al.* (2019) and Yang *et al.* (2019) reported the nano-composition of fluorosurfactants and microlithography with small-molecule biosensors in a boundary layer. Srivastava *et al*. (2016) and Kulikovsky (2009) observed that oxygen transport is an important consideration in biomedical systems and modern sustainable fuel cell designs. To simulate oxygen diffusion, a separate species conservation equation is required, additionally to the equations for the conservation of momentum and energy associated with thermal convection. In this regard, interesting studies that address proton exchange membrane (PEM) fuel cells include Bradean *et al.* (2002), in which flow dynamics was simulated near the porous cathode of a PEM fuel cell, and Jeng *et al.* (2004), in which the oxygen mass transfer was numerically analysed in PEM fuel cell gas diffusion layers. These studies emphasised the importance of utilising physically viable data for oxygen diffusion to achieve realistic estimates of the transport characteristics. Another interesting aspect of modern fuel cell design (microbes and PEM) is bio-enhanced engineering. Biological microorganisms can significantly enhance the performance of green, ecologically friendly fuel cell systems such as solar, hydrogen, and other types. In conventional multiphase flow mechanics, solid particles are either propelled by external forces or transported by fluid flow. However, mathematical models of bioconvection propulsion are immensely beneficial for the design of optimal microbial fuel cell systems. These models robustly simulate the mechanisms, which bacteria to swim in certain ways depending on the environment studied by Hill (2005) and Alloui *et al.* (2007). Studies by Deng *et al.* (2012) and Wang *et al.* (2014) were motivated by elucidating the near-wall transport phenomena in modern

biological-inspired microbial fuel cells and plant–microbial fuel cells (PMFCs), which are newly emerging devices utilising energy generated by microorganisms that use root exudates as fuel. The simultaneous presence of bioconvection and oxygen diffusion is important for developing a deeper understanding of the heat and mass transfer characteristics at the cathode wall and biofilm communities in such systems, according to (Butler (2010); Lee *et al.* (2015); and Fischer (2018)), where bacteria have shown to utilise oxygen as an electron acceptor, without having exo-electrogenic activity. Furthermore, the present simulations provide a good benchmark for more advanced computational fluid dynamics analysis, for example, solar-hybrid photo-microbial fuel cells, according to Wu *et al.* (2014) and Wang *et al.* (2014).

1.2 Problem identification

Currently, many researchers such that Waqas *et al.* (2022), Ahmad *et al.* (2020), Basha *et al.* (2000), Kada *et al.* (2023) observed gyrotactic-microbe-saturated mixed convection flow has the potential to be important in a variety of engineering and biomedical fields because of its resilient capabilities of transmitting heat, mass, and density within the solution. Despite having some heat transmission capacity, different base liquids are typically not chosen for heat transport operations because of their low thermal efficiency. According to Ahmad *et al.* (2022), Li *et al.* (2023), motile microorganisms are used in numerous bio-microsystems, including chip-shaped microdevices, microbial fuel cells, enzyme biosensors, and micro fluidic devices, such as microvolumes and bacteria-powered micromixers, to improve the rate of mass and heat transfer. Additionally, the flow through porous media is a crucial factor for improving heat and mass transmission. Based on the aforementioned problems, a study was carried out to look into the function of gyrotactic microorganisms in various flow fields near the horizontal surface, vertical surface, cylinder, cone, and lower stagnation point of a sphere, and to explore how velocity, temperature, concentration, and microorganism profiles additionally to the motile microbial density number, Sherwood, and Nusselt number are influenced by different physical parameters, such as mixed convection, buoyancy, Lewis, bioconvection Lewis, bioconvection Peclet, and Biot numbers. The influence of variable fluid properties, melting effect, isothermal and non-isothermal phenomena, dispersion effect, and Darcy and non-Darcy effect on Newtonian and non-Newtonian fluids is considered to observe the flow behaviour. Dual solutions are also

investigated for a particular range of specific parameters to explore stable and unstable flow phenomena.

1.3 Study objectives

The major research objectives are as follows:

- To examine the free-forced convection laminar boundary layer flow over various geometries through a porous medium hosting microorganisms with gyrotactic motion.
- To establish the mathematical formulation, wherein the regulating equations include the conservation of mass, heat energy, momentum, and motile microbes. To apply similarity transformations to convert the controlling partial differential equations into an array of ordinary differential equations.
- To impose a common finite difference scheme, the MATLAB bvp4c scheme, and Maple algorithm for attaining the outcomes.
- To exhibit the numerically simulated results and their features of diversified parameters for different flow fields and heat, mass and motile microorganism transfer rate profiles. To analyse the possibility of dual solutions in a specific region of free, forced, and mixed convection.

1.4 Significance and scope of the study

This study focuses on the bioconvection process in which motile gyrotactic microorganisms play a dominant role. A thorough investigation was done to determine the impact of mixed convection, motile volume fraction microorganisms, and other parameter-dependent flow features owing to its value in processing industries such biomedical devices, energy technologies, microfluidic devices, and bio-microsystems. Gyrotactic microorganisms have stronger heat and momentum transmission properties at fuel cell walls and, through their habit of up-swimming, they also play a significant role in generating electrons that lead to bioconvection. This research clearly demonstrates the advantages of using biological organisms in various fuel cell designs, such as cylindrical urine-fed microbial fuel cells and truncated conical-shaped fuel cells, and it also provides a logical foundation for the biomathematical modelling of such systems. The use of gyrotactic microorganisms has been demonstrated to

enhance heat and momentum transport characteristics at the fuel cell wall. Additionally, a mathematical study of dual solutions can identify the most plausible, reliable, and physically sound solutions that have a substantial impact on the development of these devices. Engineering applications can be utilised in a variety of situations, such as the planning and control of power systems, to predict the behaviour of systems. The significance of long-standing concepts about the industrial and technological consequences of bio-microsystems engineering is demonstrated throughout this study.

1.5 Limitations of the study

The importance of investigating free forced convection using various surface geometries while taking into account various mathematical formulations is the main emphasis of this study. Appropriate solution methodologies have been considered for simulation shows accurate findings. Additionally, the results are presented mathematically and graphically and exhibit a strong correlation with previously published works. The following are some limitations of this research:

- Though finite difference scheme, MATLAB bvp4c technique and Maple algorithm have been used for simulation in this study, some more numerical methods could be applied to compare the accuracy of the results.
- Similarity transformation are used to transform partial differential equations into ordinary differential equations to observe the boundary layer flow behaviour over the horizontal, vertical surfaces and also the flow near lower stagnation point. Non –similar model could also be developed to analyse the flow over curved surfaces.
- Dual solutions have been observed graphically which has clearly shown the stable and unstable phenomena. Additionally, stability analysis could be shown to predict stable, unstable phenomena.

1.6 Outline of the thesis

The research described in this thesis aims to provide a more comprehensive overview of gyrotactic microorganism modelling on free-forced convective flow over various geometric

surfaces. The main part of the results presented in this thesis originates from papers that have been published, submitted for publication, or presented at international conferences.

The introduction, which comprises a literature review, overview, and primary goal and significance of the thesis, is included in Chapter 1.

Chapter 2 describes the development of a combined free-forced steady bioconvection from a vertical flat plate that is solid and surrounded by a porous Darcian medium. By applying similarity transformations, an array of differential equations is created from the governing partial differential equations for density of microbe species, oxygen species, momentum, and energy. A finite difference approach with central differencing, tridiagonal matrix manipulation and an iterative process are used to numerically solve the modified nonlinear system of equations with boundary conditions. Through the aid of the symbolic Maple software, computations were verified.

The bioconvection process through a vertical structure with implications for heat generation is discussed in Chapter 3. This chapter introduces the variable fluid characteristics soaked in a variable-porosity porous medium. For the numerical computation, the Maple algorithm was used. The goal is of this investigation was to measure the rates of mass, heat, and motile microbe transmission for variable permeability and porosity.

In addition, Chapter 4 handles steady mixed convection flow variable fluid properties through a vertical surface, although investigation is conducted here for non-Newtonian fluid flow through permeable non-Darcy media having melting effect. Additionally, melting surface boundary conditions and nonlinear modified ordinary differential equations were resolved via the MATLAB bvp4c technique. This study's goal is to look into the various flow behaviours of fluids that are not Newtonian, such dilatant and pseudo-plastic fluids, in the case of variable permeability.

Chapter 5 discusses non-Darcy mixed convective flow with thermal, solutal, and motile microorganism dispersion effects over a horizontal cone. The nonlinear partial differential equations driving the flow, temperature, concentration, and microbe fields were reduced to a set of ordinary differential equations by applying the proper similarity transformations, which were then solved by the MATLAB bvp4c function. For various flow profiles, the computation of the grid independence test was analysed to demonstrate the accuracy of the points. This study's

objective was to look into the impact of Biot number on the rates of heat, mass, and motile microbe transmission as well as the effects of dispersion on the rates of simultaneous flow transfer.

Chapter 6 investigates the dual-solution phenomena of free-forced bioconvective flow through a non-isothermal inclined cylinder. To describe non-thermal phenomena, variations in wall temperature and concentrations were considered in the boundary conditions. For numerical computations, including analysing dual solutions, the MATLAB bvp4c algorithm was used in this study. The goal of this section is to examine a dual solution for an inclined cylinder with a variety of flow fields for a set of parameter ranges. In this chapter, the existence of a dual solution for cylinders with varying inclinations that considers vertical and horizontal cylinders is discussed.

The mixed convective flow with gyrotactic microbe saturation at the lower stagnation point of a solid sphere is discussed in Chapter 7. The boundary conditions include constant heat, mass, and microbial flow. Using non-dimensional variables, the governing equations and boundary conditions were first converted into a collection of non-dimensional equations. The reduced ordinary differential equations at the bottom stagnation point of the sphere were then numerically solved using the MATLAB bvp4c solver. The goal of this study is to identify the ranges of mixed convection parameters for which dual solutions can be discovered, and to assess stable and unstable solutions for aiding and opposing flows.

Chapter 8 concludes the thesis, details the findings of the entire investigation, and provides recommendations for the future.

Chapter 2

Biomathematical model for gyrotactic free-forced bioconvection with oxygen diffusion in near-wall transport within a porous medium fuel cell

This chapter investigates the significant role of gyrotactic microorganisms saturated with free forced convection over the vertical surface, which resembles their application in microbial fuel cells. Gyrotaxis is just one of the numerous taxes that may be seen in biological microscale transport; others include magneto-taxis, phototaxis, chemotaxis, and geo-taxis. Additionally, diffusing oxygen species are present in the bioconvection fuel cell, simulating cathodic behaviour in a PEM system. The emerging eight-order nonlinear coupled ordinary differential boundary value problem contains a number of crucial dimensionless control parameters, including the Lewis number *Le*, buoyancy ratio parameter (i.e., ratio of oxygen species buoyancy force to thermal buoyancy force *Nr*, bioconvection Rayleigh number *Rb*, bioconvection Lewis number *Lb*, bioconvection Peclet number *Pe*, and the mixed convection parameter λ spanning the entire range of free and forced convection. Dimensionless temperature, velocity, oxygen concentration, motile microorganism density distribution, Nusselt and Sherwood, and gradient of motile microorganism density were explored in relation to buoyancy and bioconvection parameters. The symbolic Maple program and published literature are both used to validate computations. The goal of this chapter is to observe the flow behaviours to the construction of fuel cells with vertical plate and cathode walls. Although many researchers have examined mixed convection flow with gyrotactic microorganisms, this work clearly demonstrates the advantages of using bioconvection in fuel cell design and provides a coherent biomathematical modeling framework for simulating such systems.

2.1 Gyrotactic bioconvection transport model

We took into account the steady-state boundary-layer flow of a Newtonian fluid containing gyrotactic microorganisms in two dimensions. We thought of water as the fundamental fluid for microbial survival. Owing to gravity, the liquid and microbes descend over the vertical surface downward (fuel cell cathode wall). We choose the coordinate system in a manner that the *x*-axis is oriented along the wall, and the *y*-axis is directed normal to it. Modelling physical flow is illustrated in **Fig. 2.1**. The vertical wall is preserved at isosolutal (constant oxygen volume fraction and motile microorganism density) and isothermal conditions. The flow regime consisted of four boundary layers: the momentum boundary layer (designated U in **Fig. 2.1**), thermal boundary layer (designated T in **Fig. 2.1**), oxygen species boundary layer (designated C in **Fig. 2.1**), and motile microorganism species boundary layer (designated n in **Fig. 2.1**). The vertical wall is kept at a constant temperature, T_w, oxygen volume fraction, C_w, and motile microorganism density, n_w, which are considered to be of higher magnitude than the ambient temperature and oxygen and motile microorganism concentrations, T_∞, C_∞, and n_∞, respectively.

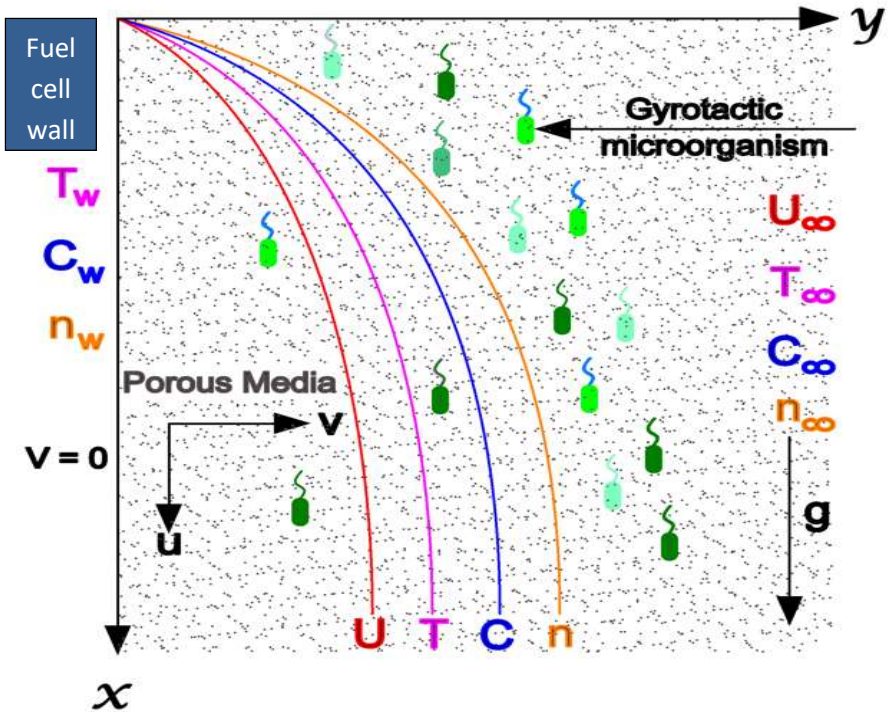

Fig. 2.1 Physical model for near-wall transport in bioconvection fuel cell

The fundamental partial differential equations that regulate the conservation of mass, momentum, energy, oxygen species, and gyrotactic motile microbial species using the Oberbeck-Boussinesq approximation can be written by neglecting nanoscale effects, following Xu *et al.* (2014) and Beg *et al.* (2013).

Mass conservation:

$$\frac{\partial u}{\partial x}+\frac{\partial v}{\partial y}=0 \tag{2.1}$$

Momentum (Darcy equation):

$$\frac{\partial u}{\partial y}=\frac{(1-C_{\infty})\rho g k}{\mu}\frac{\partial T}{\partial y}-\frac{\rho g k}{\mu}\frac{\partial C}{\partial y}-\frac{g\gamma_{n}\Delta\rho k}{\mu}\frac{\partial n}{\partial y} \tag{2.2}$$

Thermal energy equation:

$$u\frac{\partial T}{\partial x}+v\frac{\partial T}{\partial y}=\alpha\frac{\partial^{2}T}{\partial y^{2}} \tag{2.3}$$

Oxygen conservation equation:

$$u\frac{\partial C}{\partial x}+v\frac{\partial C}{\partial y}=D_{m}\frac{\partial^{2}C}{\partial y^{2}} \tag{2.4}$$

Motile microorganism conservation equation:

$$u\frac{\partial n}{\partial x}+v\frac{\partial n}{\partial y}+\frac{bW_{C}}{(C_{w}-C_{\infty})}\left[\frac{\partial}{\partial y}\left(n\frac{\partial C}{\partial y}\right)\right]=D_{n}\frac{\partial^{2}n}{\partial y^{2}} \tag{2.5}$$

The following boundary conditions are specified at the wall and boundaries of the boundary layer:

$$v=0\ ,T=T_{w}\ ,\ C=C_{\infty}\ ,\ n=n_{\infty}\qquad \text{at y} = 0 \tag{2.6}$$

$$u\to u_{\infty},\ T\to T_{\infty}\ ,\ C\to C_{\infty},\ n\to n_{\infty}\ \ \text{at y}\to\infty \tag{2.7}$$

We present the subsequent dimensionless quantities, as elaborated in previous studies, Xu *et al.* (2014) and Beg *et al.* (2013) (all scaling transformation proofs via Lie algebra symmetry are provided in these studies and are omitted here for brevity):

$$\eta = \frac{y}{x} Ra_x^{\frac{1}{3}} \left(1 + \frac{Pe_x^{\frac{1}{2}}}{Ra_x^{\frac{1}{3}}} \right), \psi = \alpha \; Ra_x^{\frac{1}{3}} \left(1 + \frac{Pe_x^{\frac{1}{2}}}{Ra_x^{\frac{1}{3}}} \right) f(\eta)$$

$$\theta(\eta) = \frac{T - T_\infty}{T_w - T_\infty} \; , \; \phi(\eta) = \frac{C - C_\infty}{C_w - C_\infty} , \; \chi(\eta) = \frac{n - n_\infty}{n_w - n_\infty}$$

$$Ra_x = \frac{(1 - C_\infty) \rho k g \beta (T_w - T_\infty) x}{\mu \alpha} , \; Pe_x = \frac{u_\infty x}{\alpha} \tag{2.8}$$

The stream function fulfils the continuity equation in a way that

$$u = \frac{\partial \psi}{\partial y} , v = - \frac{\partial \psi}{\partial x} \tag{2.9}$$

According to Nakayama and Koyama (1987), in the case of Darcy's free convective flow over a vertical flat plate, the following can be considered:

$$\frac{\mu}{k} u_\infty \text{(Darcy resistance)} \sim (1 - C_\infty) \rho g \beta (T_w - T_\infty) \text{ (Buoyancy force)} \tag{2.10}$$

In view of the aforementioned relation, it follows that:

$$u_\infty = \frac{(1 - C_\infty) k g \beta (T_w - T_\infty)}{\nu} , \text{ where } \nu = \frac{\mu}{\rho} \tag{2.11}$$

These ordinary differential equations are what we get from equations (2.1)−(2.5) using the quantities mentioned in equations (2.8)−(2.11):

$$f'' - \lambda^2 \left(\theta' - Nr \varphi' - Rb \chi' \right) = 0 \tag{2.12}$$

$$\theta'' + \frac{2 + \lambda}{6} f \theta' = 0 \tag{2.13}$$

$$\phi'' + Le \frac{2 + \lambda}{6} f \phi' = 0 \tag{2.14}$$

$$\chi'' + Lb\frac{2+\lambda}{6} f\chi' - Pe\left(\phi'\chi' + \chi\phi''\right) = 0 \tag{2.15}$$

According to Raees *et al.* (2015), we set $n_\infty = 0$, which satisfies the boundary conditions (2.6)−(2.7) at infinity, and the modified boundary conditions take on the following form:

$$\eta = 0, f = 0, \theta = 1, \phi = 1, \chi = 1 \tag{2.16}$$

$$\eta \to \infty, f' \to \lambda^2, \theta \to 0, \phi \to 0, \chi \to 0 \tag{2.17}$$

Here, the following definitions apply:

$$Nr = \frac{C_w - C_\infty}{\left(T_w - T_\infty\right)\left(1 - C_\infty\right)\beta}, Rb = \frac{\gamma_n \nabla\rho\left(n_w - n_\infty\right)}{\left(1 - C_\infty\right)\rho\beta\left(T_w - T_\infty\right)}, Le = \frac{\alpha}{D} \tag{2.18}$$

$$Lb = \frac{\alpha}{D_n}, Pe = \frac{bW_c}{D_n}, \lambda = \left(1 + \frac{Ra_x^{\frac{1}{3}}}{Pe_x^{\frac{1}{2}}}\right)^{-1}$$

Le, Nr, Rb, Lb, Pe, Ra_x, Pe_x, and λ denote the Lewis number, buoyancy ratio parameter, bioconvection Rayleigh number, bioconvection Lewis number, bioconvection Peclet number, local Darcy-Rayleigh number, local Peclet number, and mixed convection parameter, respectively. Notably, $\lambda = 0\ (Pe_x = 0)$ correlates to pure free convection, whereas $\lambda = 1\ (Ra_x = 0)$ correlates to pure forced convection. Therefore, the values of the entire regime, from $\lambda = 0$ to $\lambda = 1$ correspond to mixed convection. Here, small values of $\frac{Ra_x^{\frac{1}{3}}}{Pe_x^{\frac{1}{2}}}$ correspond to λ being close to one, which indicates a forced convection regime. By contrast, large values of $\frac{Ra_x^{\frac{1}{3}}}{Pe_x^{\frac{1}{2}}}$ correspond to λ being close to zero, which is associated with the free convection regime. According to Uddin *et al*. (2013), the quantities relevant to fuel cell design in this work are the the local Nusselt number Nu_x, the Sherwood number Sh_x and wall gradient of the local density number of the motile microorganisms Nn_x. These quantities are defined as follows:

$$Nu_x = \frac{xq_w}{k\left(T_w - T_\infty\right)}, Sh_x = \frac{xq_m}{D\left(C_w - C_\infty\right)}, Nn_x = \frac{xq_n}{D_n\left(n_w - n_\infty\right)} \tag{2.19}$$

where $q_w, q_m,$ and q_n are the wall heat, wall mass, and wall motile microorganism fluxes, respectively, which are defined mathematically as follows:

$$q_w = -k\left(\frac{\partial T}{\partial \bar{y}}\right)_{y=0}, \; q_m = -D_B\left(\frac{\partial C}{\partial \bar{y}}\right)_{y=0}, \; q_n = -D_n\left(\frac{\partial n}{\partial \bar{y}}\right)_{y=0} \tag{2.20}$$

Using the variables defined in equations (2.8) and (2.18):

$$\lambda Pe_x^{\frac{-1}{2}} Nu_x = -\theta'(0), \lambda Pe_x^{\frac{-1}{2}} Sh_x = -\phi'(0), \lambda Pe_x^{\frac{-1}{2}} Nn_x = -\chi'(0) \tag{2.21}$$

Here, $\lambda Pe_x^{\frac{-1}{2}} Nu_x$, $\lambda Pe_x^{\frac{-1}{2}} Sh_x$, $\lambda Pe_x^{\frac{-1}{2}} Nn_x$ designated Nusselt number, Sherwood number, and gradient of the local density number of motile microorganisms, respectively.

2.2 Numerical method and validation

For the numerical solution of the issue, a straightforward, precise, and effective method is used. The following principles form the foundation of this technique's numerical procedures: (i) with respect to the typical finite difference approach, (ii) on the manipulation of a tridiagonal matrix, and (iii) based on an iterative process. This numerical method has been described in detail by Nakayama (1995). According to the numerical procedure, we formulated the transformed similarity momentum, energy, concentration, and motile microorganism density equations as follows: the following is a representation of the momentum equation (2.12):

$$f'' - \lambda^2(\theta' - Nr\phi' - Rb\chi') = 0$$

The aforementioned equation is a second-order linear differential equation. By setting $y(x) = f(n)$, we obtain the following equation:

$$P(x)y''(x) + Q(x)y'(x) + R(x)y(x) = S(x) \tag{2.22}$$

$$\text{Here, } P(x) = 1, Q(x) = 0, R(x) = 0, S(x) = \lambda^2(\theta' - Nr\phi' - Rb\chi') \tag{2.23}$$

According to the aforementioned procedure, all equations can be condensed to equation (2.20). Then, for the energy equation,

$$P(x) = 1,\ Q(x) = \frac{1+\lambda}{6} f,\ R(x) = 0,\ S(x) = 0 \tag{2.24}$$

For the oxygen conservation equation:

$$P(x) = 1,\ Q(x) = Le\frac{2+\lambda}{6} f,\ R(x) = 0,\ S(x) = 0 \tag{2.25}$$

For the motile microorganism density equation:

$$P(x) = 1,\ Q(x) = \frac{2+\lambda}{6} f - Pe.\phi',\ R(x) = Pe.Le.\frac{2+\lambda}{6} f\phi',\ S(x) = 0 \tag{2.26}$$

Using a popular finite difference technique based on central differencing and tridiagonal matrix manipulation, all changed equations can be solved. We presume initial guesses to begin the solution procedure $\eta = 0$ and $\eta = \eta_\infty (\eta \to \infty)$, which satisfy boundary conditions (2.16) and (2.17). To incorporate into our numerical calculation, a proper step size $h = \Delta\eta = 0.01$ and an appropriate η_∞ value as $(y \to \infty)$ must be determined. This process continues until convergence of the solution is attained. To confirm the correctness of the current solution, we solve the equations using Maple. Using the dsolve command, this type of BVP or IVP problem is easily identified, and an appropriate algorithm is applied. The validity and accuracy of the Maple algorithm have been extensively validated in several recent studies (Uddin *et al*. (2016); Shamsuddin *et al*. (2017)). A graphical representation of the comparison is shown in **Figs. (2.2–2.4)** for temperature, oxygen concentration, and microorganism density number function, where an excellent correlation is found.

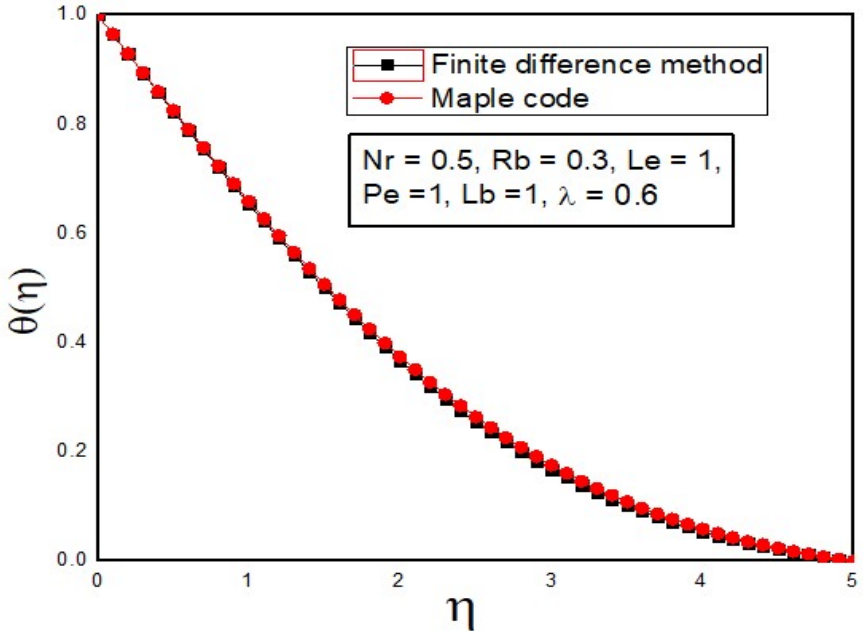

Fig. 2.2 Comparison of temperature profile

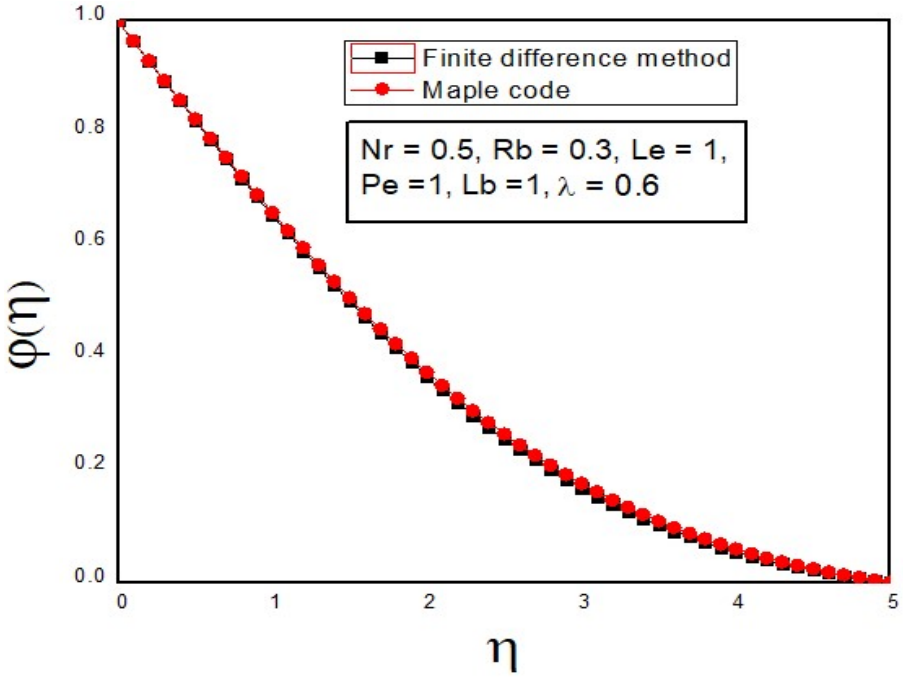

Fig. 2.3 Comparison of concentration profile

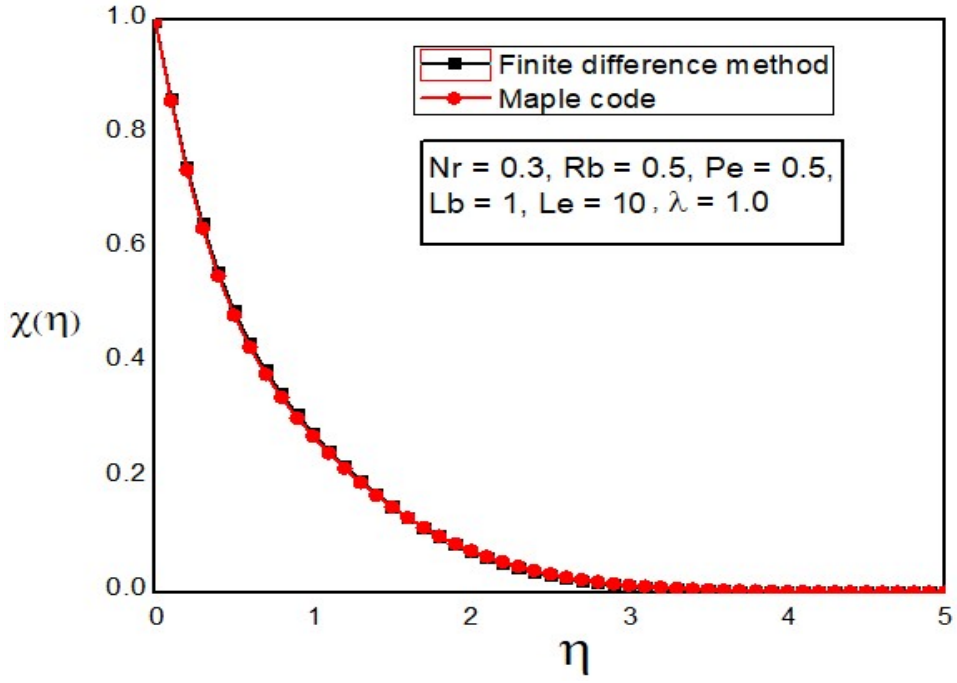

Fig. 2.4 Comparison of microorganism profile

In **Table 2.1**, comparison of $-\theta'(0)$ for a specific situation is presented for further result validation and demonstrates the accuracy of the findings.

Table 2.1 Comparison of heat transfer rate $-\theta'(0)$ for $Nr = 0, Rb = 0, Le = 0, Lb = 0, Pe = 0$

λ	Present	Cheng (1977)
1.0	0.7206	0.7205

2.3 Numerical results and discussion

In **Figs. 2.5(a–c)** we show the effect of different values of the mixed convection parameters on the temperature, concentration, and motile microorganism distribution for *Nr = 0.4, Rb = 0.1, Pe = 0.2*, *Le* = 5, and *Lb* = 1. Different values of the mixed convection parameter indicate different types of thermal convection regimes, and we can easily observe the profiles for the natural and forced convection in **Figs. 2.5(a–c)**. The temperature, oxygen concentration, and

microorganism density number are all depleted with increasing mixed convection parameter. The associated boundary layer thicknesses also decreased with a higher mixed convection parameter λ. It was also observed that the boundary layer thickness of the concentration profile was thinner than that of the temperature and motile microorganism profiles for the greater influence of Lewis number Le. For the lower values of Le, Mixed convection parameter λ shows similar impact on temperature concentration and microorganism profiles. The relative rates of diffusion (heat, oxygen, microorganisms) are therefore adjusted with mixed convection effects, indicating that fuel cell performance is tuneable in actual devices.

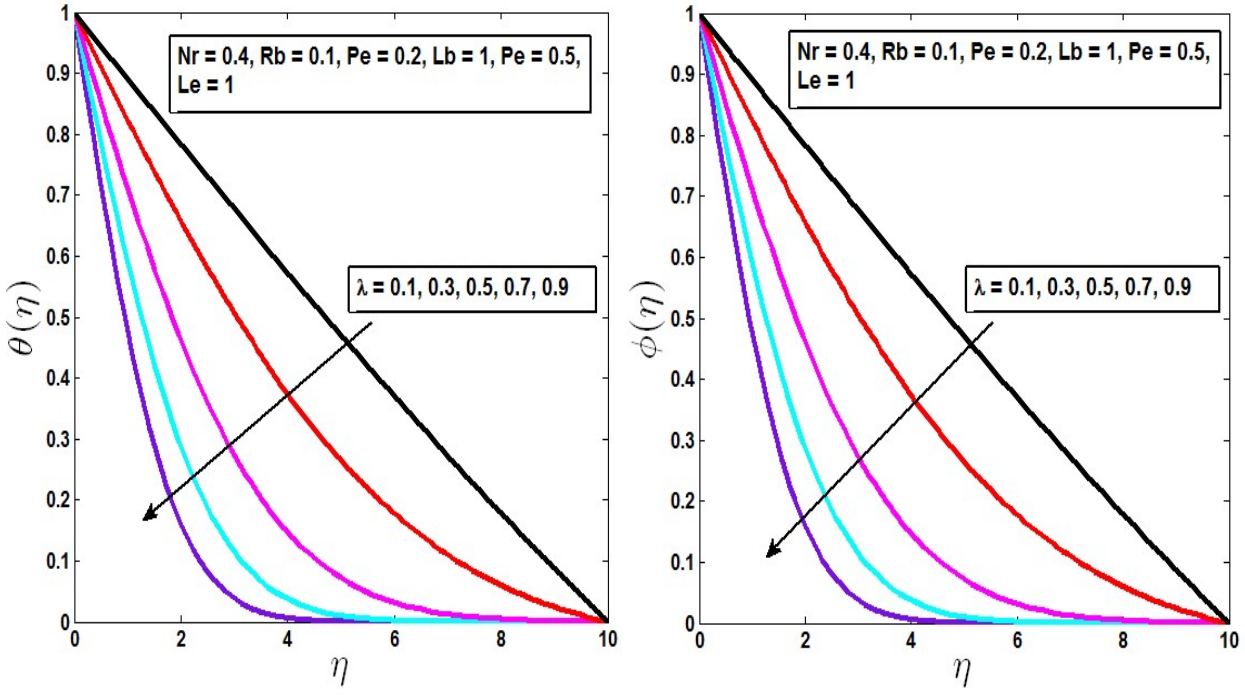

(a) **(b)**

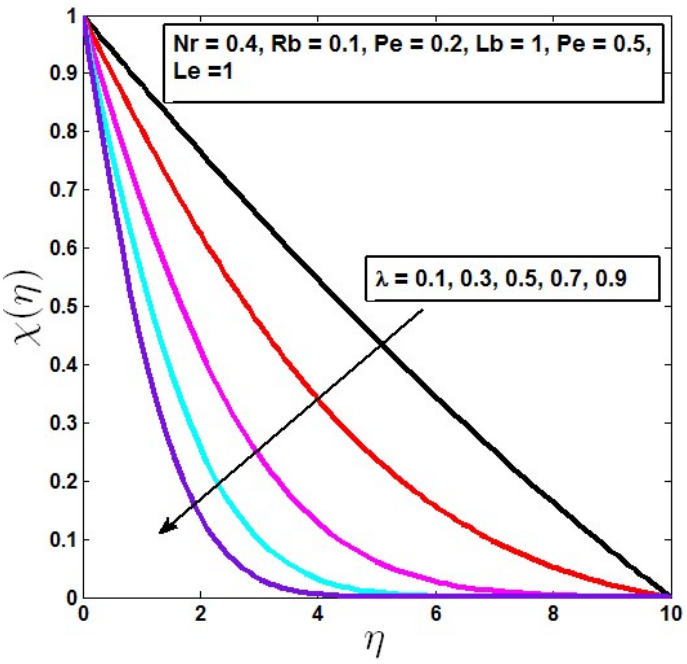

(c)

Fig. 2.5 The influence of λ on a) temperature profile b) concentration profile c) microorganism profile

The velocity profiles are demonstrated to be affected by the bioconvection Raleigh number and the buoyancy ratio parameter in **Figs. 2.6(a–b)**. The velocity profile attains its maximum value for the minimum values of the Nr and Rb. This behaviour can be attributed due to the presence of gyrotactic microorganisms, as the microorganisms in the base fluid are responsible for decline of the motion of the fluid at the surface. As the velocity profile is dependent on the mixed convection parameter, It has been noted that the velocity profile has a significant impact on the forced convection regime for the buoyancy ratio parameter and bioconvection Rayleigh number. Effects of Nr and Rb on Nusselt number, Sherwood number and motile microorganism density number in free forced and combined free forced region are shown in **Table 2.2 and Table 2.3.** The results clearly demonstrate that

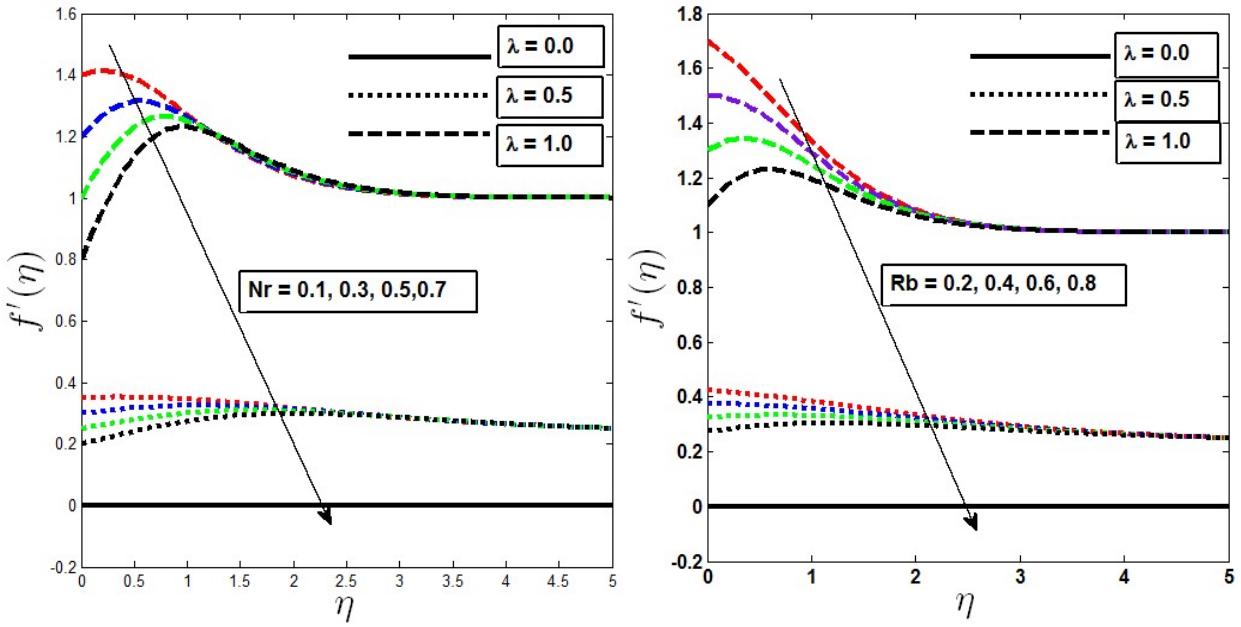

(a) **(b)**

Fig. 2.6 The influence of free forced convection on velocity profile with the a) variation of Nr b) variation of Rb

Table 2.2 Effect of Nr on Nusselt, Sherwood and density of motile microorganism in free, mixed and forced convection region for $Le = 5, Lb = 0.5, Pe = 0.3, A = 0.5, Rb = 0.3$

Nr	$\theta'(0)$			$\varphi'(0)$			$\chi'(0)$		
	$\lambda = 0.1$	$\lambda = 0.5$	$\lambda = 0.9$	$\lambda = 0.1$	$\lambda = 0.5$	$\lambda = 0.9$	$\lambda = 0.1$	$\lambda = 0.5$	$\lambda = 0.9$
0.1	0.10856	0.30519	0.59128	0.14352	0.70941	1.37518	0.13092	0.38996	0.75154
0.5	0.10775	0.28731	0.55652	0.13512	0.64642	1.25303	0.12793	0.36270	0.69819
0.8	0.10567	0.27278	0.52748	0.12863	0.59426	1.15187	0.12563	0.34006	0.65385
1.0	0.10481	0.26144	0.50619	0.12422	0.55635	1.07836	0.12467	0.32357	0.62150

Table 2.3 Effect of Rb on Nusselt, Sherwood and density of motile microorganism in free, mixed and forced convection region for $Le = 5, Lb = 0.5, Pe = 0.3, A = 0.5, Nr = 0.6$									
Rb	$\theta'(0)$			$\varphi'(0)$			$\chi'(0)$		
	$\lambda = 0.1$	$\lambda = 0.5$	$\lambda = 0.9$	$\lambda = 0.1$	$\lambda = 0.5$	$\lambda = 0.9$	$\lambda = 0.1$	$\lambda = 0.5$	$\lambda = 0.9$
0.1	0.10738	0.29716	0.57583	0.13741	0.67080	1.30043	0.12874	0.37503	0.72277
0.5	0.10565	0.26699	0.51675	0.12853	0.58552	1.13471	0.12560	0.33455	0.64244
0.8	0.10435	0.24172	0.46684	0.12185	0.51258	0.99258	0.12324	0.30039	0.57402
1.0	0.10348	0.22310	0.42967	0.11740	0.45774	0.88529	0.12168	0.27502	0.52269

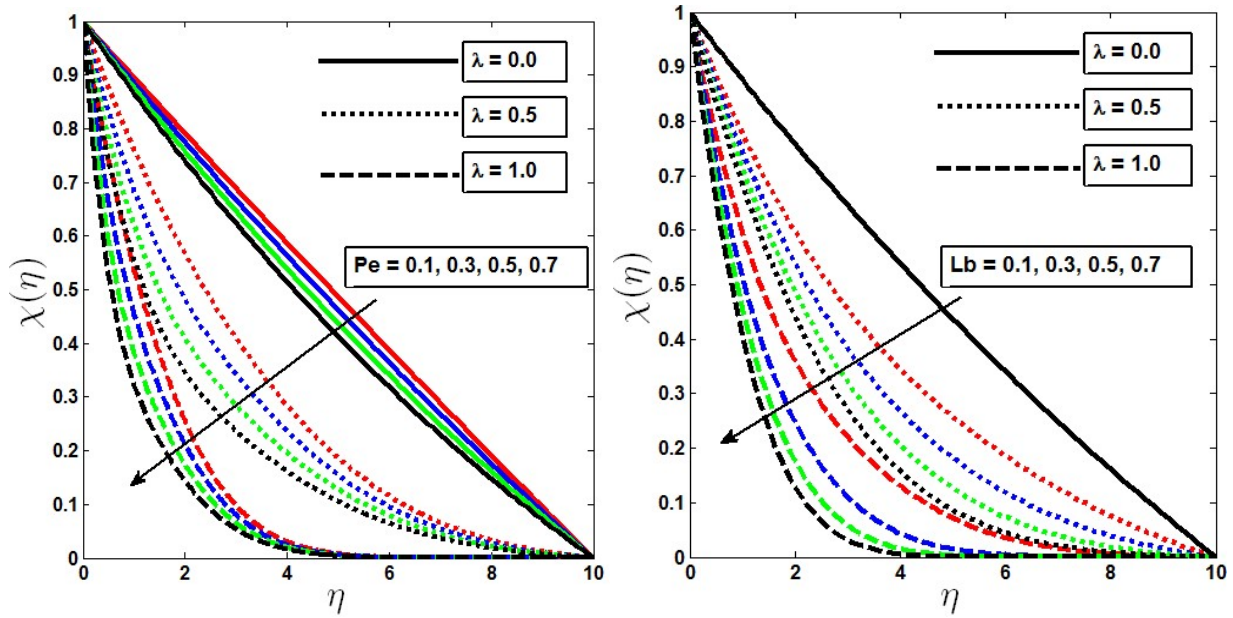

(a) **(b)**

Fig. 2.7 The influence of microorganism profile with the a) variation of Pe b) variation of Lb

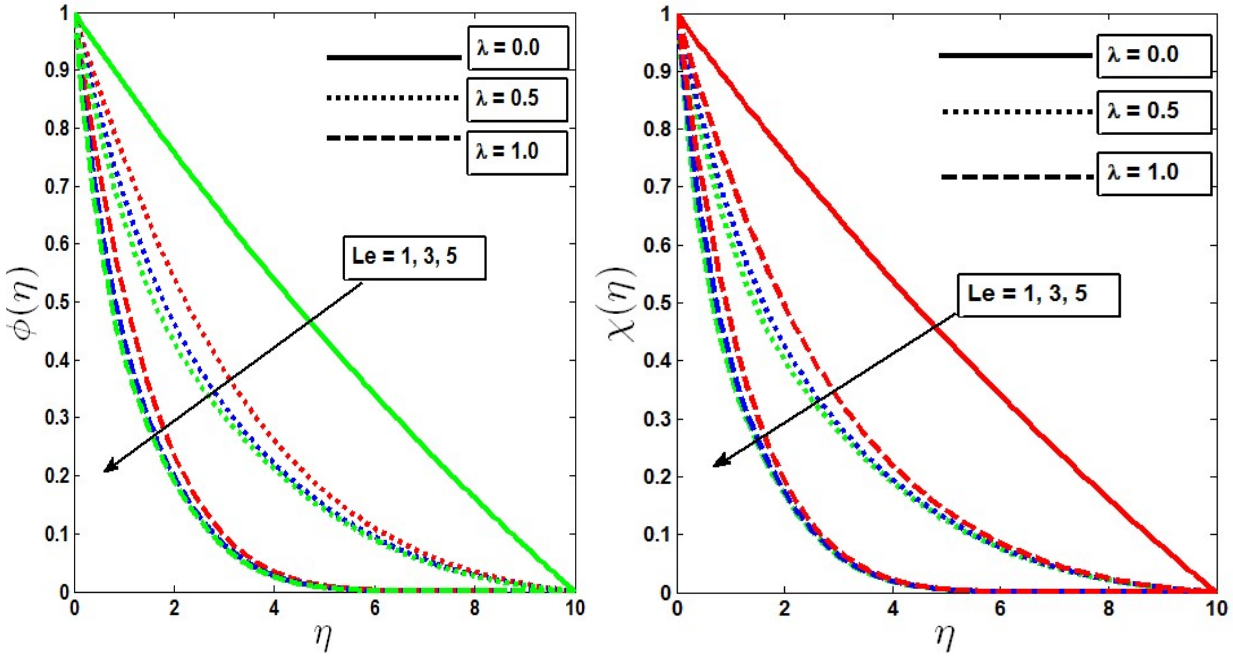

Fig. 2.8 The influence of *Le* on a) concentration profile b) microorganism profile

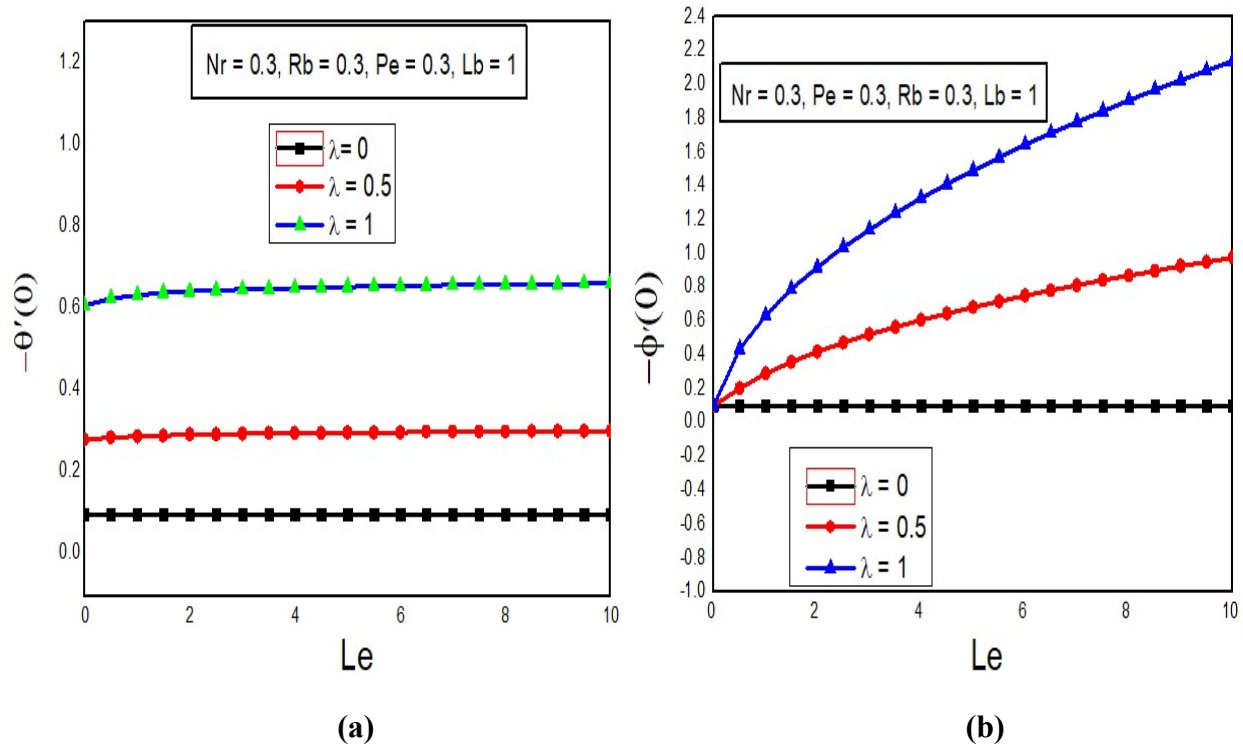

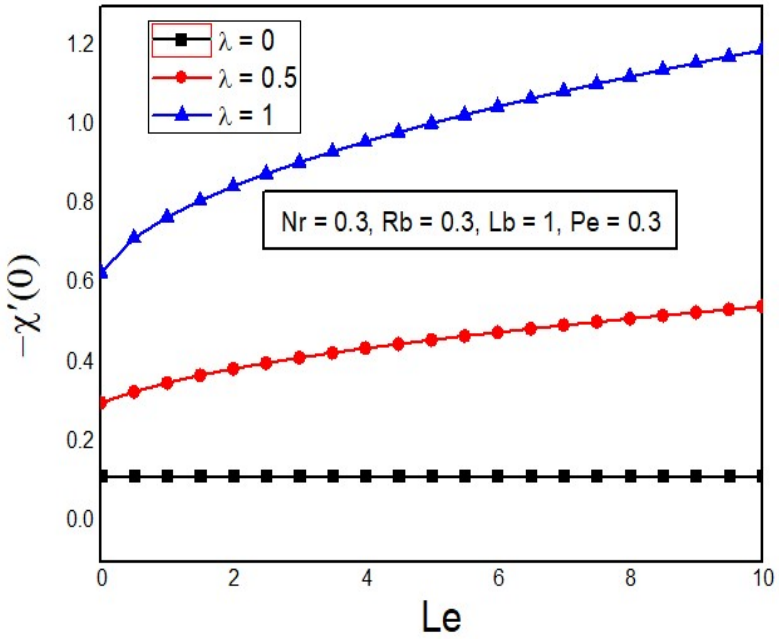

(c)

Fig. 2.9 The influence of *Le* with free forced convection on a) Nusselt number b) Sherwood number c) microorganism density number

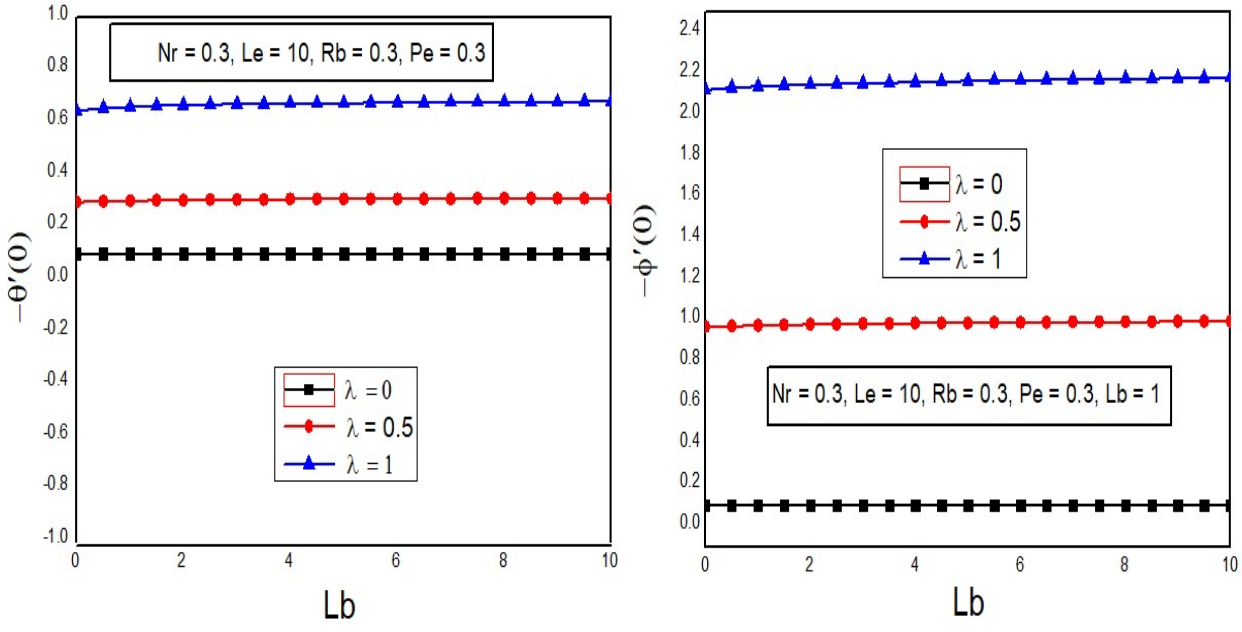

(a) **(b)**

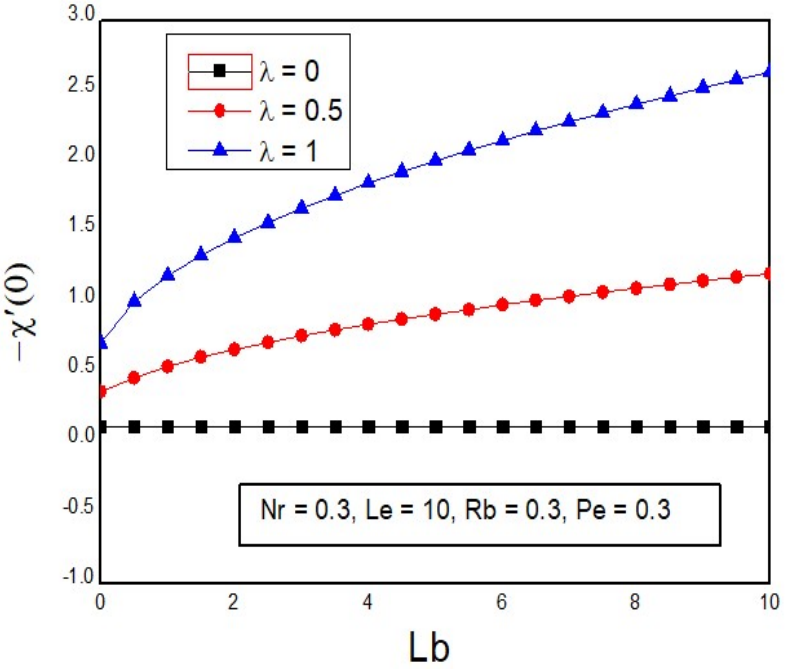

(c)

Fig. 2.10 The influence of *Lb* with free forced convection on a) Nusselt number b) Sherwood number c) microorganism density number

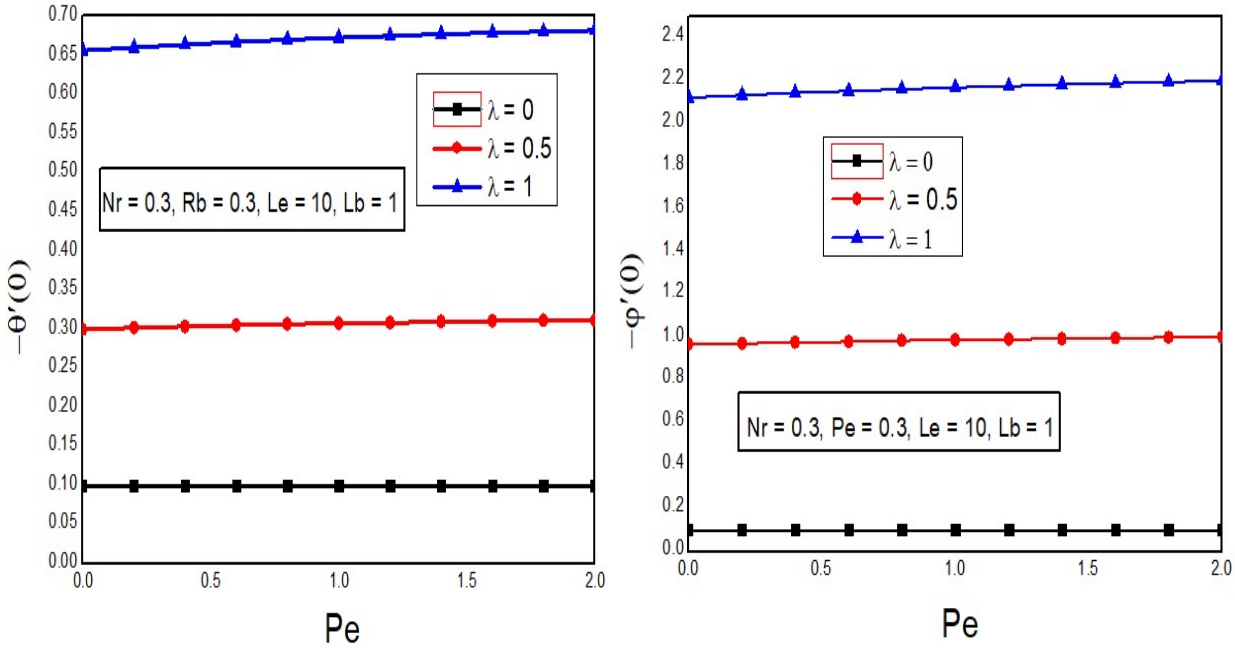

(a) **(b)**

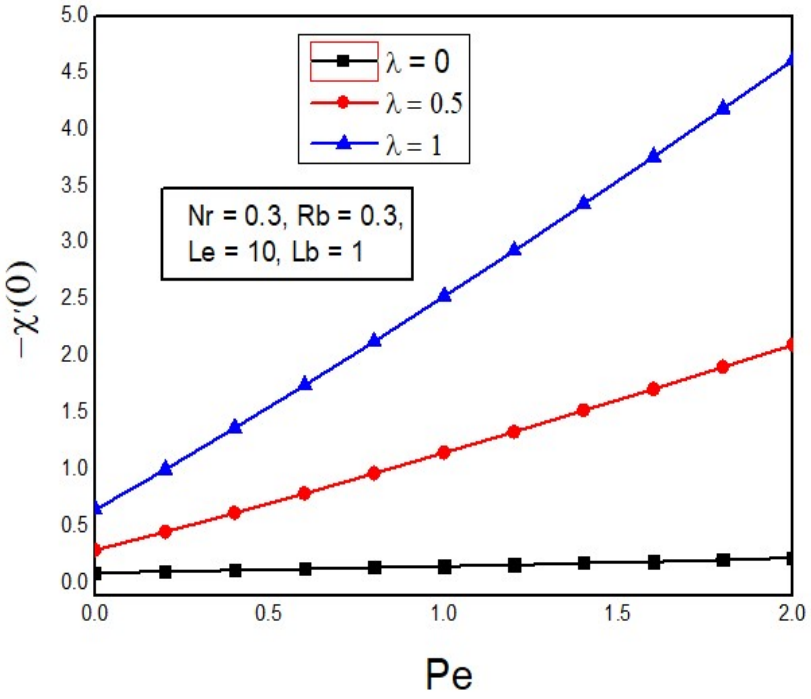

(c)

Fig. 2.11 The influence of *Pe* with free forced convection on a) Nusselt number b) Sherwood number c) microorganism density number

In **Figs. (2.7–2.8)**, the concentration and microorganism boundary layer thickness are found to decrease with increasing Lewis number, bioconvection Peclet number, and biconvection Lewis number for the pure free forced and mixed convection, and the bioconvection Lewis number and bioconvection Peclet number have a tendency to decrease microorganism profiles, as shown in **Figs. 2.7(a–b).)**. The thickness of the motile microorganisms is reduced by increasing the estimations of the bioconvection parameters because the bioconvection Lewis number and bioconvection Peclet number increase the swimming rate of the microorganisms in relation to the fluid. The depth at which the concentration boundary layer can be penetrated is decreased as the Lewis number decreases the mass diffusivity of the oxygen species, as shown in **Fig. 2.8.**

In **Figs. 2.9(a–c)**, we can observe the response in the Nusselt number, Sherwood number, and wall gradient of the density of the motile microorganisms. The Nusselt number and Sherwood number (with *Nr = 0.3, Le = 10, Rb = 0.3, and Pe = 0.3*) were both enhanced by increasing the Lewis number in the mixed and forced convection regimes. The Lewis number

has a negligible effect on the Nusselt number, indicating that the heat transfer rate at the fuel cell wall (boundary) is not modified by the ratio of the thermal diffusivity to the oxygen diffusivity ($Le = \frac{\alpha}{D}$). It is more sensitive to microorganism species diffusivity, which justifies the implementation of gyrotactic species in the fuel cell.

The behaviour of the Nusselt number, Sherwood number, and gradient of the motile microorganism density function, with increasing values of the Lb, are depicted in **Figs. 2.10(a–c)** and with increasing values of Pe are shown in **Figs. 2.11(a–c)**. Bioconvection Peclet number is the ratio between the rates of diffusion and advection, whereas Lewis number opposes the diffusion of the diffusivity of microorganisms. In contrast to diffusion, Pe causes an increase in the advective transport rate. So, both Lb and Pe have a significant impact on the rate of transmission of motile microorganisms. In both cases, the density of motile microorganisms increased in both mixed and forced convection regimes with bioconvection Lewis and Peclet numbers. This indicates that an enhancement in the near-wall transport characteristics is induced by the careful manipulation of the bioconvection parameters.

2.4 Summary

A theoretical and computational study is presented for free-forced convective flow from a vertical plate embedded in a Darcian permeable medium as a model of near-wall PEM fuel cell transport phenomena. A graphical analysis of the consequences of mixed convection and bioconvection parameters on the velocity, temperature, oxygen concentration, and microorganism density profiles was conducted. Following is a summary of the study's main conclusions:

- The effects of the buoyancy parameter Nr, bioconvection Raleigh number Rb, Lewis number Le, bioconvection Lewis number Lb, and bioconvection Peclet number Pe in the forced convection regime were more prominent than those in the pure free convection regime. Therefore, fuel cell performance can be optimised by carefully selecting these parameters.
- The Lewis number Le, bioconvection Lewis number Lb, and bioconvection Peclet number Pe have a negligible impact on the Nusselt number.

- The Sherwood number increased with increasing Lewis number Le, indicating that the wall oxygen mass transfer rate was enhanced.
- The density of motile microorganisms increases with the bioconvection Lewis number Lb, Lewis number Le, and bioconvection Peclet number Pe, which implies an enhanced performance in the near-wall zone of the fuel cell.

Chapter 3

Double-diffusivity heat generation effects on bioconvection process embedded in a vertical porous surface with variable fluid properties

This chapter examines flow gyrotactic microorganisms while considering the impact of heat generation and varied fluid characteristics. The physical laws governing the microorganism concentration and fluid flow were modelled as a collection of connected partial differential equations and then condensed into equivalent nonlinear ordinary differential equations with similarity variables. Maple built-in functions were used to get numerical solutions, which reduces the difficulty associated with nonlinear problems with high computational complexity. In accordance with the fluid physics, graphic solutions to the symbolic results are shown and completely described for the profiles of motile microbe density, temperature, concentration, and velocity for variable and uniform permeability as well as for both porous and impermeable instances. This study can be used in different geothermal engineering fields, where motile gyrotactic microorganisms play a dominant role in the bioconvection process.

3.1 Mathematical formulation

Convectional flow in an incompressible fluid along a vertical wall contained within a permeable medium containing motile microorganisms has been studied. The flow was assumed to be steady, with variable pore sizes. The coordinate system (x, y) was chosen such that the x-axis aligns with the plate, whereas the y-axis is in the transverse direction. The vertical wall is maintained at constant distributions, such as temperature T_w, the fluid concentration C_w, and microorganism density n_w, which are seen as being greater than the ambient temperature, concentrations, and density T_∞, C_∞, and n_∞, respectively.

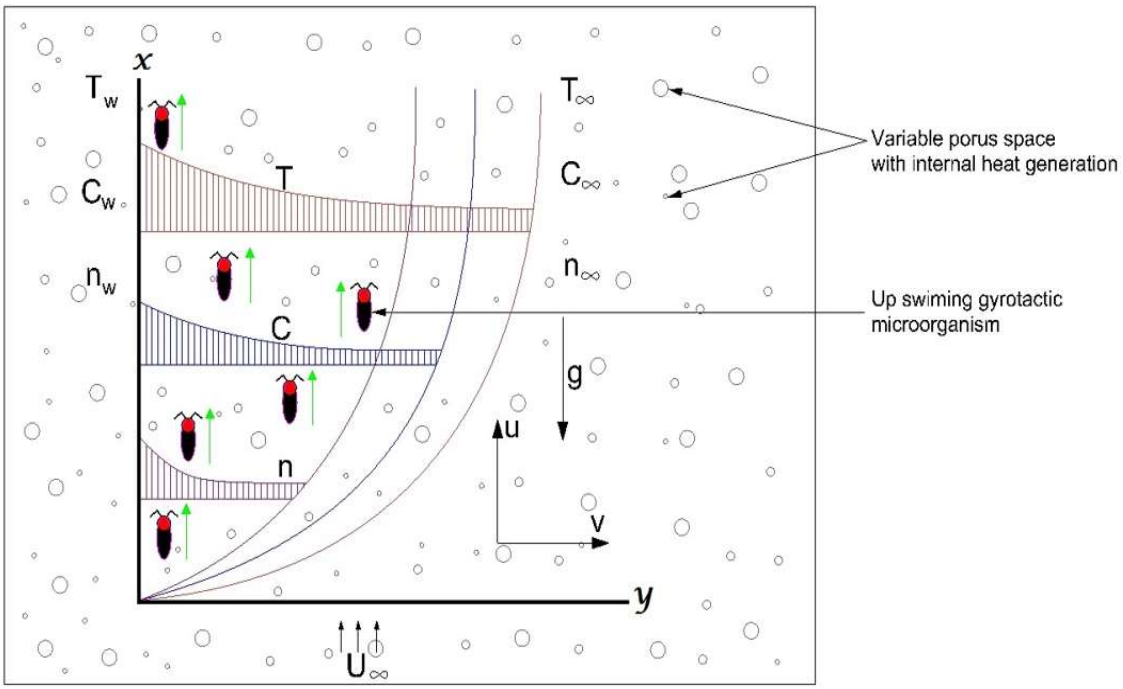

Fig. 3.1 Coordinates and the physical model

According to Cheng (2012), Ferdows and Liu (2017), and Dinesh (2015), the governing equations that form the theoretical framework for the study are from the conservation laws for mass, momentum, energy, concentration, and microorganisms, and are given in differential form as:

$$\frac{\partial u}{\partial x}+\frac{\partial v}{\partial y}=0 \tag{3.1}$$

$$u=u_\infty+\frac{gk}{\upsilon}\left(\beta_T\left(T-T_\infty\right)+\beta_C\left(C-C_\infty\right)+\beta_n\left(n-n_\infty\right)\right)-\frac{\mu}{\rho_0}\frac{\varepsilon(y)}{k(y)}u \tag{3.2}$$

$$u\frac{\partial T}{\partial x}+v\frac{\partial T}{\partial y}=\frac{\partial}{\partial y}\left(\alpha(y)\frac{\partial T}{\partial y}\right)+q''' \tag{3.3}$$

$$u\frac{\partial C}{\partial x}+v\frac{\partial C}{\partial y}=\frac{\partial}{\partial y}\left(\sigma(y)\frac{\partial C}{\partial y}\right) \tag{3.4}$$

$$u\frac{\partial n}{\partial x}+v\frac{\partial n}{\partial y}+\frac{bW_C}{\left(C_w-C_\infty\right)}\left[\frac{\partial}{\partial y}\left(n\frac{\partial C}{\partial y}\right)\right]=\frac{\partial}{\partial y}\left(\gamma(y)\frac{\partial n}{\partial y}\right) \tag{3.5}$$

Additionally, the boundary conditions have the following structure:

$$v = 0, T = T_w, C = C_w, n = n_w \qquad \text{at } y = 0 \tag{3.6}$$

$$u \to u_\infty, T \to T_\infty, C \to C_\infty, n \to n_\infty \qquad \text{at } y \to \infty \tag{3.7}$$

In (3.1)–(3.7), $k(y)$ is the variable permeability of the porous medium and $\varepsilon(y)$ is the variable porosity, $\alpha(y)$ is the thermal diffusivity, $\sigma(y)$ is the solute diffusivity, $\gamma(y)$ is the variable effective diffusivity of microorganisms, and q''' is the exponential term of internal heat generation. To solve the aforementioned nonlinear partial differential equations, we introduce the following dimensionless quantities and similarity variables following Uddin *et al.* (2013), Ferdows and Liu (2017):

$$\eta = \frac{y}{x} Ra_x^{\frac{1}{2}}, \ \psi = \alpha_0 \ Ra_x^{\frac{1}{2}} f(\eta), \tag{3.8}$$

$$\theta(\eta) = \frac{T - T_\infty}{T_w - T_\infty}, \ \chi(\eta) = \frac{n - n_\infty}{n_w - n_\infty}, \ \phi(\eta) = \frac{C - C_\infty}{C_w - C_\infty}, q''' = \frac{\alpha_0 (T_w - T_\infty) Ra_x}{x^2} e^{-\eta} \tag{3.9}$$

The definitions of the formulae for the variable fluid properties are given below in accordance with Kameswaran *et al*. (2016):

$$\begin{aligned}
k(\eta) &= k_0\left(1 + de^{-\eta}\right) \\
\varepsilon(\eta) &= \varepsilon_0\left(1 + d^* e^{-\eta}\right) \\
\alpha(\eta) &= \alpha_0\left[\left(\varepsilon_0\left(1 + d^* e^{-\eta}\right)\right) + \alpha^*\left\{1 - \varepsilon_0\left(1 + d^* e^{-\eta}\right)\right\}\right] \\
\sigma(\eta) &= \sigma_0\left[\left(\varepsilon_0\left(1 + d^* e^{-\eta}\right)\right) + \sigma^*\left\{1 - \varepsilon_0\left(1 + d^* e^{-\eta}\right)\right\}\right] \\
\gamma(\eta) &= \gamma_0\left[\left(\varepsilon_0\left(1 + d^* e^{-\eta}\right)\right) + \gamma^*\left\{1 - \varepsilon_0\left(1 + d^* e^{-\eta}\right)\right\}\right]
\end{aligned} \tag{3.10}$$

where $k(\eta)$ = variable permeability, $\alpha(\eta)$ = variable effective thermal diffusivity, $\varepsilon(\eta)$ = variable porosity, $\sigma(\eta)$ = variable effective solute diffusivity, and $\gamma(\eta)$ = variable effective diffusivity of microorganisms.

In (3.10), $k_0, \varepsilon_0, \alpha_0, \sigma_0, \gamma_0$ represents constant permeability, porosity, thermal conductivity, solute diffusivity, and microorganism diffusivity respectively. In addition, α^* provides the ratio

of solid thermal conductivity to fluid conductivity, σ^* ratios the solid thermal diffusivity with fluid diffusivity, and γ^* is the thermal diffusivity of the microorganism to the conductivity of the fluid. For variable permeability (VP), d and d^* are considered constants and for uniform permeability $d = d^* = 0$.

Using (3.9)– (3.10) in (3.1)– (3.7) leads to the following coupled differential equations:

$$\left(1+\frac{1}{kp}\frac{\left(1+d^*e^{-\eta}\right)}{\left(1+de^{-\eta}\right)}\right)f' - \lambda - \left(\theta + N_1\phi + N_2\chi\right) = 0 \tag{3.11}$$

$$\theta'' + \frac{\frac{1}{2}f\theta' + se^{-\eta} - \varepsilon_0 d^* e^{-\eta}\left(1-\alpha^*\right)\theta'}{\varepsilon_0 + \alpha^*\left(1-\varepsilon_0\right) + \varepsilon_0 d^* e^{-\eta}\left(1-\alpha^*\right)} = 0 \tag{3.12}$$

$$\phi'' + \frac{\frac{1}{2}Lef\phi' + \varepsilon_0 d^* e^{-\eta}\left(\sigma^* - 1\right)\phi'}{\varepsilon_0 + \sigma^*\left(1-\varepsilon_0\right) + \varepsilon_0 d^* e^{-\eta}\left(1-\sigma^*\right)} = 0 \tag{3.13}$$

$$\chi'' + \frac{\frac{1}{2}Lbf\chi' + \varepsilon_0 d^* e^{-\eta}\left(\gamma^* - 1\right)\chi' - Pe\left(\left(A+\chi\right)\phi'' + \chi'\phi'\right)}{\varepsilon_0 + \gamma^*\left(1-\varepsilon_0\right) + \varepsilon_0 d^* e^{-\eta}\left(1-\gamma^*\right)} = 0 \tag{3.14}$$

Together with

$$\eta = 0, f = 0, \theta = 1, \phi = 1, \chi = 1 \tag{3.15}$$

$$\eta \to \infty, f' \to \lambda, \theta \to 0, \phi \to 0, \chi \to 0 \tag{3.16}$$

where the permeability parameter $kp^* = \frac{k_0}{\varepsilon_0}$, porous parameter $kp = \frac{kp^*}{\nu}$, local Rayleigh number $Ra_x = \frac{kg\beta_T(T_w - T_\infty)}{\nu\alpha_0}$, local Peclet number $Pe_x = \frac{u_\infty x}{\alpha_0}$, convective term $\lambda = \frac{Pe_x}{Ra_x}$, Buoyancy ratio parameter $N_1 = \frac{\beta_C(C_w - C_\infty)}{\beta_T(T_w - T_\infty)}$, Buoyancy ratio parameter $N_2 = \frac{\beta_n(n_w - n_\infty)}{\beta_T(T_w - T_\infty)}$,

Lewis number $Le = \frac{\alpha_0}{\sigma_0}$, bioconvection Lewis number $Lb = \frac{\alpha_0}{\gamma_0}$, bioconvection Peclet number $Pe = \frac{bW_c}{\gamma_0}$, and microorganism concentration difference parameter $A = \frac{n_\infty}{n_w - n_\infty}$.

Other quantities of interest provided by

$$Nu_x = \frac{xq_w}{k(T_W - T_\infty)}, Sh_x = \frac{xq_m}{\sigma_0(C_W - C_\infty)}, Nn_x = \frac{xq_n}{\gamma_0(n_w - n_\infty)} \tag{3.17}$$

where Nu_x denotes the rate of heat transfer, Sh_x denotes the Sherwood number, and Nn_x denotes the density parameter for the motile microorganisms. Moreover, $q_{w,}\, q_m$, and q_n represent the constant wall heat, mass, and microorganism fluxes, respectively, which are written as follows:

$$q_w = -k(\frac{\partial T}{\partial \bar{y}})_{y=0},\ q_m = -\sigma_0(\frac{\partial C}{\partial \bar{y}})_{y=0},\ q_n = -\gamma_0(\frac{\partial n}{\partial \bar{y}})_{y=0} \tag{3.18}$$

Using variables (3.9), (3.10), (3.17), and (3.18), we obtain:

$$Ra_x^{-\frac{1}{2}} Nu_x = -\theta'(0),\ Ra_x^{-\frac{1}{2}} Sh_x = -\phi'(0),\ Ra_x^{-\frac{1}{2}} Nn_x = -\chi'(0) \tag{3.19}$$

where $Ra_x \frac{-1}{2} Nu_x$, $Ra_x^{-\frac{1}{2}} Sh_x$, and $Ra_x^{-\frac{1}{2}} Nn_x$ are the Nusselt number, Sherwood number, and local density number of the motile microorganisms, respectively.

3.2 Solution methodology

Making use of similarity transformations, the governing partial differential equations (3.1) – (3.7) were changed into ordinary differential equations (3.11) – (3.16) respectively, and then mathematically resolved using Maple through the use of **dsolve** command. The type of BVP or IVP problem was easily recognised, and suitable algorithms were executed. The correctness and dependability of Maple's algorithm have been confirmed many times in recent studies. For

additional proof, the current results for the special cases were contrasted with the results of Hsieh (1993) and Cheng (2012). The asymptotic boundary conditions provided by equation (3.15) – (3.16) were supplanted by using a value of eight for the similarity variable η_{max} as follows:

$$\eta_{\max} = 8,\ f'(8) = 0,\ \theta(8) = 0,\ \phi(8) = 0,\ \sigma(8) = 0$$

3.3 Numerical results and discussion

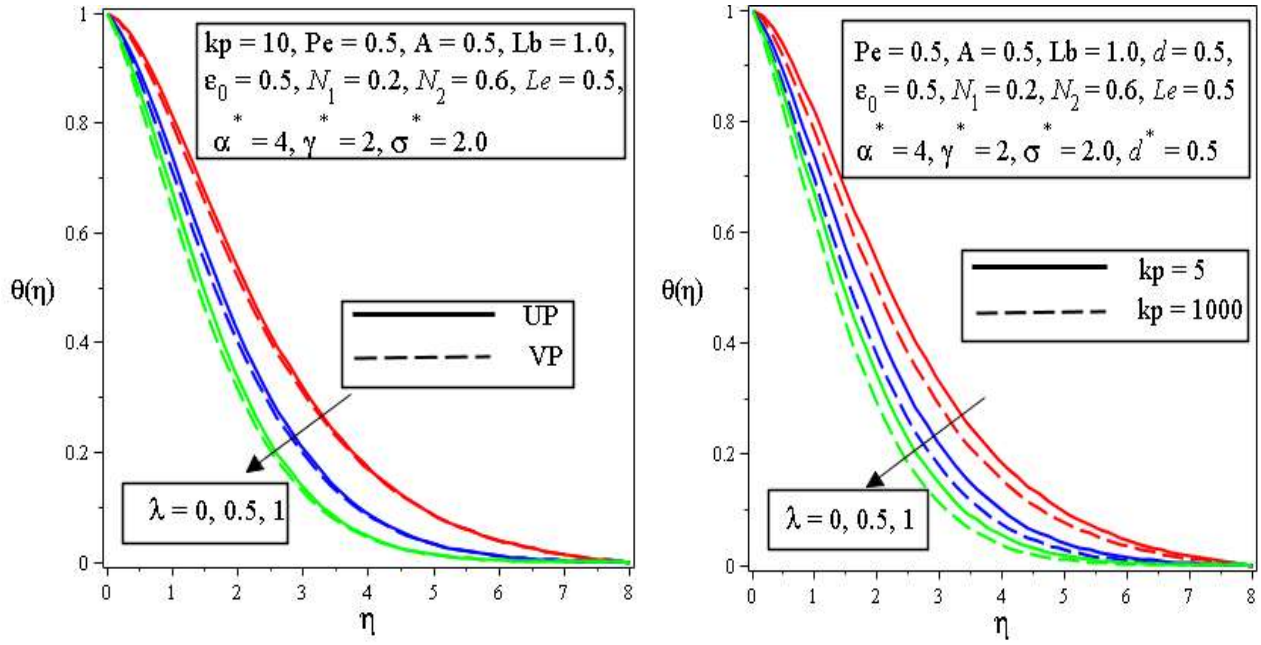

(a) **(b)**

Fig. 3.2 Temperature profile on varying values of λ a) for UP and VP cases b) for the presence and absence of porous media

In **Fig. 3.2(a)** temperature profile for various mixed convection parameter λ values is shown, where λ = 0 represents pure free convection, and λ = 1 represents pure forced convection. The temperature profile decreased with increasing values of the mixed-convection parameter. The temperature profile with the mixed convection parameter decreases more with variable permeability than with uniform permeability, where d and d^* are considered fixed constant values for VP $d = d^* = 0$ and for UP. In **Fig. 3.2(b)**, the behaviour of the temperature profile

with a mixed convection parameter is shown to determine whether porous media are present or not. A higher value of *kp* is considered to represent the absence of a porous matrix. The boundary layer thickness of the temperature profile shown in **Fig. 3.2(b)** increases in the presence of a porous matrix.

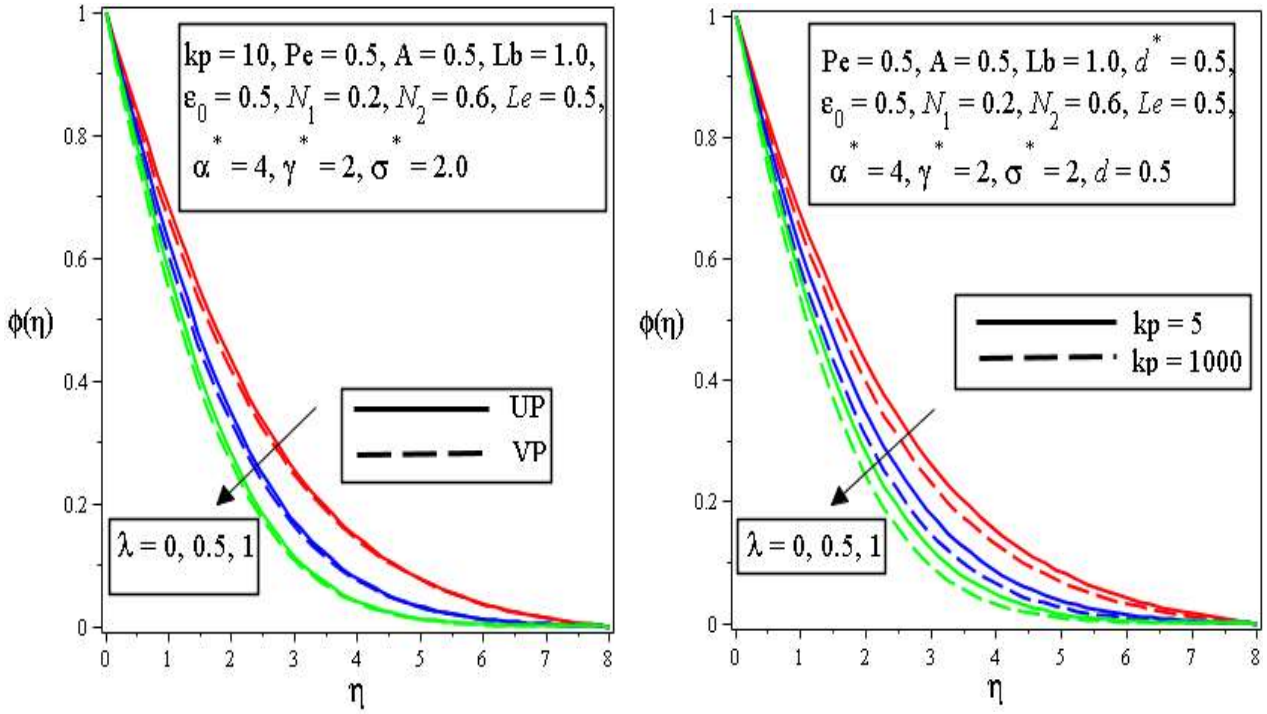

(a) **(b)**

Fig. 3.3 Concentration profile on varying values of λ a) for UP and VP cases b) for the presence and absence of porous media

In **Figs. 3.3(a–b),** the concentration profile decreases because of the rising value of the mixed convection parameter, and behaviour for uniform permeability and VP the presence or absence of a porous matrix is also observed. Increasing mixed convection parameter and permeability of porous medium increase mass transfer causes reduction of solutal boundary layer thickness. Similarly, the microorganism profile for the mixed convection parameter with UP and VP in porous and non-porous media is shown in **Figs. 3.4(a–b),** wherein the microorganism profile decreases with mixed convection parameters mostly for non-porous cases.

A lower value of kp is considered to represent the porous matrix. Large pores in a porous medium may lead to a reduction in the medium's resistance leads to the rise in the flow of fluid through it. As a result, the temperature, solute, and microorganism profiles have increased for lower values of kp compared with non-porous medium.

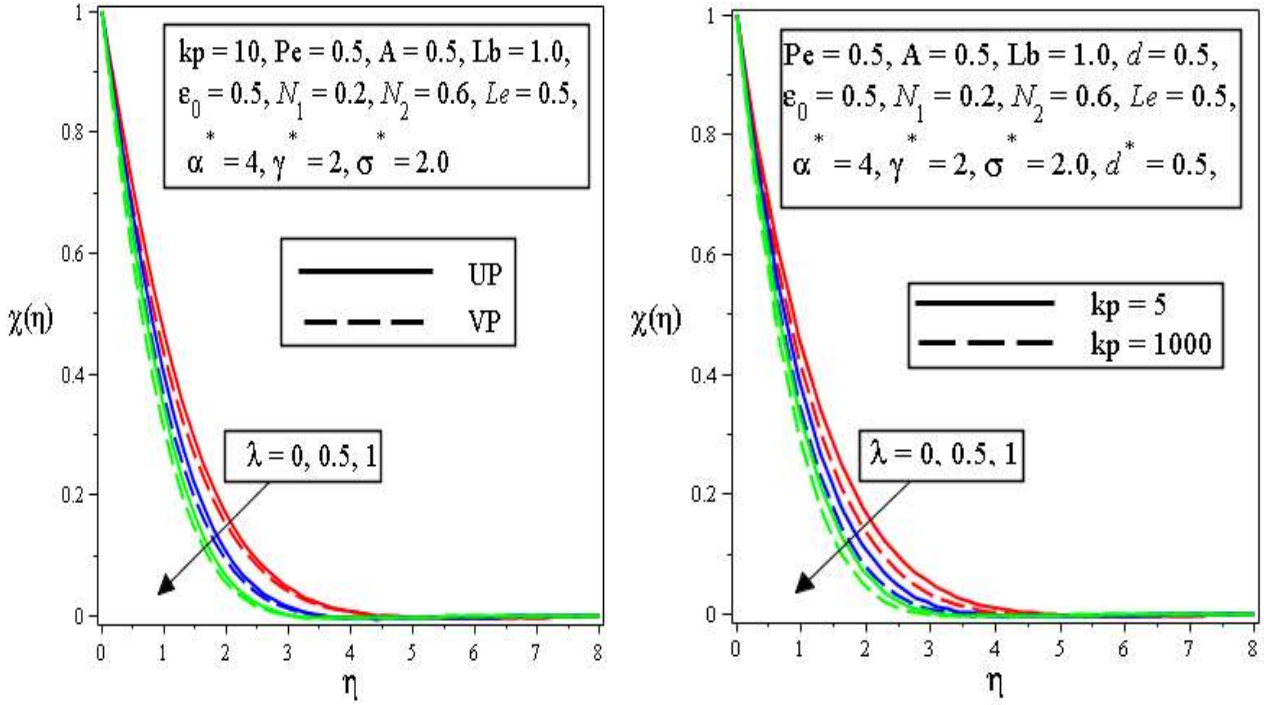

(a) **(b)**

Fig. 3.4 Microorganism profile on varying values of λ a) for UP and VP cases b) for the presence and absence of porous media

Effects of the Lewis number on the concentration profile is shown for the UP and VP cases in **Fig. 3.5(a)** and for the porous and non-porous matrices in **Fig. 3.5(b).** The Lewis number Le is oppositely correlated with the diffusion coefficient; therefore, an increase in Le results in a decrease in the concentration profile. A similar impact on the microorganism profile is observed in **Figs. 3.6(a–b),** wherein the microorganism profile initially decreases for greater Lewis number values, although after $\eta \approx 1.9$, it slightly increases. Physically, the increase of Le means decrease of microorganism diffusion. Hence the concentration of microorganism is higher for lower values of Lewis number.

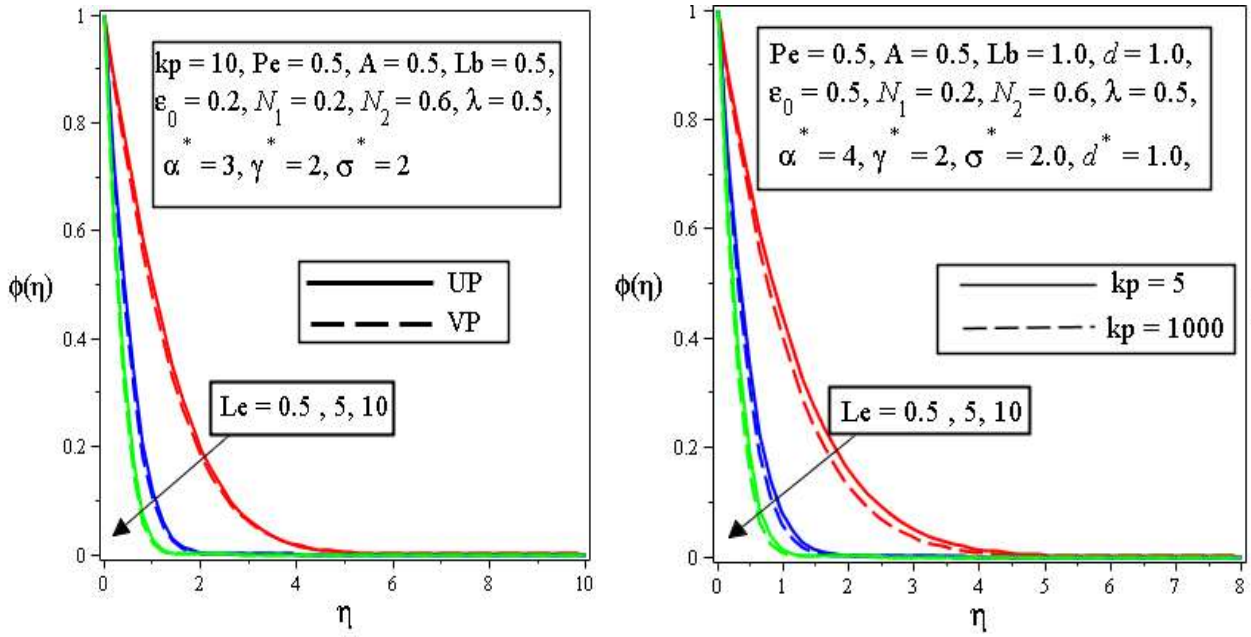

(a) **(b)**

Fig. 3.5 Concentration profile on varying values of *Le* a) for UP and VP cases b) for the presence and absence of porous media

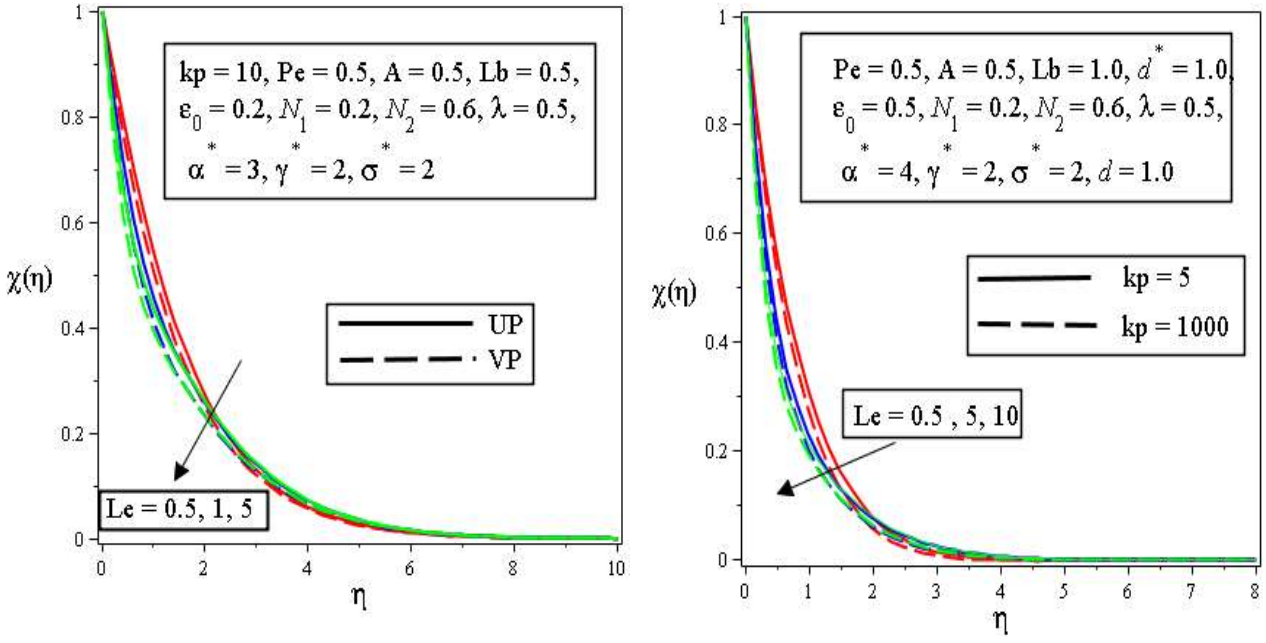

(a) **(b)**

Fig. 3.6 Microorganism profile on varying values of *Le* a) for UP and VP cases b) for the presence and absence of porous media

The bioconvection Lewis number has a noticeable impact on the microorganism boundary. The microorganism profiles for increasing values of the Lb and Pe are shown in **Figs. (3.7–3.8).** For every case, the microorganism profile decreased. A rise in the Peclet number, Pe, caused a decrease in the diffusivity of microorganisms. Owing to the decline in the diffusivity of microorganisms with increasing values of Lb and Pe, the motile density of the fluid decreases. The boundary layer thickness declines mostly in the VP case and in non-porous matrix. Variable permeability and non-porous phenomena is inversely related to the species dispersion stream. As a result, when compared to UP, VP causes the microbe concentration profile to decrease.

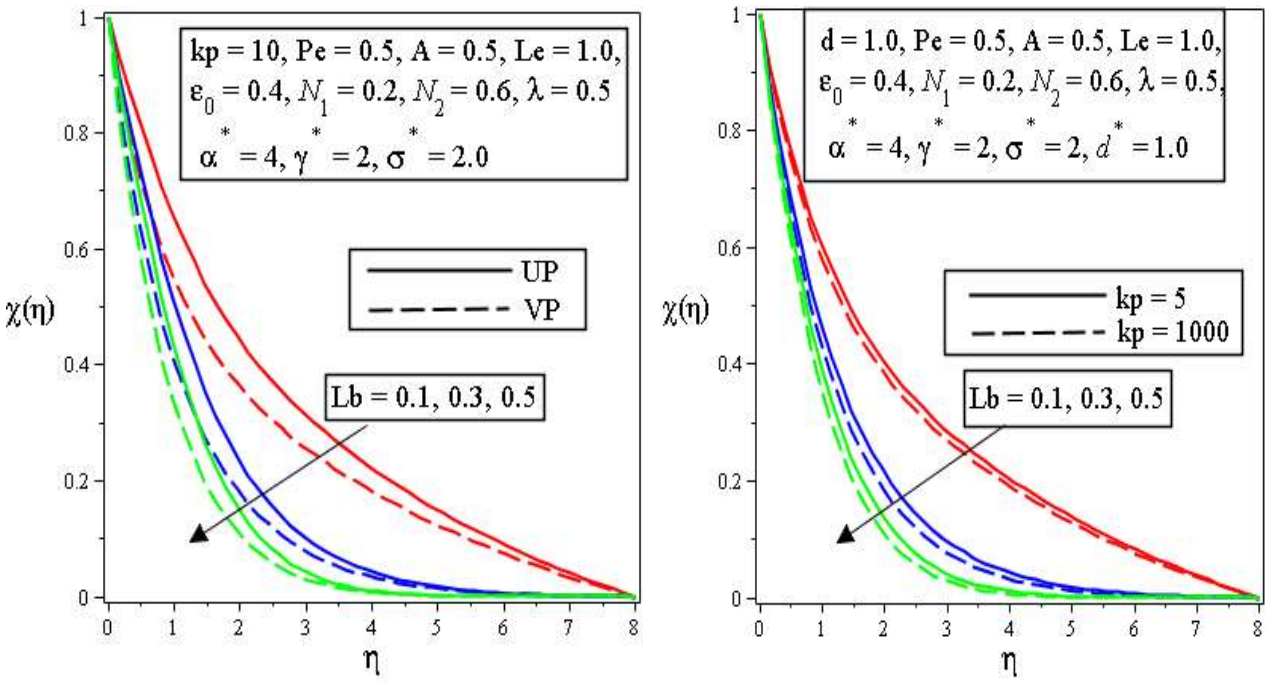

(a) **(b)**

Fig. 3.7 Microorganism profile on varying values of Le a) for UP and VP cases b) for the presence and absence of porous media

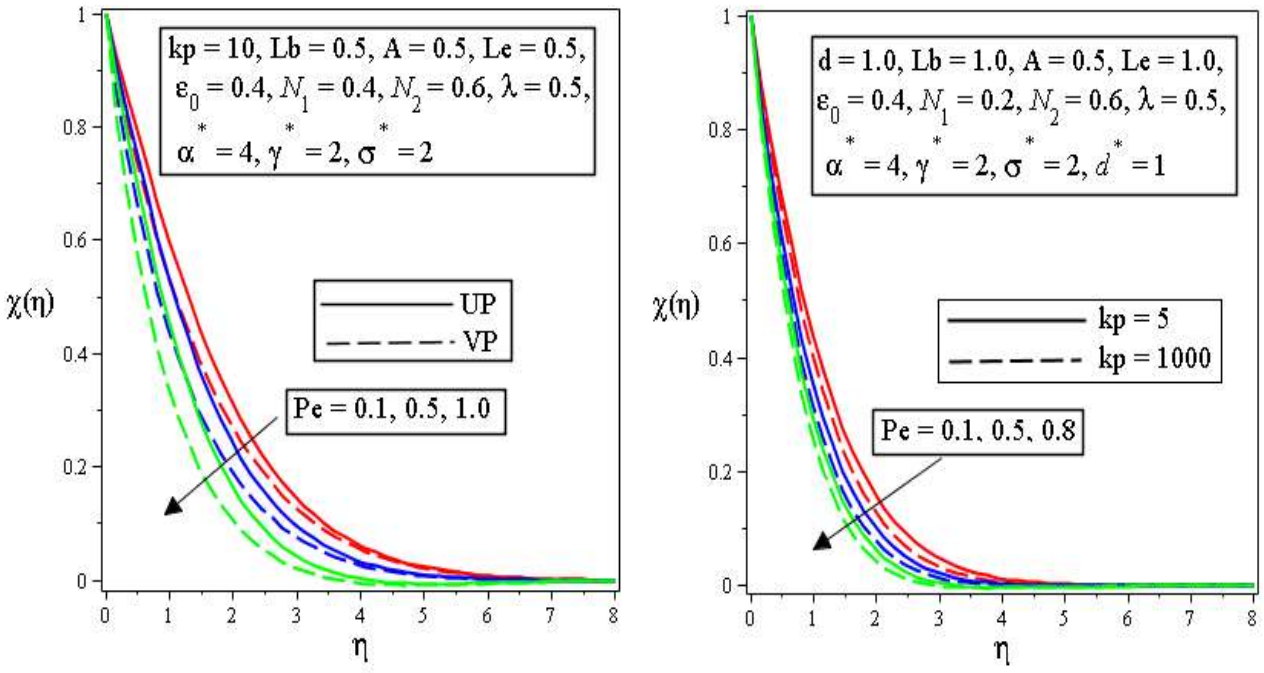

(a) **(b)**

Fig. 3.8 Microorganism profile on varying values of Pe a) for UP and VP cases b) for the presence and absence of porous media

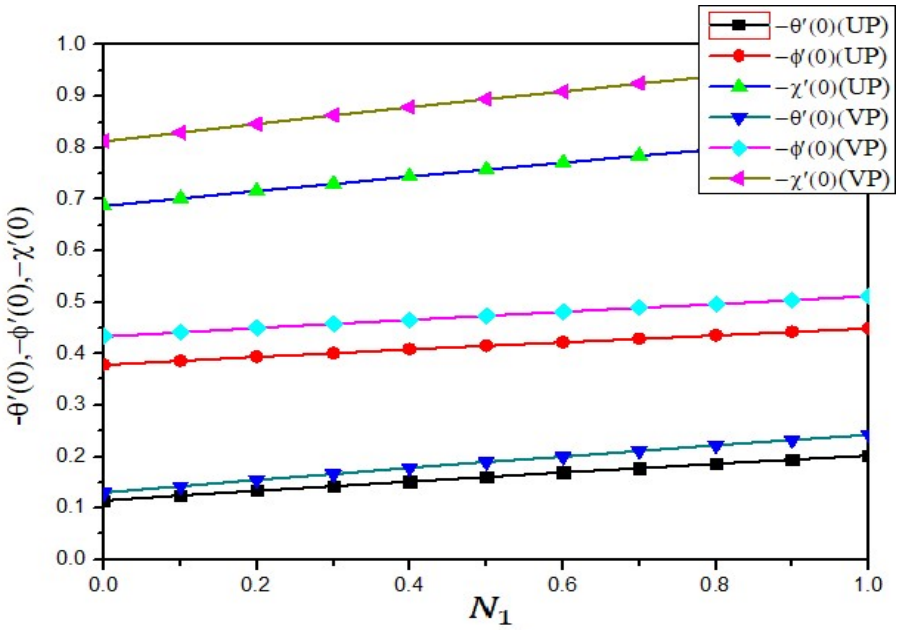

Fig. 3.9 Effect of N_1 on Nusselt number, Sherwood number, and density of motile microorganism for UP and VP cases

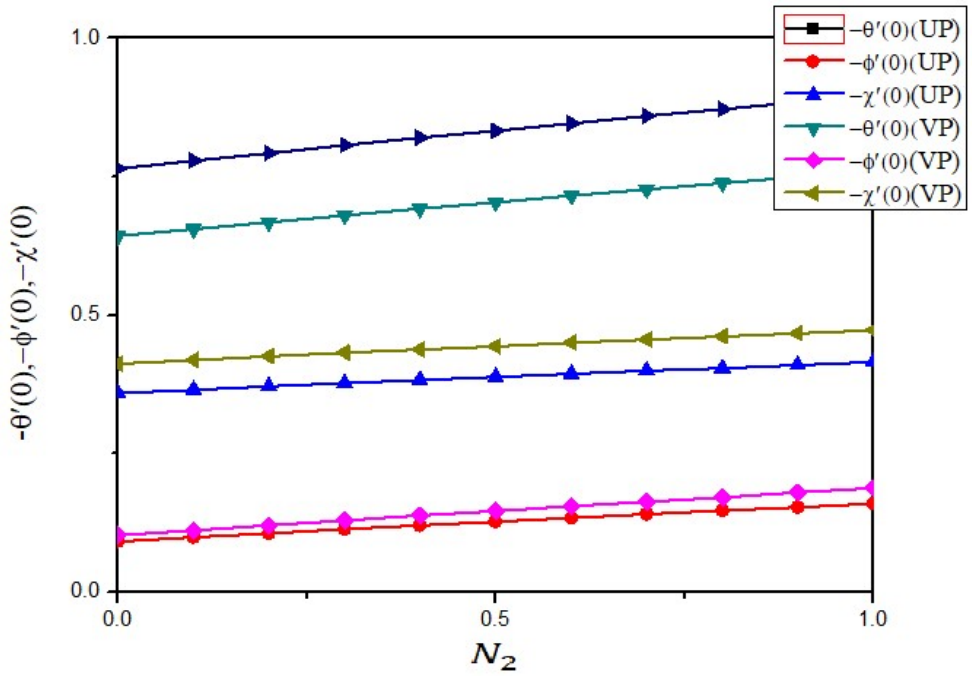

Fig. 3.10 Effect of N_2 on Nusselt number, Sherwood number, and density of motile microorganism for UP and VP cases

Figs. 3.9 and **3.10** demonstrate the impact of the buoyancy ratio parameter N_1, N_2 on the Nusselt number, Sherwood number, and motile microbial density for both the UP and VP cases, where in every case the numbers increase considering the rising worth of buoyancy parameters. Buoyancy parameters boost the buoyancy force due to bioconvection causes to increase heat, mass and motile microorganism transfer rate. Additionally, a greater effect of varying permeability is seen on the density of microorganisms. The mixed-convection parameter λ indicates the entire region of free, mixed, and forced convection, as shown in **Table 3.1.** Assuming higher values of the density of moving microorganisms, the Sherwood number, and the Nusselt number for increasing values of the mixed convection parameter λ are listed for uniform permeability (UP) and variable permeability (VP). With respect to free convection to forced convective regime heat, the mass and motile microorganism transfer rate is higher, particularly for VP.

Table 3.1 Effect of mixed convection parameter λ on heat and mass transfer, and density of motile microorganism for $Le = 0.5, Lb = 1, Pe = 0.5, A = 0.5, kp = 10, N_1 = 0.2, N_2 = 0.6, \alpha^* = 4, \sigma^* = 2, \gamma^* = 2$ for UP and VP case

λ	$-\theta'(0)$		$-\varphi'(0)$		$-\chi'(0)$	
	UP	VP	UP	VP	UP	VP
0.0	0.04875	0.04459	0.32915	0.37722	0.61210	0.72591
0.1	0.06681	0.06816	0.34267	0.39244	0.63412	0.75150
0.2	0.08430	0.09095	0.35589	0.40732	0.65543	0.77627
0.3	0.10123	0.11296	0.36878	0.42185	0.67610	0.80029
0.4	0.11761	0.13422	0.38135	0.43600	0.69619	0.82364
0.5	0.13347	0.15476	0.39360	0.44977	0.71575	0.84635
0.6	0.14884	0.17461	0.40552	0.46318	0.73481	0.86849
0.7	0.16374	0.19383	0.41713	0.47624	0.75342	0.89008
0.8	0.17820	0.21246	0.42845	0.48896	0.77160	0.91118
0.9	0.19227	0.23054	0.43949	0.50136	0.78939	0.93180
1.0	0.20595	0.24810	0.45027	0.51346	0.80680	0.95197

Table 3.2 lists the variation in heat and mass transfer and density of motile microorganisms for the porous parameter kp, where higher values of kp indicate non-porous medium. The use of a porous medium resulted in a higher heat-transfer rate. The heat transfer rate in a porous medium is higher than that in a non-porous medium because of the existence of porosity. Therefore, we can conclude that in both UP and VP cases, the values of Nusselt

number, Sherwood number, and density of motile microorganisms are lower in porous medium compared to the non-porous medium.

Table 3.2 Effect of porous parameter kp on heat and mass transfer, and density of motile microorganism for $Le = 0.5, Lb = 1, Pe = 0.5, A = 0.5, N_1 = 0.4, N_2 = 0.6, \alpha^* = 4, \sigma^* = 2, \gamma^* = 2, \lambda = 0.5$ for UP and VP cases

	$-\theta'(0)$		$-\varphi'(0)$		$-\chi'(0)$	
kp	UP	VP	UP	VP	UP	VP
1	0.022463	0.011892	0.307043	0.353380	0.554489	0.661173
3	0.105821	0.119347	0.371862	0.425605	0.676720	0.8015870
5	0.130391	0.150785	0.391271	0.447161	0.712678	0.8427941
10	0.151638	0.177896	0.408147	0.465883	0.743811	0.8784396
50	0.170798	0.202288	0.423434	0.482825	0.771930	0.9106097
100	0.173348	0.205531	0.425473	0.485084	0.775677	0.9148945
1000	0.175676	0.208490	0.427335	0.487146	0.779097	0.9188050

Table 3.3 Comparison of heat transfer rate $-\theta'(0)$ for $\lambda = 0, N_1 = 0, N_2 = 0, S = 0, \varepsilon_0 = 1, \alpha^* = 1, \sigma^* = 1, \gamma^* = 1, Le = 0, Lb = 0, Pe = 0$

	Present	Hsieh et al (1993) when $\xi = 0$	Ching-Yang Cheng (2012) when $\xi = 0$
$-\theta'(0)$	0.4445	0.4438	0.4438

For higher values of kp, we can consider that $\frac{1}{kp}$ is negligible, and if we use $\lambda = 0, N_1 = 0, N_2 = 0, s = 0, \varepsilon_0 = 1, \alpha^* = 1, \sigma^* = 1, \gamma^* = 1, Le = 0, Lb = 0, Pe = 0$, then the value of the Nusselt number is similar to the values of the Nusselt number presented in Hsieh (1993) and Cheng (2012).

3.4 Summary

A numerical model is established for the study of mixed-convection heat flow and mass transfer over a vertical plate in a saturated porous medium containing gyrotactic microorganisms by considering variable fluid properties. Following are the findings from the analysis:

- Increasing the mixed convection parameter λ results in a drop in the temperature profile; this implies that the temperature profile gradually decreases from free convection to forced convection. The boundary layer thickness mostly decreases for VP and non-porous media.
- Concentration profile decreases between the regimes of forced and free convection with the increasing value of mixed convection parameter λ and declines with an increase in Lewis number Le.
- Thickness of the microorganism profile's boundary layer decreases for increasing values of mixed convection parameter λ, bioconvection Lewis number Lb, and bioconvection Peclet number Pe. In every case decreasing effect is mostly shown for variable permeability and non-porous matrix.
- Nusselt number, Sherwood number, and density of motile microorganism increases with buoyancy ratio parameters N_1 and N_2, mixed convection parameter λ, and porous parameter kp for UP and for VP.

Chapter 4

Melting effect on non-Newtonian fluid flow in gyrotactic microorganism saturated non-Darcy porous media with variable fluid properties

This chapter elaborates on previous studies by considering the melting effect on a non-Newtonian fluid with gyrotactic microorganisms flowing steadily in mixed convection along a vertical plate embedded in a saturated non-Darcy porous medium. Variable fluid properties are considered in this chapter to describe the variations in permeability, porosity, and thermal conductivity, which are estimated by an exponential function. The changed non-dimensional governing ordinary differential equations via similarity transformation characterising the flow phenomena subjected to melting surface boundary conditions were solved numerically by the MATLAB bvp4c solver. To analyse the consequences of the flow-influencing parameters, the flow variables are tabulated and visualised graphically. Comparisons with previous studies show a strong agreement between the results.

4.1 Mathematical formulation

We take into account the continuous two-dimensional flow of a non-compressible non-Newtonian power-law fluid containing gyrotactic microorganisms in a non-Darcy porous medium over a vertical plate, in the presence of a melting effect and variable fluid properties. The coordinate system is chosen such that the positive x −plane is measured along the direction of motion, with the slot at the origin, whereas the positive y −plane is normal to the surface of the plate, as depicted in **Fig. 4.1**. The fluid flow over the vertical surface is induced by the action of the temperature and concentration buoyancy numbers and the uniform movement of the plate in its own plane. The plate was maintained at a constant temperature, T_m, at which the material that occupies the porous matrix melts. The liquid-phase temperature $T_0\left(T_0 < T_m\right)$ and the solid's temperature distant from the interface are $T_\infty\left(T_\infty < T_m\right)$. The vertical wall was retained at

constant distributions of the fluid concentration C_w and the motile microorganism concentration n_w, which was assumed to be greater than the far-field ambient concentrations C_∞ and n_∞. If there isn't viscous dissipation and the Hall current effect, the induced magnetic field was neglected owing to the low Reynolds number. The thermal conductivity and viscosity are supposed to change depending on temperature.

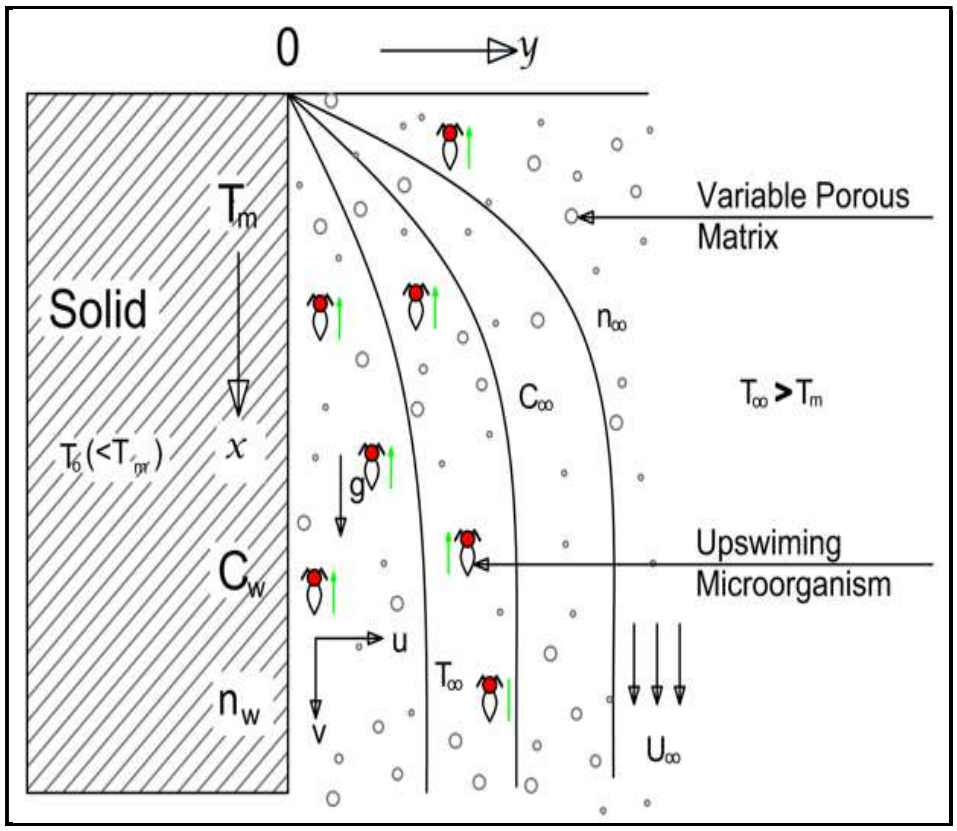

Fig. 4.1 Coordinates and the physical model

In the essence of aforementioned suppositions and estimates, the equations that describe the motion of a continuous mixed convection flow of non-Newtonian containing microorganisms over a vertical plate encased in non-Darcy porous media with melting effects and variable fluid properties adopts the form using (Mahdy *et al*. (2013); Shoba *et al*. (2010); Kameswaran *et al*. (2016)). The equations 3.1, 3.4, and 3.5 from chapter 3 that represent continuity, mass

conservation, and conservation of microorganisms have been examined in this chapter. The following are newly considered momentum and thermal energy equations:

$$\frac{\partial u^n}{\partial y}+\frac{c_f}{\nu}\left(2\sqrt{k}u\frac{\partial u}{\partial y}+\frac{u^2}{2\sqrt{k}}\frac{\partial k}{\partial y}\right)+\frac{g}{\upsilon}\begin{pmatrix}k\beta_T\frac{\partial T}{\partial y}+\beta_T(T_\infty-T_m)(\theta-1)\frac{\partial k}{\partial y}+k\beta_C\frac{\partial C}{\partial y}\\+\beta_C(C_\infty-C_w)(\phi-1)\frac{\partial k}{\partial y}+k\beta_n\frac{\partial n}{\partial y}+\beta_n(n_\infty-n_w)(\chi-1)\frac{\partial k}{\partial y}\end{pmatrix}=0$$

(4.1)

$$u\frac{\partial T}{\partial x}+v\frac{\partial T}{\partial y}=\frac{\partial}{\partial y}\left(\alpha(y)\frac{\partial T}{\partial y}\right)+\frac{\mu}{\rho C_P}\frac{u^2}{k} \tag{4.2}$$

In equations (3.1), (4.1), (4.2), (3.4) and (3.5), u and v are the velocity components along the x and y directions, respectively. T, C, n are the temperature, concentration, and volume fraction of motile microorganism, c_f is the Forchheimer Empirical constant, k is the permeability of porous medium, ν is the kinematic viscosity, and g is the acceleration because of gravity. In addition, β_T, β_C, β_n is the thermal, solutal, and motile microorganism expansion coefficient, respectively. ρ_∞ is the density, C_p is the specific heat at constant pressure, $\alpha(y)$ is thermal diffusivity, $\sigma(y)$ is solute diffusivity, and $\gamma(y)$ is the effective diffusivity of microorganism. According to study of RamReddy and Kairi (2015), n is the power law index ($n<1, n=1, n>1$), representing pseudo-plastic, Newtonian and dilatants fluids, respectively.

The boundary conditions are of the following form:

$$k_{eff}\frac{\partial T}{\partial y}=\rho[h_{sf}+c_s(T_m-T_0)]\nu, T=T_m, C=C_w, n=n_w \qquad \text{at} \quad y=0 \tag{4.3}$$

$$u\to u_\infty, T\to T_\infty, C\to C_\infty, n\to n_\infty \qquad \text{at} \quad y\to\infty \tag{4.4}$$

According to Epstein and Cho (1976) and Cheng and Lin (2007), the physical meaning of the boundary condition $k_{eff}\dfrac{\partial T}{\partial y}=\rho[h_{sf}+c_s(T_m-T_0)v$ signifies that the heat conducted to the melting surface is equal to the heat of melting plus the sensible heat required to increase the solid temperature to its melting temperature T_m.

Non-dimensional quantities and similarity variables were introduced to solve the aforementioned nonlinear partial differential equations.

$$\eta=\frac{y}{x}Pe_x^{1/2},\quad \psi=\alpha_\infty Pe_x^{1/2}f(\eta), \tag{4.5}$$

$$\theta(\eta)=\frac{T-T_m}{T_\infty-T_m},\ \phi(\eta)=\frac{C-C_\infty}{C_w-C_\infty},\ \chi(\eta)=\frac{n-n_\infty}{n_w-n_\infty} \tag{4.6}$$

Following the study by Kameswaran *et al.* (2016), the expressions for variable fluid properties are defined as follows:

$$\begin{aligned}
k(\eta)&=k_\infty\left(1+be^{-\eta}\right)\\
\varepsilon(\eta)&=\varepsilon_\infty\left(1+de^{-\eta}\right)\\
\alpha(\eta)&=\alpha_\infty\left[\left(\varepsilon_\infty\left(1+de^{-\eta}\right)\right)+\alpha^*\left\{1-\varepsilon_\infty\left(1+de^{-\eta}\right)\right\}\right]\\
\sigma(\eta)&=\sigma_\infty\left[\left(\varepsilon_\infty\left(1+de^{-\eta}\right)\right)+\sigma^*\left\{1-\varepsilon_\infty\left(1+de^{-\eta}\right)\right\}\right]\\
\gamma(\eta)&=\gamma_\infty\left[\left(\varepsilon_\infty\left(1+de^{-\eta}\right)+\gamma^*\left\{1-\varepsilon_\infty\left(1+de^{-\eta}\right)\right\}\right]\right.
\end{aligned} \tag{4.7}$$

where $k(\eta)=$ variable permeability, $\varepsilon(\eta)=$ variable porosity, $\alpha(\eta)=$ variable effective thermal diffusivity, $\sigma(\eta)=$ variable effective solutal diffusivity, and $\gamma(\eta)=$ variable effective diffusivity of microorganism. $k_\infty,\varepsilon_\infty,\alpha_\infty,\sigma_\infty,\gamma_\infty$ represents the permeability, porosity, thermal conductivity, solutal diffusivity, and microorganism diffusivity at the edge of the boundary layer. In addition, α^* provides the ratio of solid thermal conductivity to fluid conductivity, σ^* ratios the solid thermal diffusivity with fluid diffusivity, and γ^* is the thermal diffusivity of the microorganism to the conductivity of the fluid. For variable permeability (VP), d was considered constant.

Using Equations (4.5) – (4.7) in ((3.1), (4.1), (4.2), (3.4) and (3.5)) leads to following coupled differential equations:

$$n(f')^{n-1}f''+F\sqrt{1+be^{-\eta}}\,ff''-\frac{F}{4}\frac{be^{-\eta}}{\sqrt{1+be^{-\eta}}}(f')^2\pm(\lambda)^n\begin{bmatrix}(1+be^{-\eta})\theta'-be^{-\eta}(\theta-1)+N_1\{(1+be^{-\eta})\phi'\\-be^{-\eta}(\phi-1)\}+N_2\{(1+be^{-\eta})\chi'-be^{-\eta}(\chi-1)\}\end{bmatrix}=0 \tag{4.8}$$

$$\left[\varepsilon_\infty(1+de^{-\eta})(1-\alpha^*)+\alpha^*\right]\theta''+\varepsilon_\infty de^{-\eta}(\alpha^*-1)\theta'+\frac{1}{2}f\theta'+Ec.\Pr(f'')^2=0 \tag{4.9}$$

$$\left[\varepsilon_\infty(1+de^{-\eta})(1-\sigma^*)+\sigma^*\right]\phi''+\varepsilon_\infty de^{-\eta}(\sigma^*-1)\phi'+\frac{1}{2}Lef\phi'=0 \tag{4.10}$$

$$\left[\varepsilon_\infty(1+de^{-\eta})(1-\gamma^*)+\gamma^*\right]\chi''+\varepsilon_\infty de^{-\eta}(\gamma^*-1)\chi'+\frac{1}{2}Lbf\chi'-Pe\left[(A+\chi)\phi''+\chi'\phi'\right]=0 \tag{4.11}$$

Where λ, F, Ra_x, Pe_x, Ec, Pr, N_1, N_2, Le, Lb, Pe and A are the parameters, namely, the mixed convection parameter, non-Darcy parameter, local Rayleigh number, local Peclet number, Eckert number, Prandtl number, buoyancy ratio parameter due to concentration, buoyancy ratio parameter owing to microorganisms, Lewis number, bioconvection Lewis number, bioconvection Peclet number, and microorganism concentration difference parameter, respectively which occurred in equations (4.11) – (4.14) are defined as follows:

$$\begin{aligned}&\lambda=\frac{Ra_x}{Pe_x},\ F=\frac{2c_f\sqrt{k_\infty}(u_\infty)^{2-n}}{\upsilon},\ Ra_x=\left[\frac{k_\infty g\beta_T(T_\infty-T_m)}{\nu}\right]^{\frac{1}{n}}\frac{x}{\alpha_\infty},\ Pe_x=\frac{u_\infty x}{\alpha_\infty},\\&Ec=\frac{{u_\infty}^2}{C_p(T_\infty-T_m)},\ \Pr=\frac{\upsilon}{\alpha_\infty},\ N_1=\frac{\beta_C(C_w-C_\infty)}{\beta_T(T_w-T_\infty)},\ N_2=\frac{\beta_n(n_w-n_\infty)}{\beta_T(T_w-T_\infty)},\ Le=\frac{\alpha_\infty}{\sigma_\infty},\\&Lb=\frac{\alpha_\infty}{\gamma_\infty},Pb=\frac{bW_c}{\gamma_\infty},\ A=\frac{n_\infty}{n_w-n_\infty}\end{aligned} \tag{4.12}$$

The modified boundary conditions are changed to:

$$\eta\to 0: f(0)+2M\theta'(0)=0,\phi(0)=0,\chi(0)=0 \tag{4.13}$$

$$\eta\to\infty: f'(\infty)\to 1,\theta(\infty)\to 1,\phi(\infty)\to 1,\chi\to 1 \tag{4.14}$$

$M = \frac{C_p(T_\infty - T_m)}{h_{sf} + C_s(T_m - T_0)}$ is a dimensionless melting parameter, which is a combination of the Stefan numbers $\frac{C_f(T_\infty - T_m)}{h_{sf}}$ and $\frac{C_s(T_m - T_0)}{h_{sf}}$ for the liquid and solid phases, respectively.

The heat transfer rate, Sherwood number, and density parameter for the motile microorganisms can be defined as follows:

$$Nu_x = \frac{xq_w}{k_{eff}(T_\infty - T_m)}, Sh_x = \frac{xq_m}{\sigma_\infty(C_W - C_\infty)}, Nn_x = \frac{xq_n}{\gamma_\infty(n_w - n_\infty)} \tag{4.15}$$

where q_w, q_m, and q_n depict the continual fluxes of mass, heat, and microbes through the wall, respectively, which are stated as follows:

$$q_w = -k_{eff}(\frac{\partial T}{\partial \bar{y}})_{y=0}, q_m = -\sigma_\infty(\frac{\partial C}{\partial \bar{y}})_{y=0}, q_n = -\gamma_\infty(\frac{\partial n}{\partial \bar{y}})_{y=0} \tag{4.16}$$

Using variables (4.5-4.7), (4.18), and (4.19), we obtained the dimensionless Nusselt number and Sherwood number local density number of the motile microorganisms.

$$Pe_x^{-\frac{1}{2}} Nu_x = -\theta'(0), Pe_x^{-\frac{1}{2}} Sh_x = -\phi'(0), Pe_x^{-\frac{1}{2}} Nn_x = -\chi'(0) \tag{4.17}$$

4.2 Solution methodology

With the aid of similarity transformations, the guiding partial differential equations were converted into ordinary differential equations and then mathematically solved using the MATLAB bvp4c solver, where sol = bvp4c(odefun,bcfun,solinit) integrates a array of differential equations of the interval [a, b] depending on general two-point boundary conditions of the form bc(y(a),y(b)) = 0 and the initial solution guess solinit. The bvpinit function is used to create the initial guess solinit, in addition to defining the points with which the boundary conditions in bcfun are satisfied. In the light of the aforementioned bvp4c function, we need to transform the governing equations into a first-order differential equation, allowing $\eta = x$

$$\begin{aligned} &y_1 = f, y_2 = f', \ y_3 = \theta, \ y_4 = \theta', \\ &y_5 = \phi, \ y_6 = \phi', \ y_7 = \chi, \ y_8 = \chi', \end{aligned} \tag{4.18}$$

Following transformation, the first order differential equations are as follows:

$$\frac{dy_1}{dx} = f' = y_2$$

$$\frac{dy_2}{dx} = f'' = \frac{\frac{F}{4}\frac{be^{-\eta}}{\sqrt{1+be^{-\eta}}}(y_2)^2 \mp \lambda^n \begin{pmatrix} \left(1+be^{-\eta}\right)y_4 - be^{-\eta}\left(y_3-1\right) + N_1\left\{\left(1+be^{-\eta}\right)y_6 - be^{-\eta}\left(y_5-1\right)\right\} \\ + N_2\left\{\left(1+be^{-\eta}\right)y_4 - be^{-\eta}\left(y_3-1\right)\right\} \end{pmatrix}}{\left(n(y_2)^{n-1} + F\sqrt{1+be^{-\eta}}\, y_1\right)}$$

$$\frac{dy_4}{dx} = \theta'' = \frac{\begin{pmatrix} -\varepsilon_\infty de^{-\eta}(\alpha^*-1)y_4 - \frac{1}{2}y_1y_4 - E_C.\Pr \\ \left(\begin{array}{l} \frac{F}{4}\frac{be^{-\eta}}{\sqrt{1+be^{-\eta}}}(y_2)^2 \mp \\ \lambda^n\left[\begin{array}{l} \left(1+be^{-\eta}\right)y_4 - be^{-\eta}\left(y_3-1\right) + N_1\left\{\left(1+be^{-\eta}\right)y_6 - be^{-\eta}\left(y_5-1\right)\right\} \\ + N_2\left\{\left(1+be^{-\eta}\right)y_4 - be^{-\eta}\left(y_3-1\right)\right\} \end{array}\right] \\ \left(n(y_2)^{n-1} + F\sqrt{1+be^{-\eta}}\, y_1\right) \end{array} \right)^2 \end{pmatrix}}{\left(\varepsilon_\infty(1+de^{-\eta})(1-\alpha^*)+\alpha^*\right)}$$

$$\frac{dy_6}{dx} = \phi'' = \frac{-\varepsilon_\infty de^{-\eta}(\sigma^*-1)y_6 - \frac{1}{2}Ley_1y_6}{\left(\varepsilon_\infty(1+de^{-\eta})(1-\sigma^*)+\sigma^*\right)}$$

$$\frac{dy_8}{dx} = \chi'' = \frac{\begin{pmatrix} -\varepsilon_\infty de^{-\eta}(\gamma^*-1)y_8 - \frac{1}{2}Lby_1y_8 + Pe\left((A+y_7)\left(\frac{-\varepsilon_\infty de^{-\eta}(\sigma^*-1)y_6 - \frac{1}{2}Ley_1y_6}{\left(\varepsilon_\infty(1+de^{-\eta})(1-\sigma^*)+\sigma^*\right)} \right) + y_8y_6 \right) \end{pmatrix}}{\left(\varepsilon_\infty(1+de^{-\eta})(1-\gamma^*)+\gamma^*\right)}$$

(4.19)

Considering yp be the left edge and yq be the right edge, the boundary conditions become the following:

$$\begin{aligned} &yp(1) + 2Myp(4) = 0, yq(2) - 1 = 0, \\ &yp(3) = 0, yq(3) - 1 = 0, \\ &yp(5) = 0, yq(5) - 1 = 0, \\ &yp(7) = 0, yq(7) - 1 = 0, \end{aligned} \tag{4.20}$$

Comparing the numerical results for the special instances to some published findings looked into by (Sobha *et al.* (2010); Kameswaran *et al.* (2016)).

4.3 Numerical results and discussion

For clarity and a smooth representation of the results, diverse diagrams are presented for different parameter-dependent flow characteristics. In all the results obtained, some terms are fixed, whereas others vary to examine their impact on the gyrotactic microorganism non-Newtonian liquid in a saturated nonlinear porous medium. For variable fluid properties with a melting effect, different flow, heat, species, and microorganism distribution behaviours as well as the wall effects with variation in the microorganism volume fraction, are achieved.

4.3.1. Velocity distribution for various dependent parameters:

Fig 4.2(a) depicts the response of the non-Newtonian variable properties of the liquid to an increase in the nonlinear porosity term F at various microorganism fractional volumes. The flow rate decreased for various motile microorganisms as the nonlinearity of the porous medium increased. As the flow medium is saturated with pores, the viscoelastic fluid material permeability is opposed, which leads to an overall damping in the flow velocity, as observed in the plot. A remarkable shrinkage in the velocity profile is shown in **Fig. 4.2(b)** as the mixed convective term increases with diverse volume fractions of microorganisms. The gyrotactic microorganism conducted heat away from the non-Newtonian fluid, thereby increasing the liquid viscoelastic strength, which resulted in a gradual decline in the flow magnitude. Hence, gyrotactic microorganisms will help in encouraging the viscoelastic effect of a fluid for the optimal performance of industrial lubricants. **Figs. 4.2(c−d)** show the impact of the buoyancy ratio of the species and microorganism, respectively, on the flow velocity with various motile volume fractions. Retaining all other terms fixed, the buoyancy ratios N_1 and N_2 increase the flow field. The internal heat source terms are enhanced as the buoyancy ratio increases, which in turn breaks the fluid bonding force and causes the liquid to move rapidly near the fixed plate. However, the flow rate steadily decreases towards the unrestricted stream until it becomes uniform in saturated permeable media. **Fig. 4.2(e)** shows the consequence of the melting term M on the non-Newtonian fluid with different motile microorganism volume fractions. As shown

in the plot, an increase in the moulting term values encourages the thermal layer and heat source terms in the temperature equation. This increases the heat distribution in the system, which leads to a decrease in the viscoelastic material strength; however, the microorganism particle makeup is stimulated, thereby progressively increasing the flow velocity near the stationary plate towards the flow centre medium. Therefore, a general increase is observed in the flow field magnitude.

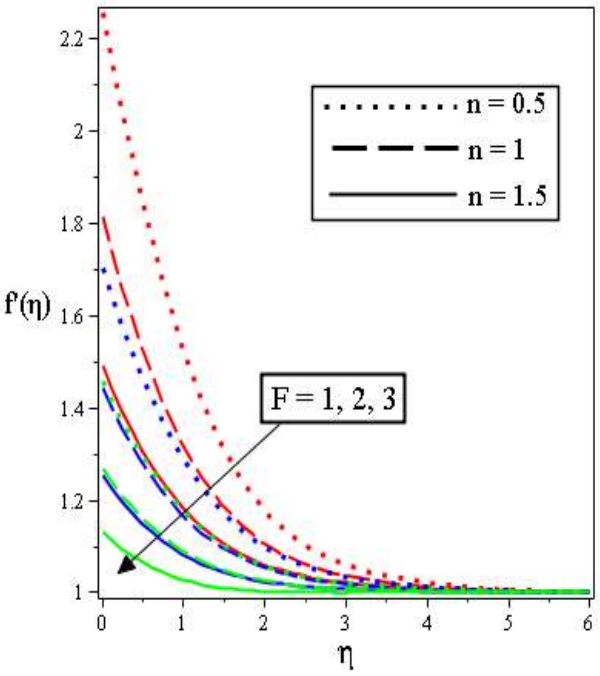

(a)

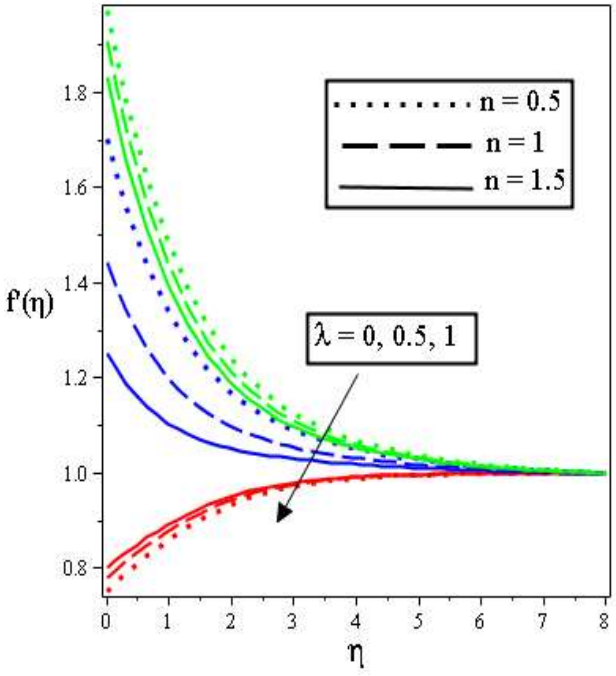

(b)

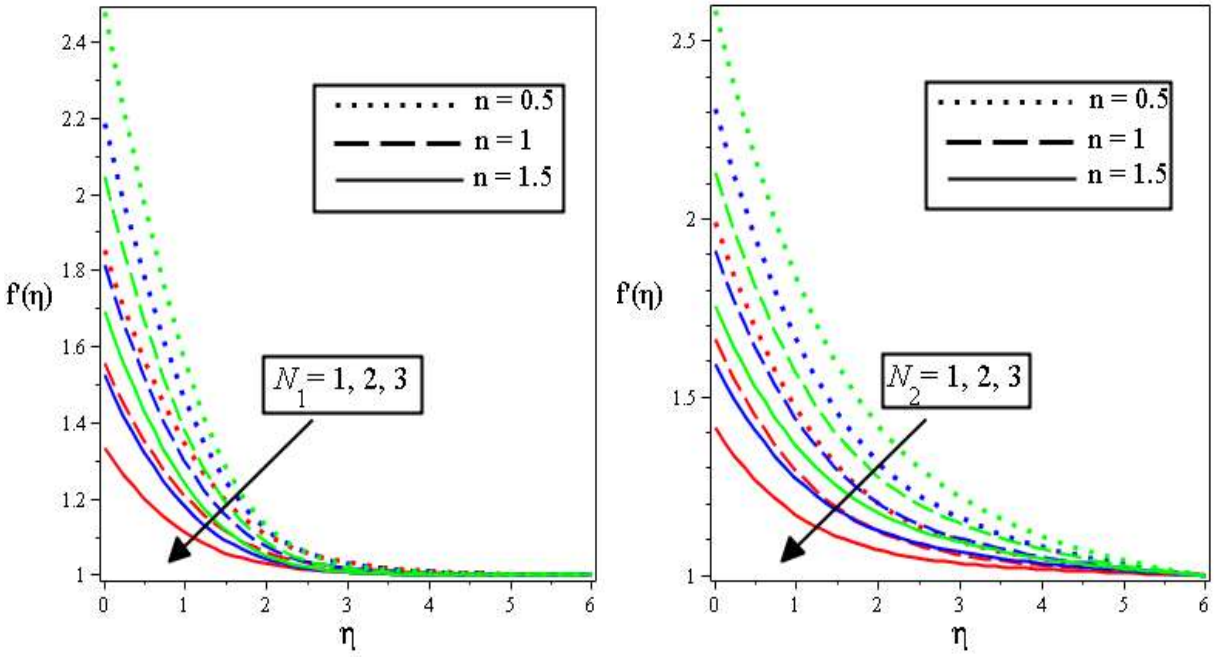

(c) **(d)**

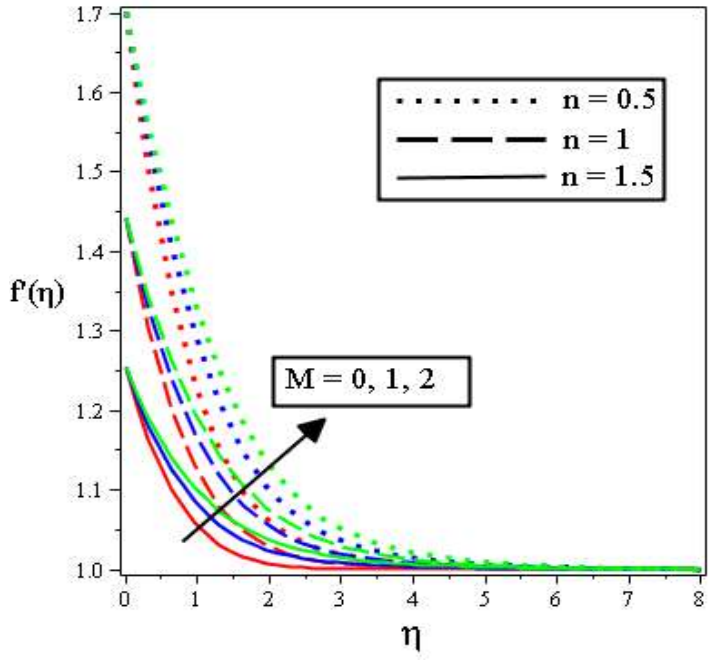

(e)

Fig. 4.2 Velocity profile with the a) variation of F b) variation of λ c) variation of N_1 d) variation of N_2 (e) variation of M in case of VP when
$\varepsilon_\infty = 0.1, b = 3, d = 1.5, Pe = 0.3, Lb = 0.3, Le = 5, \alpha^* = 2, \sigma^* = 4, \gamma^* = 2$

4.3.2. Temperature distribution and heat transfer rate parameters dependent:

The plots in the $(\eta,\theta(\eta))$ plane for the temperature distribution in a permeable medium with various microorganism volume fractions are presented in **Figs. 4.3(a)** and **4.3(b)**. With different parameter values for the mixed convection term λ and melting term M , an upsurge and shrinkage is observed in the heat profiles. In **Fig. 4.3(a)**, the heat transfer in the medium increases as the heat-conducting microorganisms up-swim and spin in the vertical plate. Thus, the heat field in the confined system proliferates as the fluid–particle collision increases. By contrast, in **Fig. 4.3(b)**, an increase in the melting term discourages the up-swimming of the heat-conducting microorganism because it melts increasingly in the non-Newtonian fluid flow system, which then leads to a weakening in the temperature magnitude in the medium. In addition, the temperature field decreases because of the thinner thermal layer, which enables heat to diffuse away from the vertical system. Hence, a complete decrease in the heat profile is obtained.

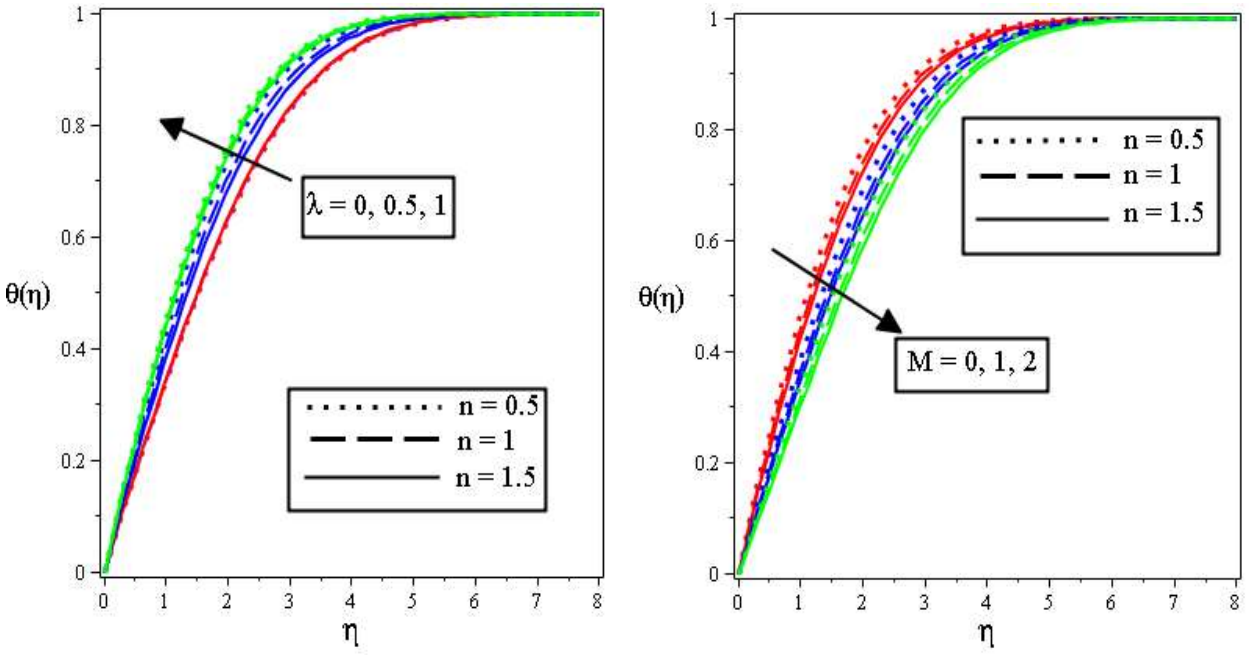

(a) **(b)**

Fig. 4.3 Temperature profile with the (a) variation of λ (b) variation of M in case of VP when $\varepsilon_\infty = 0.1, b = 3, d = 1.5, Pe = 0.3, Lb = 0.3, Le = 5, \alpha^* = 2, \sigma^* = 4, \gamma^* = 2, N_1 = 0.6, N_2 = 0.2$

Different plots demonstrating the heat-transfer gradient at the vertical plate surface are shown in **Figs. 4.4(a–d)**. As shown in **Fig. 4.4(a),** for the plot of Nusselt number Nu against the nonlinearity porous term F with diverse values of n, the thermal layer viscosity thinning is enhanced. Consequently, the plate surface heat transfer is propelled, causing an upsurge in the wall energy gradient. **Figs. 4.4(b), 4.4(c), and 4.4(d)** depict the Nusselt effect as the mixed convection λ, melting parameter M , and Prandtl number Pr increases with increasing values of the volume of microorganism fraction n in VP when the other terms remain unchanged**.** A decrease in the rate of wall energy transport was observed in all cases as the thermal viscosity layer stickiness was enriched. This increased the amount of heat within the confined infinite plate, which encouraged molecular diffusion in the system.

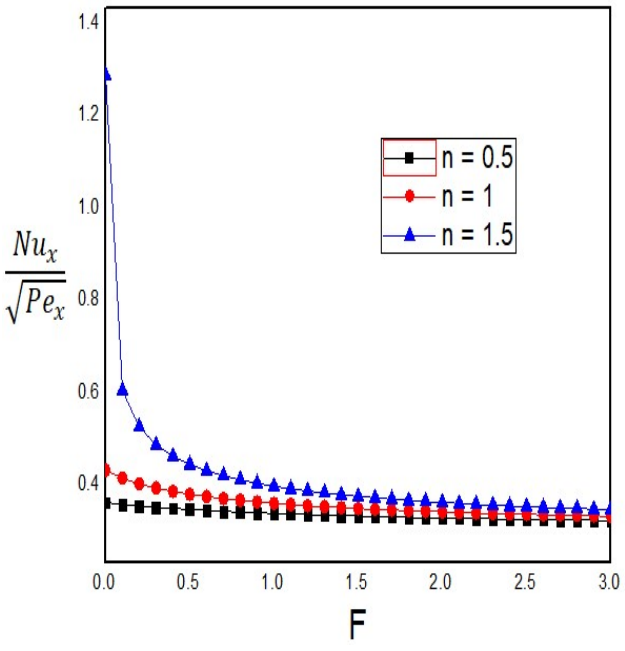

(a)

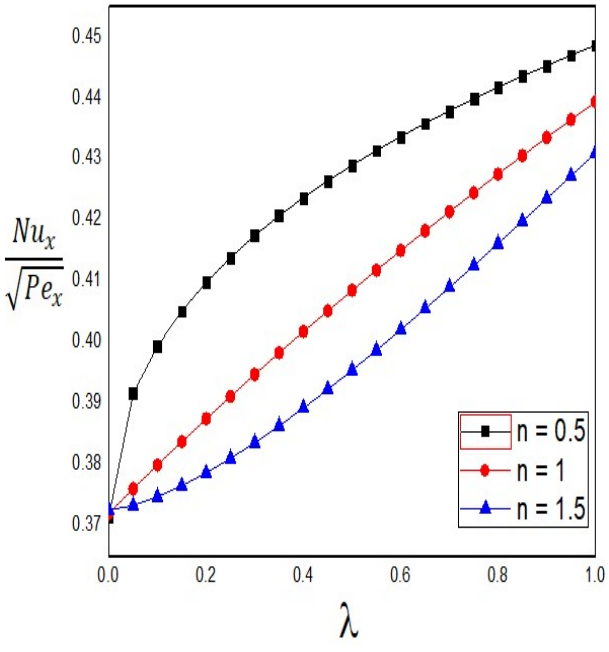

(b)

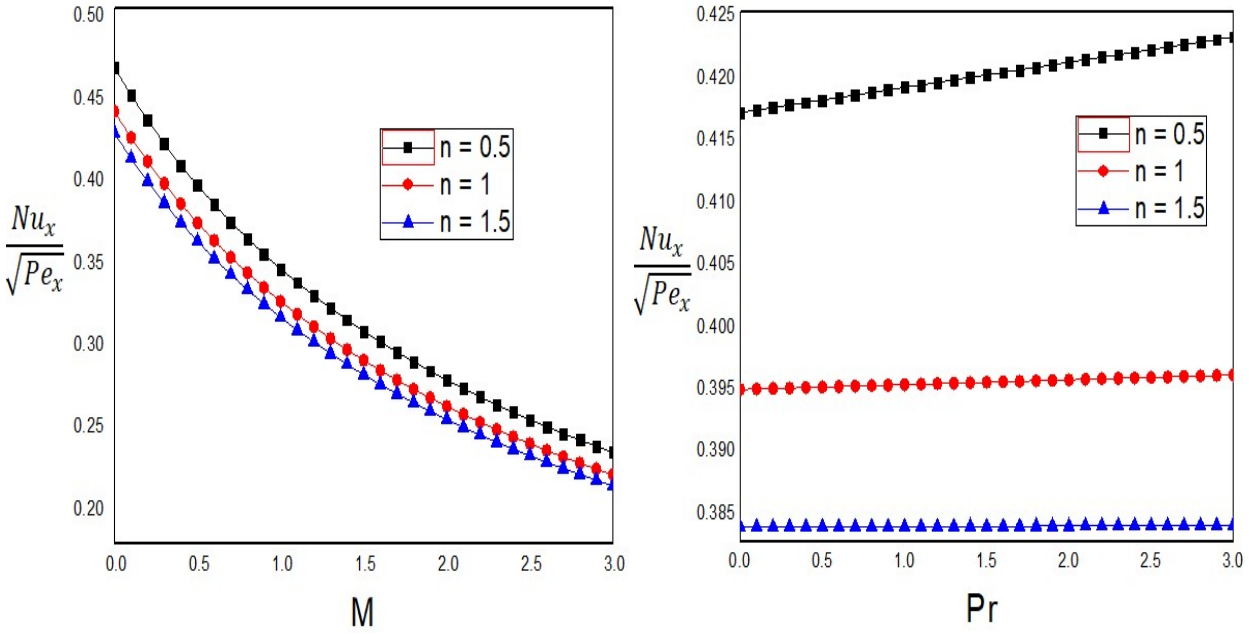

(c) **(d)**

Fig. 4.4 Nusselt number with the (a) variation of F (b) variation of λ (c) variation of M (d) variation of Pr in case of VP when

$\varepsilon_\infty = 0.1, b = 0.3, d = 1.5, Pe = 0.3, Lb = 0.3, Le = 0.5, N_1 = 0.6, N_2 = 0.2, \alpha = 4, \gamma^* = 2$

4.3.3. Concentration profile and mass transfer rate for dependent parameters:

Figs. 4.5(a) and 4.5(b) portray the reaction of the concentration distribution in a saturated permeable medium to arise in the melting term M and Lewis number Le with variable fluid properties. As shown in **Fig. 4.5(a)**, the non-Newtonian fluid species transfer decreases regularly towards the centre of the vertical plate medium from the stationary plate. This is because the concentration layer viscosity is reduced, allowing the microorganism particles to move slowly in a nonlinear porous medium. The flow species became constant away from the centre medium as it tended towards the free concentration direction. In addition, the reverse is the case for rising Lewis number that turn to increase the magnitude of mass transfer over the entire vertical plate medium. The heat generation terms are boosted as the Lewis number increases, which in turn increases reactive molecular diffusion in the system. This results in a high rate of species transfer, which causes an overall increase in the concentration field.

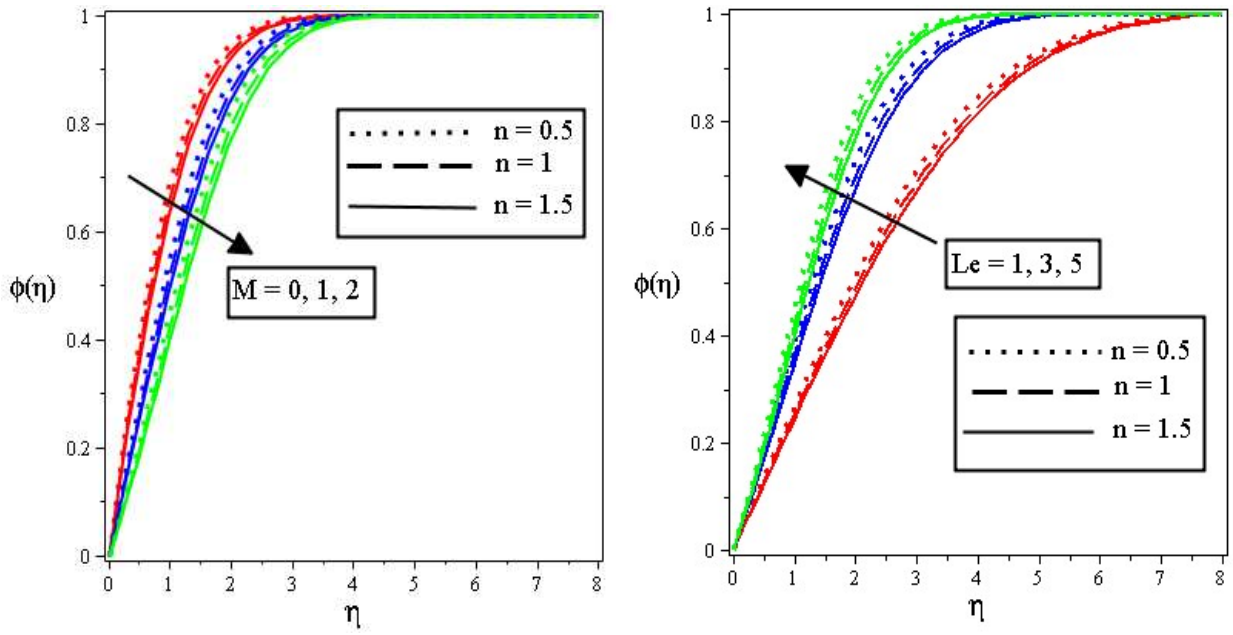

(a) **(b)**

Fig. 4.5 Concentration profile with the (a) variation of *M* (b) variation of *Le* in case of VP when

$\varepsilon_\infty = 0.1, b = 0.3, d = 1.5, Pe = 0.3, Lb = 0.3, \lambda = 0.5, N_1 = 0.6, N_2 = 0.2, \alpha^* = 4, \sigma^* = 4, \gamma^* = 2$

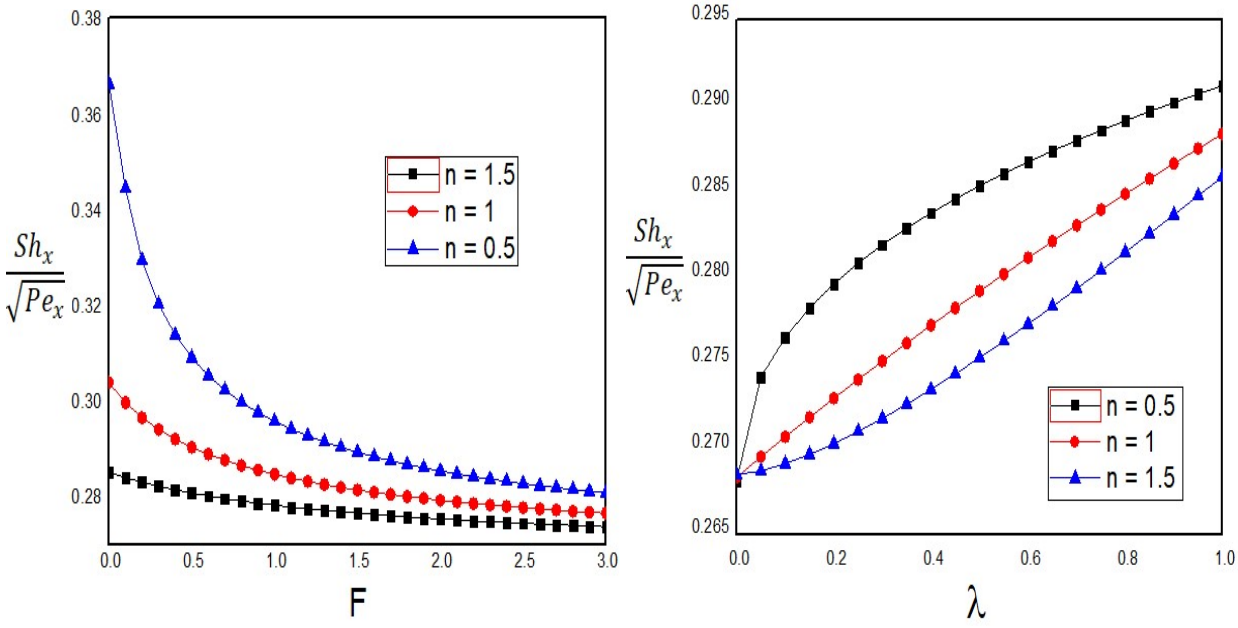

(a) **(b)**

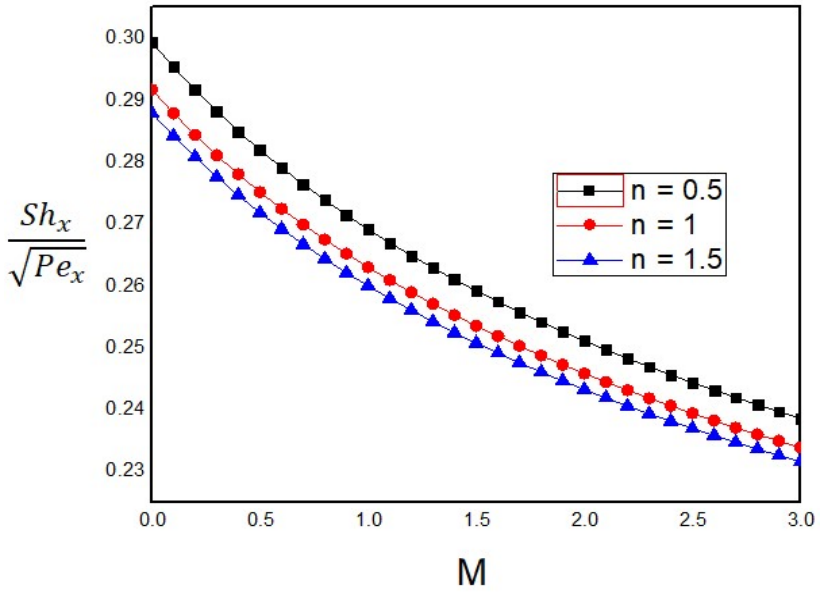

(c)

Fig. 4.6 Sherwood number with the (a) variation of *F* (b) variation of λ (c) variation of *M* in case of VP when

$\varepsilon_\infty = 0.1, b = 0.3, d = 1.5, Pe = 0.3, Lb = 0.3, \lambda = 0.5, N_1 = 0.6, N_2 = 0.2, \alpha^* = 4, \sigma^* = 4, \gamma^* = 2$

The Sherwood effect with distinct values of the volume fraction (n) for some fluid thermo-physical terms is shown in **Figs. 4.6(a–c)**. An increase in the porosity term is observed to have increased the species gradient transfer because the pore size is increased as the nonlinearity porous term is increased. An upsurge in the term F increases the resistance to microorganism species diffusion, raising the Sherwood wall effect, as shown in **Fig. 4.6(a).** Nevertheless, increasing the mixed convection and melting terms discourages the Sherwood impact on the transfer of microorganism concentration at the plate surface, as shown in **Figs. 4.6(a−b)**. Hence, the concentration gradient profiles decreased as the number of terms increased.

4.3.4. Microorganism profile and motile microorganism transfer rate:

The effects of some pertinent dependent terms on microorganisms are depicted in **Figs. 4.7(a) and 4.7(b)**. The bioconvection Lewis number Lb and bioconvection Peclet number Pe with VP enhanced microorganism distribution in non-Darcy media. As observed, the gyrotactic microorganism nonlinear permeable medium increases as the bioconvection Lewis number and

bioconvection Peclet number increase because of the stimulation of heat owing to molecular diffusion of species and high-rate collision of the non-Newtonian fluid particles. A significant increase was noticed, which diminished steadily until it became uniform far from the fixed wall. **Figs. 4.8(a–c)** show the motile density number effect for increasing values of the non-Darcy term F, mixed convection term λ, and melting term M. An increase in the nonlinear porous term increases the influence of motile density on the permeability of the medium and plate surfaces, as shown in **Fig. 4.8(a).** Furthermore, **Figs. 4.8(b) and 4.8(c)** show the decreasing effect of motile density as the mixed convection and melting terms increase. This is because of the thinner gyrotactic microorganism boundary layer, which reduces the up-swimming strength of the microorganism particle composition.

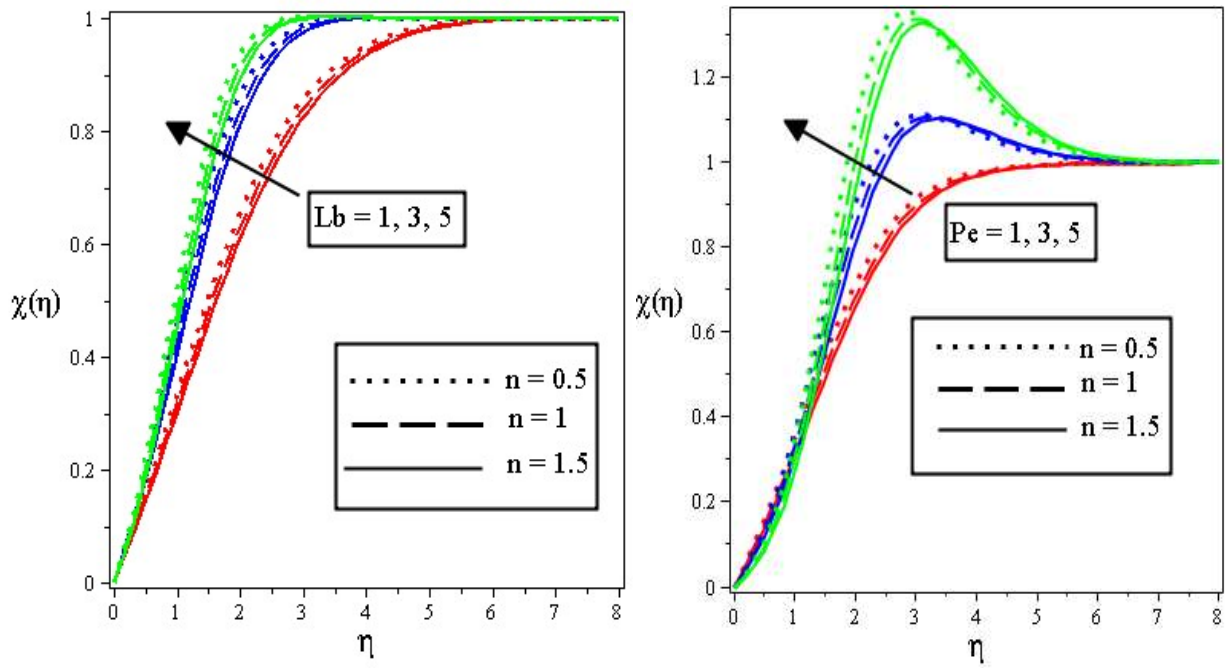

Fig. 4.7 Microorganism profile with the (a) variation of *Lb* (b) variation of *Pe* in case of VP when $\varepsilon_\infty = 0.1, b = 0.3, d = 1.5, M = 2, \lambda = 0.5, N_1 = 0.6, N_2 = 0.2, \alpha^* = 2, \sigma^* = 4, \gamma^* = 2$

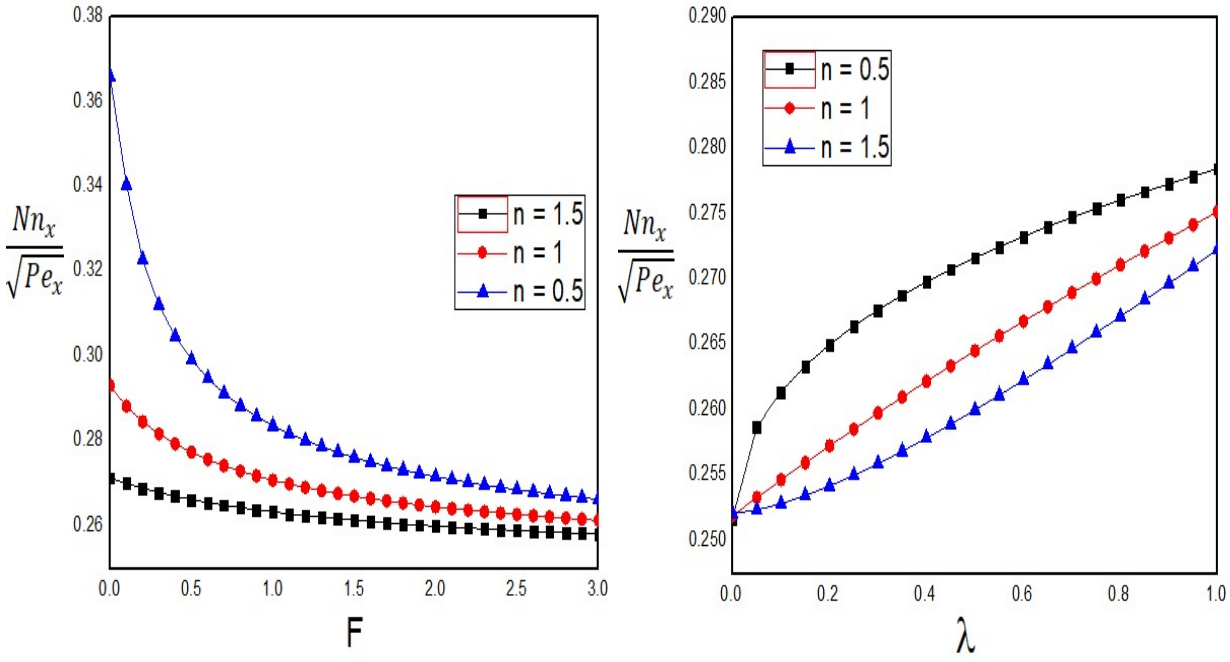

(a) **(b)**

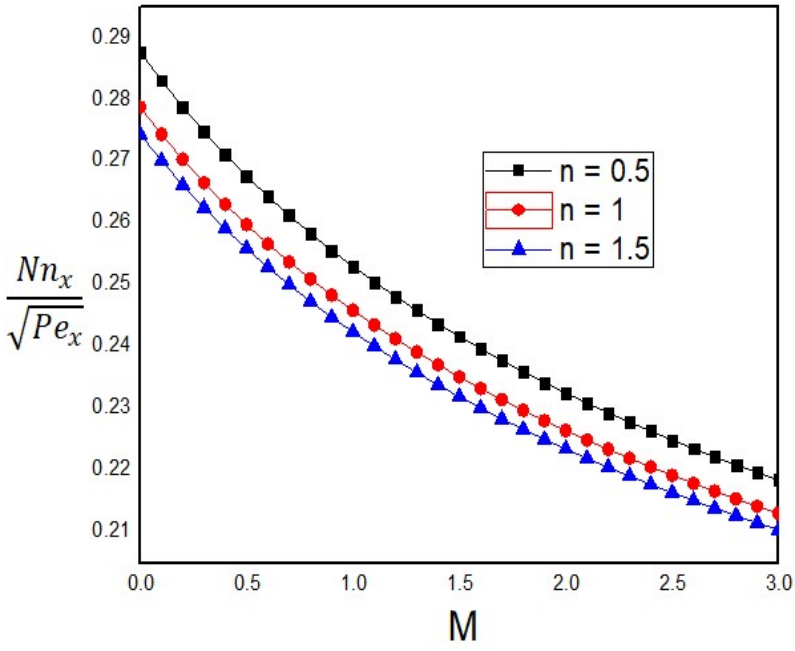

(c)

Fig. 4.8 Microorganism density number with the (a) variation of *F* (b) variation of λ (c) variation of *M* in case of VP when

$\varepsilon_\infty = 0.1, \Pr = 0.3, b = 0.3, d = 1.5, Pe = 0.3, Lb = 0.3, Le = 0.5, N_1 = 0.6, N_2 = 0.2, \alpha^* = 2, \sigma^* = 4, \gamma^* = 2$

The results shown above are for varying permeability. For dilatants, Newtonian, and pseudo-plastic fluids, **Table 4.1** illustrates the effects of varying permeability $(b = 0.5, d = 2)$ in comparison to uniform permeability $(b = 0, d = 0)$ on the Nusselt, Sherwood, and microbe density profiles. The rate of heat, mass, and microbial transport is increased for both Newtonian and non-Newtonian fluids when varying permeability is taken into account.

Table 4.1 Effect of pseudo-plastic $(n < 1)$, Newtonian $(n = 1)$, and dilatant $(n > 1)$ fluid on Nusselt, Sherwood and density of motile microorganism for UP and VP case

$\lambda = 0.5, Le = 0.5, Lb = 0.3, Pe = 0.3, A = 0.5, kp = 10, N_1 = 0.6, N_2 = 0.4, \alpha^* = 2, \sigma^* = 4, \gamma^* = 2,$
$M = 1, Ec = 0.5, \Pr = 0.3, F = 2$

n	$\theta'(0)$		$\varphi'(0)$		$\chi'(0)$	
	UP	VP	UP	VP	UP	VP
0.5	0.36435	0.38759	0.22847	0.25207	0.23062	0.24648
1	0.34497	0.36079	0.22228	0.24517	0.22295	0.23821
1.5	0.33264	0.34726	0.21833	0.24073	0.21806	0.23287

4.3.5. Comparison of Results:

Comparisons of $f'(0)$ and $\theta'(0)$ with published results by Shobha *et al.* (2010) and Kameswaran *et al.* (2016) for regular fluid n = 1 and, $F = 0, N_1 = 0, N_2 = 0, b = 0, d = 0,$ $\varepsilon_\infty = 1, \alpha^* = 1, \sigma^* = 1, \gamma^* = 1, Le = 0, Lb = 0, Pe = 0$ are tabulated in **Tables 4.2** and **4.3,** where $f'(0)$ and $\theta'(0)$ both increase with some specific increased values of λ. The computed results agreed with previously obtained numerical values. This indicates that the present study is open to further research.

Table 4.2 Effect of mixed convection parameter λ on $f'(0)$				
M	λ	$f'(0)$ present	$f'(0)$ Kameswaran *et al.* (2016)	$f'(0)$ Shoba *et al*. (2010)
	0.0	1.000	1.000	1.000
	1.4	2.400	2.400	2.400
2	3.0	4.000	4.000	4.000
	8.0	9.000	9.000	9.000
	10	11.00	11.00	11.00
	20	21.00	21.00	21.00

Table 4.3 Effect of mixed convection parameter λ on $\theta'(0)$				
M	λ	$\theta'(0)$ present	$\theta'(0)$ Kameswaran *et al.* (2016)	$\theta'(0)$ Shoba *et al*. (2010)
	0.0	0.2706	0.27062	0.27062
	1.4	0.3800	0.3800	0.3801
2	3.0	0.4744	0.4745	0.4745
	8.0	0.69016	0.6902	0.69019
	10	0.75938	0.7594	0.75939
	20	1.0382	1.0383	1.0384

4.4 Summary

The steady mixed convective flow of a non-Newtonian power-law fluid containing microorganisms over a vertical plate embedded in a non-Darcy porous medium with melting effects is modelled and mathematically analysed. There was a thorough discussion of the effects of different flow-influencing parameters. To affirm the current outcomes, appraisal is formed using earlier outcomes and it is clinched that both results are favourable to each other. The key reviews are summarised as follows:

- Non-Newtonian velocity profiles decayed for rising values of non-Darcy and mixed convection parameters. However, the velocity contours changed their behaviour for the melting parameter M, temperature, and concentration buoyancy numbers N_1, N_2 at the free-stream boundary.

- Non-Newtonian fluid temperature increases for the mixed convection parameter λ, whereas this nature is opposite to that of the melting parameter M.
- For high-melting-effect concentration profiles, it decelerates in nature, although the reverse trend is observed in the Lewis number case.
- Bioconvection Lewis number Lb and Peclet number Pe has an increasing impact on the microorganism profiles.
- Non-Darcy melting parameters show a pronounced impact on the Sherwood number, Nusselt number, and motile microorganism density profiles, although they decrease mostly for dilatant fluids.
- Mixed convection parameters show a pronounced impact on the Sherwood number, Nusselt number, and motile microorganism density profiles, although they decrease mostly for pseudo-plastic fluids.

Chapter 5

Effects of non-Darcy mixed convection over a horizontal cone with different convective boundary conditions incorporating gyrotactic microorganisms on dispersion

This chapter examines the impact of the dispersion on mixed convection flow along a horizontal cone in a non-Darcy porous material. A non-Darcy model that incorporates temperature, solutal, and microbial dispersion effects is considered for mathematical formulation, which has many biological and environmental applications, and different convective boundary conditions are also taken into consideration. To solve the transformed ordinary differential equations, the MATLAB bvp4c technique is used. This chapter's key discovery is that variations in Biot numbers, in the absence of dispersion, favour heat, mass, and motile microbe transmission most in the range of mixed convection parameters to pure forced convection, and thermal, solutal, and microorganism dispersion coefficients a_1, b_1, c_1, and higher modified Peclet number values cause increased dispersion effects, which lower flow transfer rates mostly in the forced convection regime. Therefore, it is feasible to adjust the rates at which heat, mass, and microorganisms are transmitted in many useful systems, such as a truncated conical-shaped microbial fuel cell, by carefully choosing the effects of dispersion. In a few instances, the research provided a decisive conclusion by comparing the findings of the current study with those of previously published studies.

5.1 Mathematical formulation

We consider the steady flow of the mixed convection boundary layer past a semi-vertically angled horizontal cone immersed in a porous fluid-saturated medium with ambient temperature T_∞ and concentration C_∞, n_∞. The coordinate x is measured from the tip of the cone to the end of the ray, and the longitudinal coordinate y is measured normal to it, as shown in **Fig.**

5.1. Convection from a warmed flowing fluid is expected to heat the surface of the cone with gyrotactic microorganisms at constant temperature T_f and constant concentrations C_f, n_f with variable heat, mass, and motile microorganism coefficients $h_f(x), h_m(x)$, and $h_n(x)$, respectively. The diffusion-thermo and thermo-diffusion effects are also believed to be minimal when the diffusing species is present in small amounts.

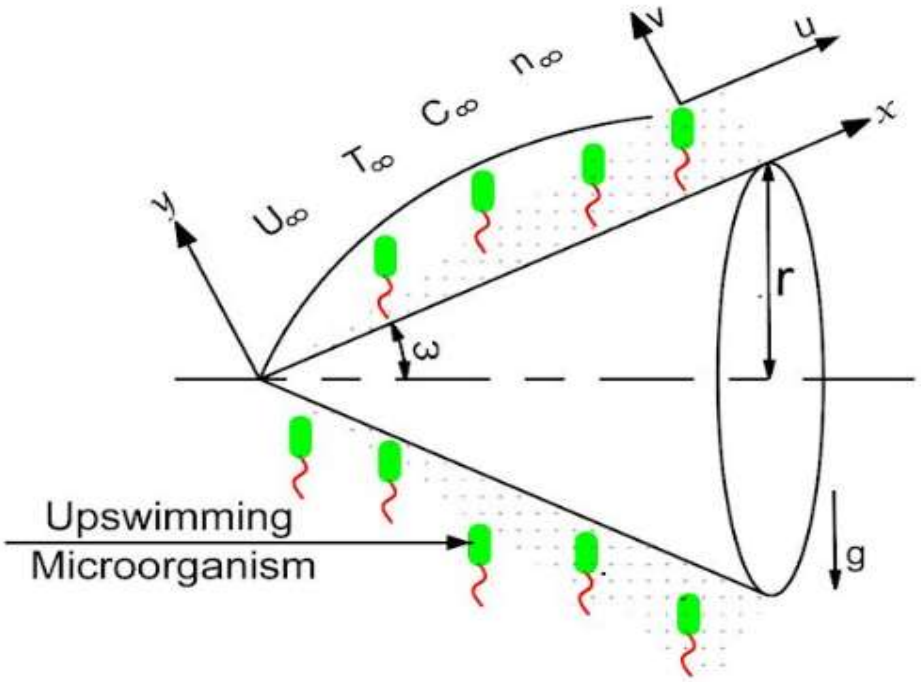

Fig. 5.1 Coordinates and the physical model

Making use of the Boussinesq approximation and non-Darcy model, the conservation equations such as continuity, momentum equations (Kumari (2010)), thermal energy, mass conservation equations (Kairi (2011)) and the equation of microorganism (Khan *et al.* (2019)) modification to the convective boundary condition (Latiff *et al.* (2017)) are considered as follows:

Continuity equation

$$\frac{\partial(ru)}{\partial x}+\frac{\partial(rv)}{\partial r}=0 \tag{5.1}$$

Momentum equation

$$\frac{\partial u}{\partial y}+\frac{\partial}{\partial y}\left(\rho\frac{bK^{*}}{\mu}u^{2}\right)=-\frac{\partial}{\partial x}\left[\frac{\rho gK\cos\omega}{\mu}\left\{\beta_{T}(T-T_{\infty})+\beta_{C}(C-C_{\infty})+\beta_{n}(n-n_{\infty})\right\}\right] \tag{5.2}$$

Thermal energy equation

$$u\frac{\partial T}{\partial x}+v\frac{\partial T}{\partial y}=\frac{\partial}{\partial y}\left(\alpha_{e}\frac{\partial T}{\partial y}\right) \tag{5.3}$$

Mass conservation equation

$$u\frac{\partial C}{\partial x}+v\frac{\partial C}{\partial y}=\frac{\partial}{\partial y}\left(D_{c}\frac{\partial C}{\partial y}\right) \tag{5.4}$$

Conservation equation for microorganism

$$u\frac{\partial n}{\partial x}+v\frac{\partial n}{\partial y}+\frac{bW_{c}}{C_{w}-C_{\infty}}\left(\frac{\partial}{\partial y}\left(n\frac{\partial C}{\partial y}\right)\right)=\frac{\partial}{\partial y}\left(D_{e}\frac{\partial n}{\partial y}\right) \tag{5.5}$$

The boundary conditions are of the following form:

$$v=0\ ,\ -k\frac{\partial T}{\partial y}=h_{f}(x)(T_{f}-T)\ ,\ -D_{m}\frac{\partial C}{\partial y}=h_{m}(x)(C_{f}-C)\ ,$$

$$-D_{n}\frac{\partial n}{\partial y}=h_{n}(x)(n_{f}-n)\ \text{at}\ y=0 \tag{5.6}$$

$$u\to u_{\infty},\ T\to T_{\infty},C\to C_{\infty},n\to n_{\infty}\ \text{at}\ y\to\infty \tag{5.7}$$

where T, C, and n are the temperature, concentration, and volume fraction of motile microorganisms, respectively.

Furthermore, α_{e},D_{c},D_{e} represents the effective thermal, solutal, and microorganism diffusivities, which can be written according to Kairi (2011), as follows:

$$\alpha_e = \alpha + a_1 du$$
$$D_c = D_m + b_1 du$$
$$D_e = D_n + c_1 du$$

Where α, D_m, D_n is the constant thermal, molecular, and microorganism diffusivities, and a_1, b_1, c_1 is the coefficient of the solute, thermal, and microbial dispersions. These lie between $\frac{1}{7}$ and $\frac{1}{3}$.

We introduce the dimensionless quantities, as follows:

$$\eta = \frac{y}{x} Pe_x^{\frac{1}{2}} \left(1 + \frac{Ra_x^{\frac{1}{3}}}{Pe_x^{\frac{1}{2}}} \right), \psi = \alpha r \; Pe_x^{\frac{1}{2}} \left(1 + \frac{Ra_x^{\frac{1}{3}}}{Pe_x^{\frac{1}{2}}} \right) f(\eta), \tag{5.8}$$
$$\theta(\eta) = \frac{T - T_\infty}{T_f - T_\infty}, \phi(\eta) = \frac{C - C_\infty}{C_f - C_\infty}, \chi(\eta) = \frac{n - n_\infty}{n_f - n_\infty}$$

$$h_f(x) = x^{-\frac{1}{2}} h_f, h_m(x) = x^{-\frac{1}{2}} h_m, h_n(x) = x^{-\frac{1}{2}} h_n \tag{5.9}$$

where ψ denotes the stream function, and it is customarily defined as follows:

$$u = \frac{1}{r} \frac{\partial \psi}{\partial y}, v = -\frac{1}{r} \frac{\partial \psi}{\partial x}$$

Using the transformations (5.8)-(5.9) in the equations (5.2)-(5.7), we have got the following transformed ordinary differential equations and boundary conditions:

$$f''' + 2\lambda^2 \,\mathrm{Re}\, f f'' + (1-\lambda)^3 \left[-\frac{\eta\theta'}{2} - \frac{\eta\theta'}{6}(1-\lambda) + N_1 \left(-\frac{\eta\phi'}{2} - \frac{\eta\phi'}{6}(1-\lambda) \right) + N_2 \left(-\frac{\eta\chi'}{2} - \frac{\eta\chi'}{6}(1-\lambda) \right) \right] = 0 \tag{5.10}$$

$$\theta'' + \frac{1}{2} f\theta' - \frac{f\theta'}{6}(1-\lambda) + \lambda^2 a_1 Pe_d \left(f'\theta'' + f''\theta' \right) = 0 \tag{5.11}$$

$$\phi'' + \frac{1}{2} Lef\phi' - Le\frac{f\phi'}{6}(1-\lambda) + Le\lambda^2 b_1 Pe_d\left(f'\phi'' + f''\phi'\right) = 0 \tag{5.12}$$

$$\chi'' + \frac{1}{2} Lbf\chi' - Lb\frac{f\chi'}{6}(1-\lambda) + Lb\lambda^2 c_1 Pe_d\left(f'\chi'' + f''\chi'\right) - Pe\left[\phi'\chi' + (\chi+\omega)\phi''\right] = 0 \tag{5.13}$$

Boundary condition

$$f(0) = 0, \theta'(0) = -\lambda B_i\left(1-\theta(0)\right), \phi'(0) = -\lambda B_{i,m}\left(1-\phi(0)\right), \chi'(0) = -\lambda B_{i,n}\left(1-\chi(0)\right) \quad \text{at } \eta = 0$$

$$f'(\infty) = \lambda^2, \theta(\infty) == 0, \phi(\infty) = 0, \chi(\infty) = 0 \qquad \text{at } \eta \to \infty \tag{5.14}$$

where local Rayleigh number $Ra_x = \frac{kg\beta_T(T_f - T_\infty)\cos\omega.x}{\nu\alpha}$, local Peclet number $Pe_x = \frac{u_\infty x}{\alpha}$, mixed convective term $\lambda = \left(1 + \frac{Ra_x^{\frac{1}{3}}}{Pe_x^{\frac{1}{2}}}\right)^{-1}$, buoyancy ratio parameter $N_1 = \frac{\beta_C(C_f - C_\infty)}{\beta_T(T_f - T_\infty)}$, buoyancy ratio parameter $N_2 = \frac{\beta_n(n_f - n_\infty)}{\beta_T(T_f - T_\infty)}$, Lewis number $Le = \frac{\alpha}{D_m}$, bioconvection Lewis number $Lb = \frac{\alpha}{D_n}$, bioconvection Peclet number $Pe = \frac{bW_c}{D_n}$, microorganism concentration difference parameter $A = \frac{n_\infty}{n_w - n_\infty}$, mixed convection parameter $\lambda = \left(1 + \frac{Ra_x^{\frac{1}{3}}}{Pe_x^{\frac{1}{2}}}\right)^{-1}$, Biot number $B_i = -\frac{h_f \alpha^{\frac{1}{2}}}{k u_\infty^{\frac{1}{2}}}$, Biot number of mass transfer $B_{i,m} = \frac{h_m \alpha^{\frac{1}{2}}}{D_m u_\infty^{\frac{1}{2}}}$, Biot number of microorganism transfer $B_{i,n} = \frac{h_n \alpha^{\frac{1}{2}}}{D_n u_\infty^{\frac{1}{2}}}$, inertia coefficient dependent Reynolds number $\mathrm{Re} = \frac{K^* b}{\nu} u_\infty$.

Local Nusselt number Nu_x, Sherwood number Sh_x, and local density number of motile microorganisms Nn_x are expressed as follows:

$$Nu_x = \frac{xq_w}{k\left(T_f - T_\infty\right)}, Sh_x = \frac{xq_m}{D\left(C_f - C_\infty\right)}, Nn_x = \frac{xq_n}{D_n\left(n_f - n_\infty\right)} \tag{5.15}$$

where the wall heat, wall mass, and wall motile microorganism fluxes are specified as q_w , q_m, and q_n, respectively, and they are defined as follows:

$$q_w = -k\left(\frac{\partial T}{\partial y}\right)_{y=0}, \; q_m = -D_B\left(\frac{\partial C}{\partial y}\right)_{y=0}, \; q_n = -D_n\left(\frac{\partial n}{\partial y}\right)_{y=0} \tag{5.16}$$

The dimensionless forms of the local Nusselt number, local Sherwood number, and local motile microorganisms are as follows:

$$\lambda Pe_x^{\frac{-1}{2}} Nu_x = -\theta'(0), \lambda Pe_x^{\frac{-1}{2}} Sh_x = -\phi'(0), \lambda Pe_x^{\frac{-1}{2}} Nn_x = -\chi'(0) \tag{5.17}$$

5.2 Solution methodology

Simulation of the transformed Equations (5.1)−(5.13) within the confines of the boundary condition (5.14) was found for a range of values of the flow regulating parameters using the MATLAB bvp4c numerical technique. The governing equations must be transformed into first-order differential equations in the context of the aforementioned bvp4c function. First Equations (5.10) – (5.13) can be rearranged as follows:

$$f'' = \frac{-(1-\lambda)^3\left(\frac{\lambda}{6} - \frac{2}{3}\right)\eta\left[\theta' + N_1\phi' + N_2\chi'\right]}{\left(1 + 2\,\mathrm{Re}\, f'\right)}$$

$$\theta'' = -\left(\frac{\lambda}{6} + \frac{1}{3}\right) f\theta' - \lambda^2 a Pe_d\left(f'\theta'' + f''\theta'\right)$$

$$\phi'' = -\left(\frac{\lambda}{6} + \frac{1}{3}\right) Lef\phi' - Le\lambda^2 b Pe_d\left(f'\phi'' + f''\phi'\right)$$

$$\chi'' = -\left(\frac{\lambda}{6} + \frac{1}{3}\right) Lbf\chi' - Lb\lambda^2 c Pe_d\left(f'\chi'' + f''\chi'\right) + Pe\left[\phi'\chi' + (\chi + A)\phi''\right]$$

This equation must be transformed into a first-order differential equation: For this let $\eta = x$ and

$$y_1 = f, y_2 = f'$$

$$y_3 = \theta, y_4 = \theta', y_5 = \phi,$$

$$y_6 = \phi', y_7 = \chi, y_8 = \chi$$

The first order differential equations are as follows:

$$\frac{dy_1}{dx} = f' = y_2$$

$$\frac{dy_2}{dx} = f'' = \frac{-(1-\lambda)^3 \eta\left(\frac{\lambda}{6}-\frac{2}{3}\right)\left(y_4 + N_1 y_6 + N_2 y_8\right)}{\left(1 + 2\lambda^2 \operatorname{Re} y_2\right)}$$

$$\frac{dy_4}{dx} = \theta'' = \frac{-\left(\frac{\lambda}{6}+\frac{1}{3}\right) y_1 y_4 - \lambda^2 a Pe_d y_4 \left(- \frac{-(1-\lambda)^3 \eta\left(\frac{\lambda}{6}-\frac{2}{3}\right)\left(y_4 + N_1 y_6 + N_2 y_8\right)}{\left(1 + \lambda^2 \operatorname{Re} y_2\right)} \right)}{\left(1 + \lambda^2 a Pe_d y_2\right)}$$

$$\frac{dy_6}{dx} = \phi'' = \frac{-Le\left(\frac{\lambda}{6}+\frac{1}{3}\right) y_1 y_6 - Le\lambda^2 b Pe_d y_6 \left(- \frac{-(1-\lambda)^3 \eta\left(\frac{\lambda}{6}-\frac{2}{3}\right)\left(y_4 + N_1 y_6 + N_2 y_8\right)}{(1 + \lambda^2 \operatorname{Re} y_2)} \right)}{(1 + Le\lambda^2 b Pe_d y_2)}$$

$$\frac{dy_8}{dx} = \chi'' = \frac{\left(\begin{array}{l} y_6 y_8 + \\ \left(y_7 + A\right) \left(\dfrac{-Le\left(\frac{\lambda}{6}+\frac{1}{3}\right) y_1 y_6 - Le\lambda^2 b Pe_d y_6 \left(- \dfrac{-(1-\lambda)^3 \eta\left(\frac{\lambda}{6}-\frac{2}{3}\right)\left(y_4 + N_1 y_6 + N_2 y_8\right)}{\left(1 + \lambda^2 \operatorname{Re} y_2\right)} \right)}{\left(1 + Le\lambda^2 b Pe_d y_2\right)} \right) \end{array} \right)}{1 + Lb\lambda^2 c Pe_d y_2}$$

$$- Lb\left(\frac{\lambda}{6}+\frac{1}{3}\right) y_1 y_8 - Lb\lambda^2 c Pe_d y_8 \left(- \frac{(1-\lambda)^3 \eta(\frac{\lambda}{6}-\frac{2}{3})(y_4 + N_1 y_6 + N_2 y_8)}{\left(1 + \lambda^2 \operatorname{Re} y_2\right)} \right) + Pe$$

The boundary conditions are changed such that yp represents the left boundary and yq represents the right boundary.

$$yp(1) = 0, yq(2) - \lambda^2 = 0$$
$$yp(4) + \lambda B_i(1 - yp(3)) = 0, yq(3) = 0$$
$$yp(6) + \lambda B_{i,m}(1 - yp(5)) = 0, yq(5) = 0$$
$$yp(8) + \lambda B_{i,n}(1 - yp(7)) = 0, yq(7) = 0$$

The MATLAB algorithm's accuracy and dependability have been proven in a number of recent researches papers. **Tables. (5.1−5.3)** show a clear comparison of the current findings with those of Reddy *et al*. (2018) for a few special circumstances, with a strong correlation.

Table 5.1 Comparison of $f'(0)$ for

$Le = 0, \lambda = 1, \mathrm{Re} = 0, Pe_d = 0, Lb = 0, Pe = 0, B_i \to \infty, B_{i,m} \to \infty$

$f'(0)$	
Present Result	Reddy *et al*. (2018)
1.0000	1.0000

Table 5.2 Comparison of $-\theta'(0)$ for $\lambda = 1, \mathrm{Re} = 0, Pe_d = 0, Lb = 0, Pe = 0, B_i \to \infty, B_{i,m} \to \infty$

$-\theta'(0)$			
$Le = 1$		$Le = 10$	
Present Result	Reddy *et al*. (2018)	Present Result	Reddy *et al*. (2018)
0.5644	0.5642	0.5644	0.5642

Table 5.3 Comparison of $-\phi'(0)$ for $\lambda = 1, \mathrm{Re} = 0, Pe_d = 0, Lb = 0, Pe = 0, B_i \to \infty, B_{i,m} \to \infty$			
$-\phi'(0)$			
$Le = 1$		$Le = 10$	
Present Result	Reddy *et al*. (2018)	Present Result	Reddy *et al*. (2018)
0.5644	0.5642	1.7841	1.7841

5.3 Numerical results and discussion

In **Fig. 5.2,** the effect of mixed convection and buoyancy parameters on the velocity profile is demonstrated. As shown in **Fig. 5.2(a),** with rising λ values, the velocity profile increases, indicating that velocity profile gradually increases for free to forced convection for the inciting attitude of buoyancy forces for up-swimming microorganism. **Figs. 5.2(b−c)** depicts that increase in buoyancy parameters N_1, N_2 results in an increase in the velocity profile. Because the buoyancy parameter is proportional to the buoyancy, the larger the buoyancy parameter, the greater the buoyancy. These higher levels of buoyancy operate as agents, increasing fluid velocity. Furthermore, in every case, the velocity profile for Darcy porous media is observed to be higher than for non-Darcy case.

Effect of temperature profile with the growing values of mixed convection parameter and Biot number are observed in **Fig. 5.3. Fig. 5.3(a)** depicts temperature profile increases which mixed convection parameter λ in the presence of dispersion effect because of the increment of motion of the fluid average kinetic energy increases which causes increment of temperature profile. But it is seen when dispersion effect is absent temperature profile increases from free to mixed convection regime, then again decreases to forced convection regime. In **Fig. 5.3(b),** As the Biot number rises, the temperature profile rises with it. The Biot number helps to increase the temperature profiles of the fluid by increasing internal heat in solid surfaces. When there is a dispersion effect, the thickness of the boundary layer of the temperature profile increases.

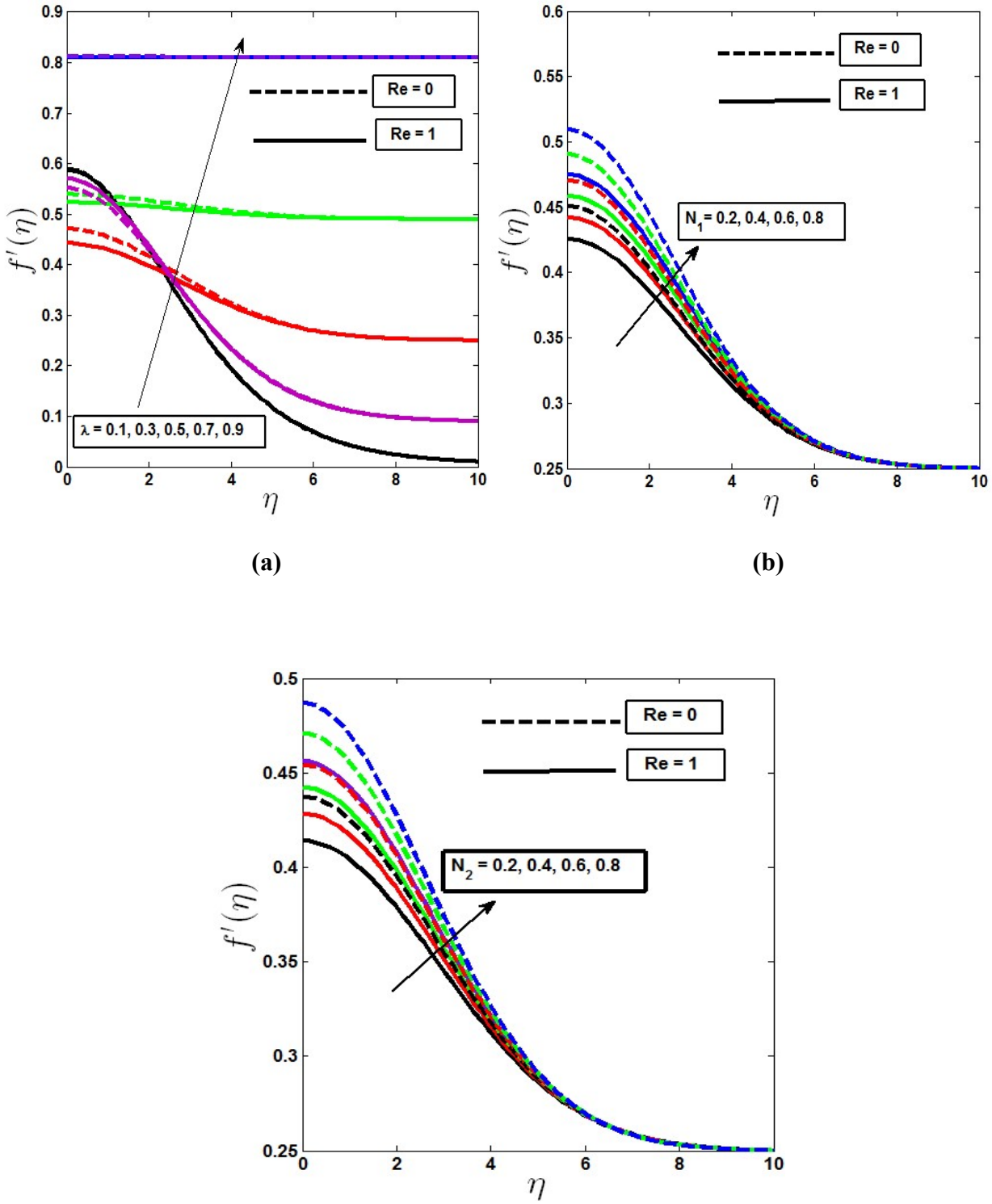

Fig. 5.2 Velocity profile with the a) variation of λ b) variation of N_1 c) variation of N_2 for Darcy and non-Darcy cases

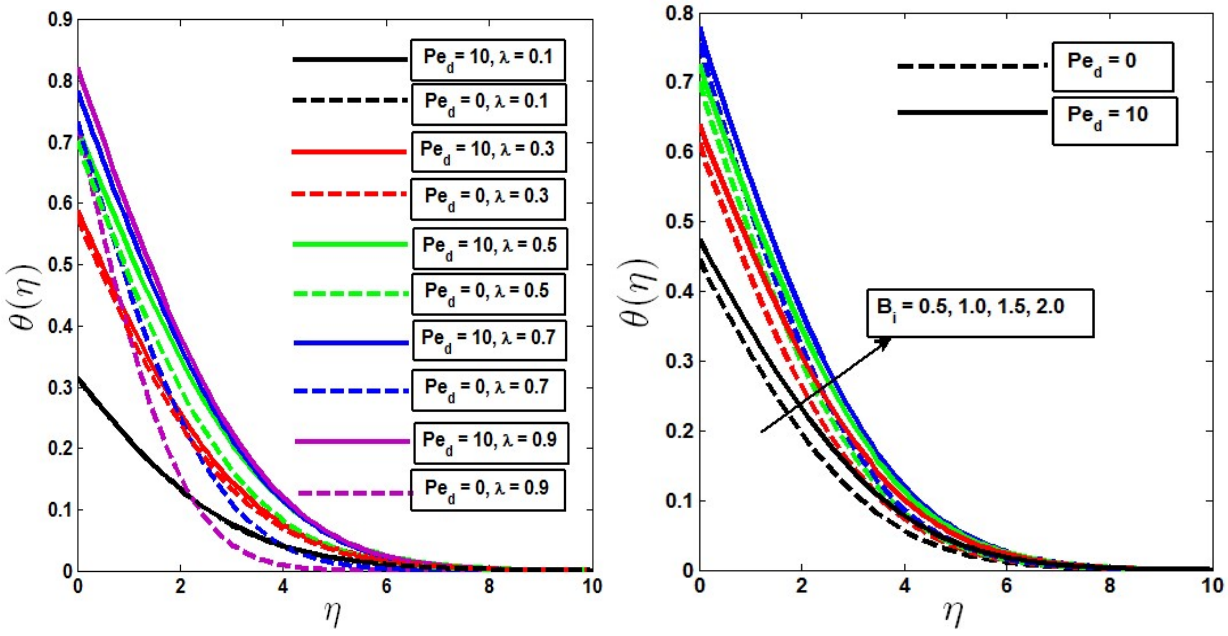

(a) **(b)**

Fig. 5.3 Temperature profile with the a) variation of λ b) variation of B_i in the presence and absence of thermal dispersion effect

The impact of the mixed convection parameter on the concentration and microorganism profile is demonstrated in **Figs. 5.4(a)** and **5.5(a),** respectively. In both cases boundary layer thickness is increasing with λ in the presence of dispersion effect. Without dispersion effect both profiles increase from pure free convection (λ = 0) to pure mixed convection (λ = 0.5) and then decreases to pure forced convection (λ = 1). **Figs. 5.4(b)** and **5.5(b)** depict that the concentration and microorganism profiles increase within the boundary layer when Biot number of mass transfer $B_{i,m}$ and Biot number of motile microorganism transfer $B_{i,n}$ increase from least to large value. Biot numbers are placed as a boundary condition in the enhanced wall boundary condition in Equation (5.13). With the rise in Biot numbers, more heat and species of motile microorganisms are conveyed to the fluid, energising the temperature, concentration, and microorganism profile boundary layer.

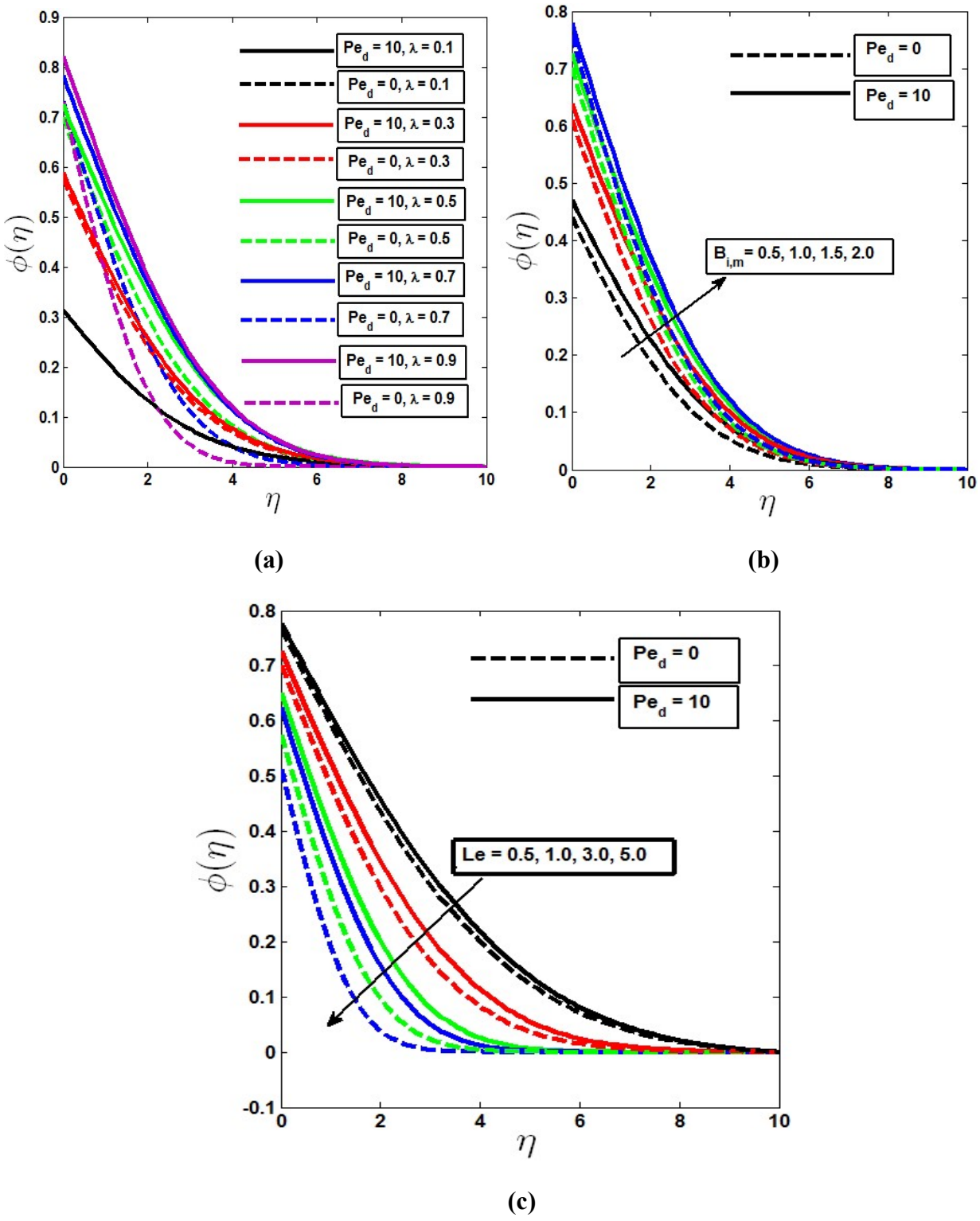

Fig. 5.4 Concentration profile with the a) variation of λ b) variation of $B_{i,m}$ c) variation of Le in the presence and absence of solutal dispersion effect

The Lewis number is a measure of the relationship between thermal diffusivity and mass (Nanoparticle) species diffusivity. $Le = 1$ denotes that the fluid's thermal diffusivity and species diffusivity are both the same, as is the thickness of both boundary layers. When Le is less than one, mass diffusivity is greater than thermal diffusivity, and vice versa when Le is greater. As shown in **Fig. 5.4(c),** the mass diffusivity of the concentration boundary layer declines as the Lewis number decreases, lowering the penetration depth. Without the dispersion effect, the concentration profile deteriorates. The bioconvection Peclet number Pe and bioconvection Lewis number Lb have a propensity to lower the motile microorganism density. The bioconvection Peclet number Pe and the quantity of motile microbe thickness decrease as the Lewis number Lb of the bioconvection increases fluid mobility, as shown in **Figs. 5.5(c)** and **5.5(d).** The behaviour of the microorganism profile with and without dispersion effects are also shown.

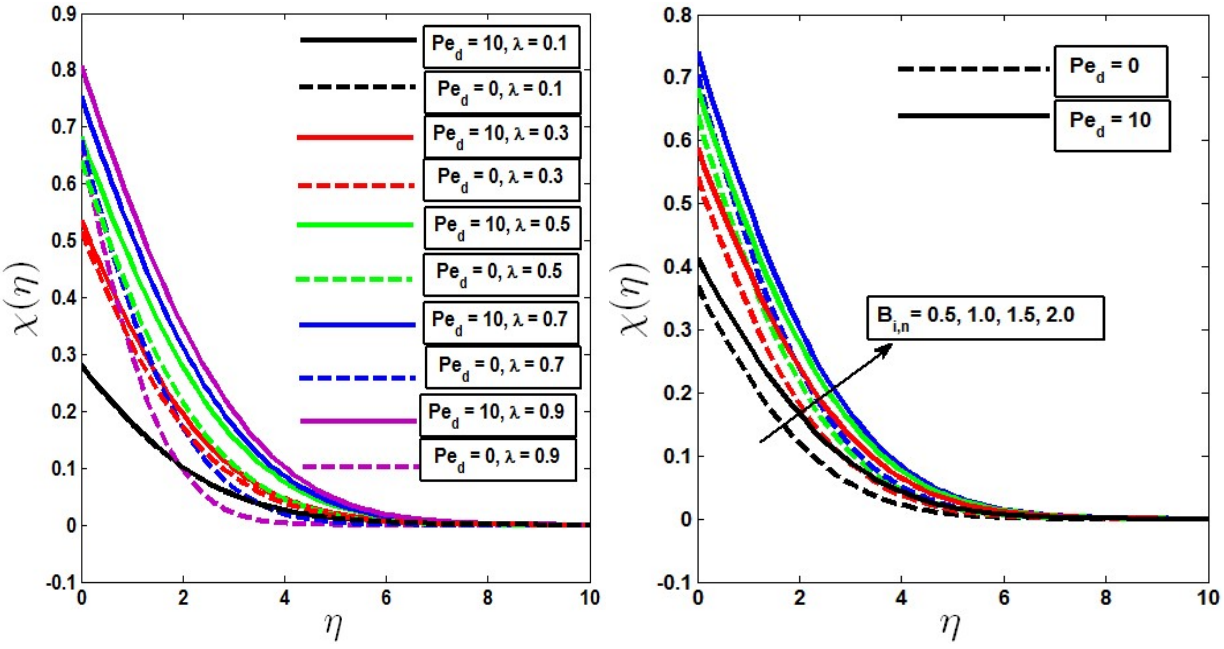

(a) **(b)**

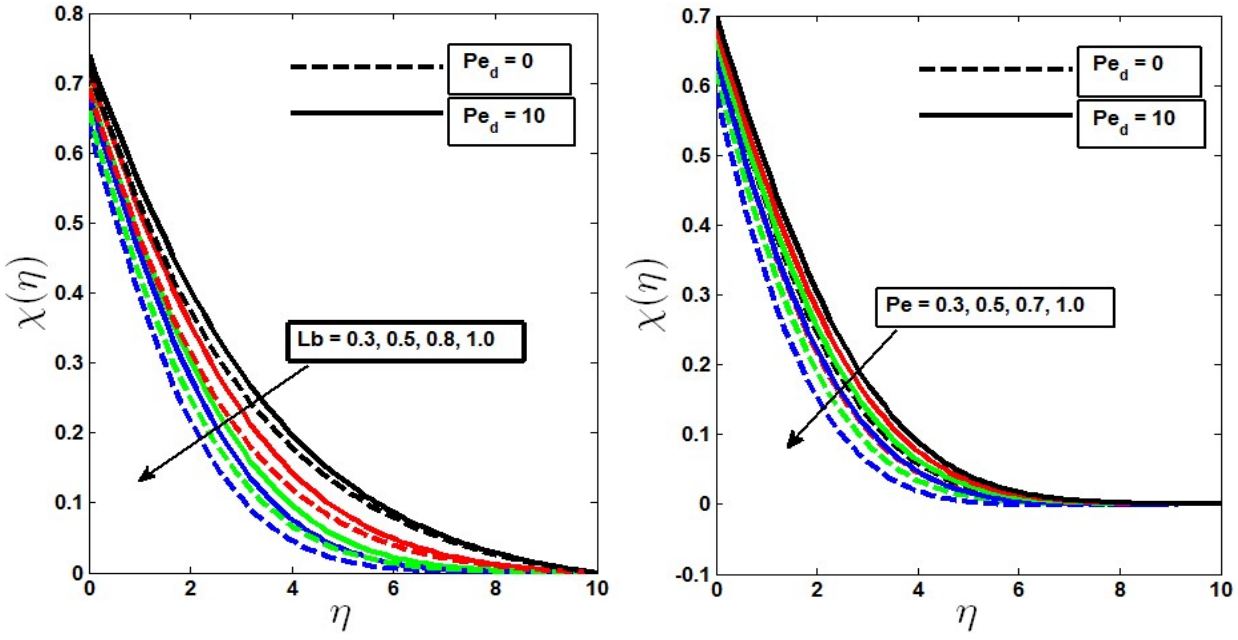

(c) **(d)**

Fig. 5.5 Microorganism profile with the a) variation of λ b) variation of $B_{i,n}$ c) variation of Le d) variation of Pe in the presence and absence of microorganism dispersion effect

Fig. 5.6 shows the impacts of dispersion on heat, mass, and motile microbe transfer rates as the mixed convection parameter is varied, and the rate of heat transmission increases as the dispersion parameter decreases. **Fig. 5.6(a)** shows that the rate of heat transmission is faster in the absence of the dispersion effect. Because λ closer to zero indicates free convection regime and closer to one indicates forced convection regime, we can observe in **Fig. 5.6(a)** that dispersion effect on heat transfer rate is negligible in free convection region. By contrast, effects are prominent in forced convection region. Similarly, **Figs. 5.6(b)** and **5.6(c)** depict that mass and motile microorganism transfer rates increase with the growing values of when the dispersion effect is negligible. When c = 0.3 and $Pe_d = 5$, mass and motile microorganism transfer rates increase from λ = 0 to λ = 0.82 and when c = 0.3 and $Pe_d = 10$, mass and motile microorganism transfer rates increase from λ = 0 to λ = 0.69, subsequently in both cases mass and microorganism transfer rate gradually decrease. Therefore, decreasing phenomena is observed in forced convective region in the presence of dispersion effect.

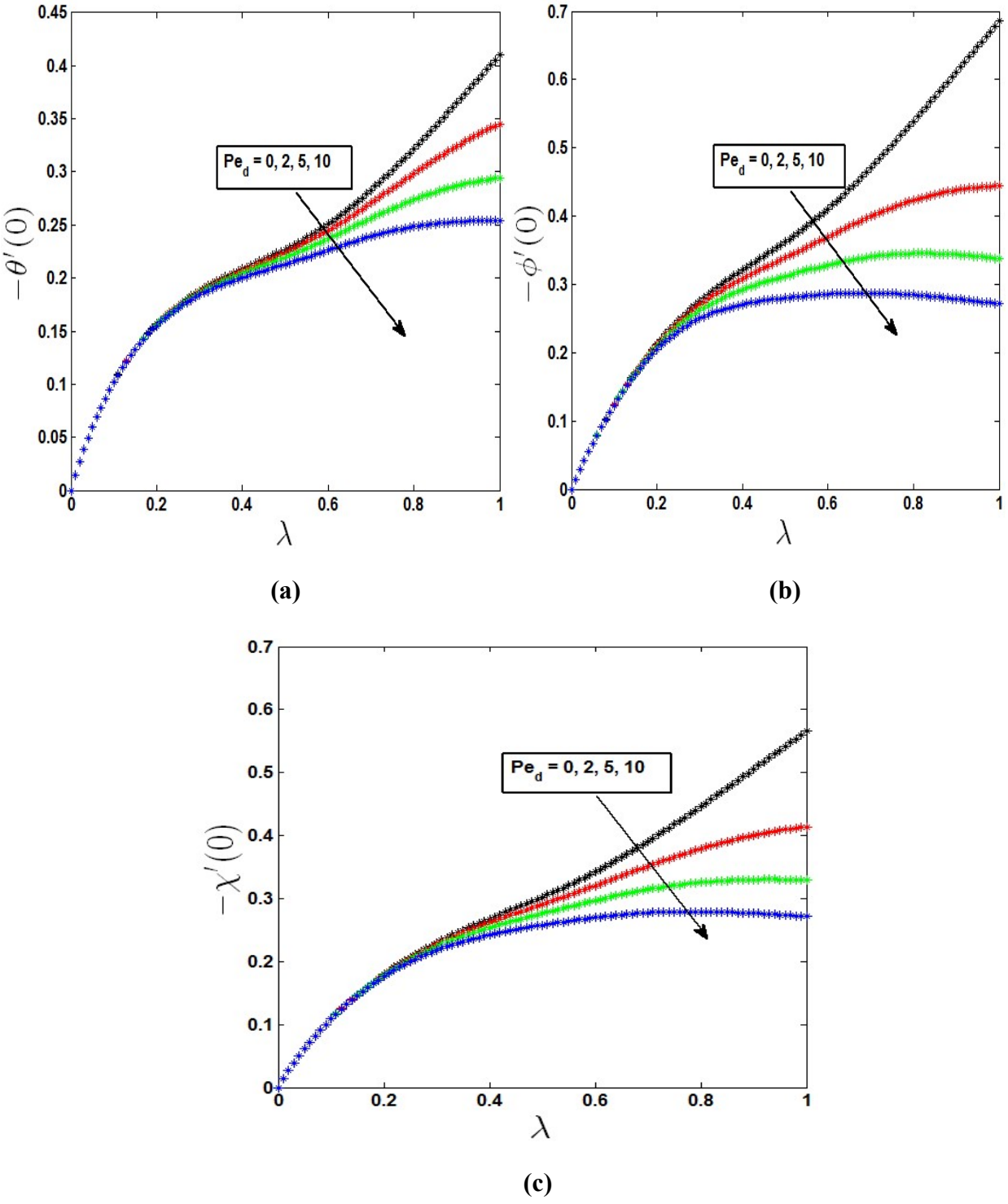

Fig. 5.6 Dispersion effects on a) heat transfer rate b) mass transfer rate c) motile microorganism transfer rate in free, forced and mixed convection regime

For the growing effects of Biot numbers, the heat, mass, and microbe transfer rates are shown in **Fig. 5.7,** as the mixed convection parameter is varied. An increase in the Biot number increased the fluid temperature, and because of convective heat transfer from the hot fluid to the surface of the cone, the surface was heated, which in turn increased the heat transfer rate from the surface to the fluid. Therefore, in **Fig. 5.7** we can observe that heat, mass, and motile microorganism transfer rates are increasing from $\lambda = 0$ to $\lambda = 1$ when dispersion effect is absent. Although this increasing rate is not similar in all regions, **Figs. 5.7(a−c)** show that in the mixed convection region, increasing phenomena is comparatively slower than free and forced convective region. By contrast, when dispersion effects are present, heat transfer rate decreases after when $B_i = 1.5$ for $\lambda = 0.98$ and $B_i = 2$ for $\lambda = 0.94$, which is closer to pure forced convection regime. Furthermore, mass transfer rate decreases after when $B_{i,m} = 1$ for $\lambda = 0.79$, $B_{i,m} = 1.5$ for $\lambda = 0.69$, and $B_{i,m} = 2$ for $\lambda = 0.62$. Similarly when $B_{i,n} = 1$ for $\lambda = 0.86$, $B_{i,n} = 1.5$ for $\lambda = 0.80$, and $B_{i,n} = 2$ for $\lambda = 0.74$, motile microorganism transfer rate decreases.

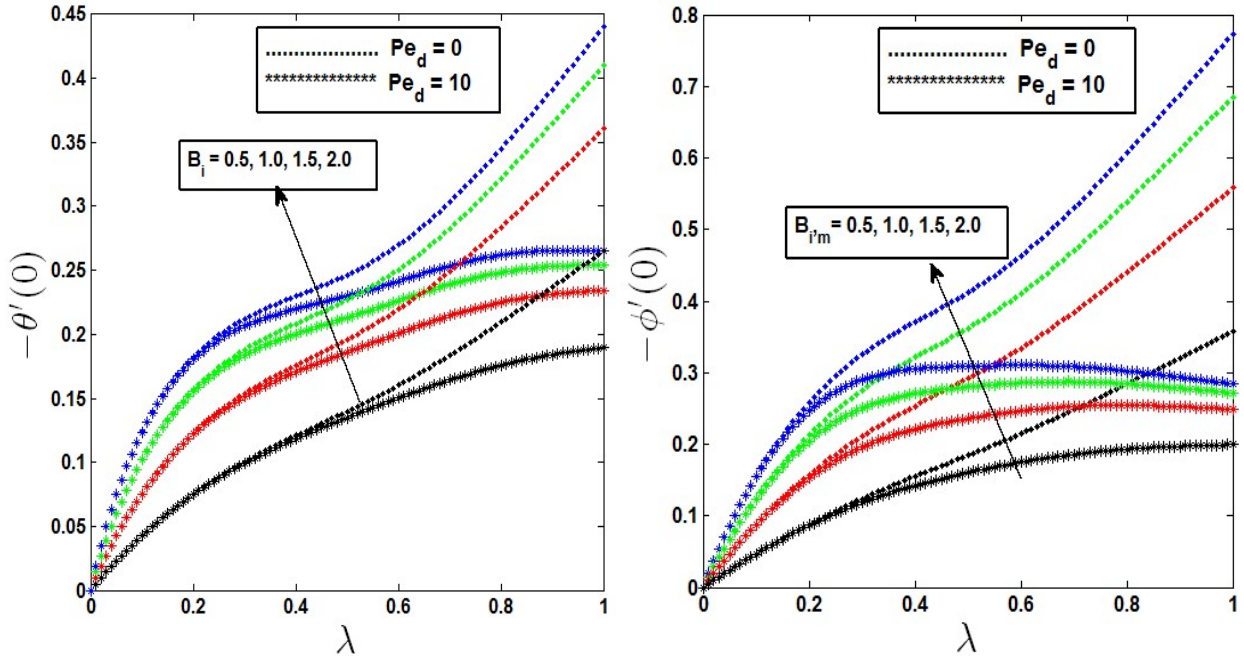

(a) **(b)**

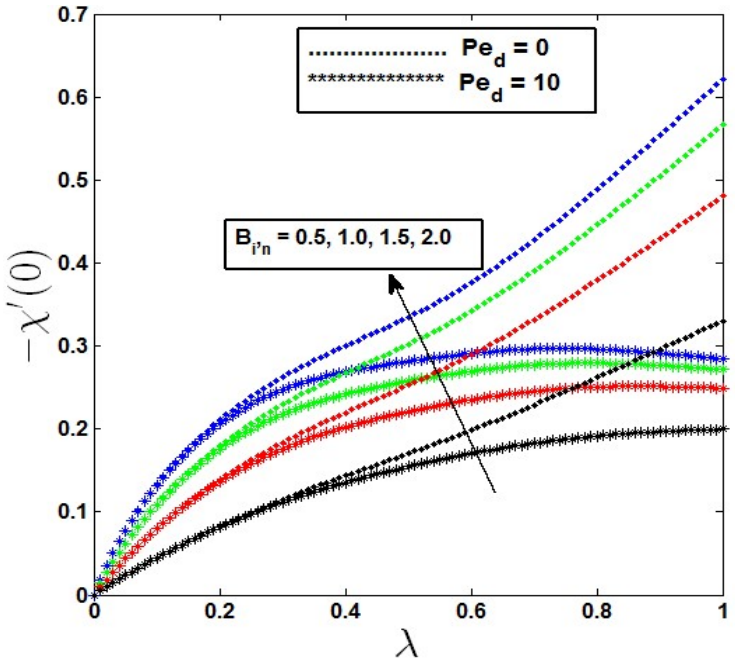

(c)

Fig. 5.7 Effects of Biot numbers on a) heat transfer rate b) mass transfer rate c) motile microorganism transfer rate in free, forced, and mixed convection regime

Fig. 5.8 depicts the grid-independence test, which is used to maintain the point of exactness. It starts with a common mesh of 50 points. We obtained a medium mesh, 100 points of accuracy, and a suitable mesh with 200 points of accuracy for velocity, temperature, concentration, and microorganism profiles by increasing the number of points twice and thrice. When the number of points exceeds the suitable mesh number, the precision is unaffected, although the set time is increased.

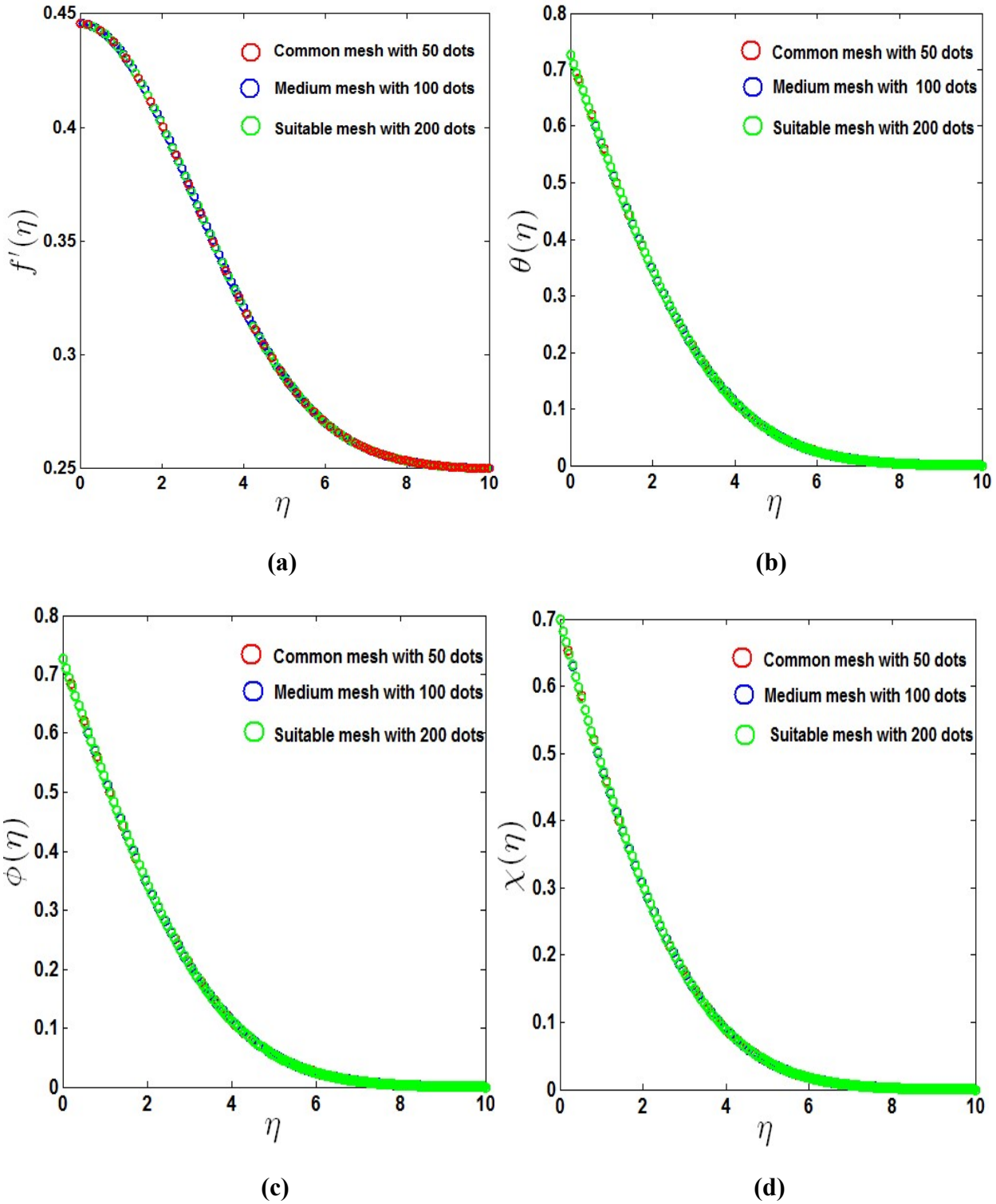

Fig. 5.8 Grid Independence test a) velocity profile b) temperature profile c) concentration profile d) microorganism profile

5.4 Summary

Theoretical and numerical studies conducted on a new mathematical framework for a stable flow of mixed convection in two dimensions via a horizontal cone containing gyrotactic microorganisms with convective boundary conditions are presented. The effects of dispersion on the rate of transport of heat, mass, and motile microorganisms, along with velocity, temperature, concentration, and microorganism profiles, were observed. The following is a summary of the main conclusions of this analysis:

- As the value of the mixed convection parameter λ increases, the velocity profile and buoyancy parameters N_1, N_2 increase, particularly for Darcy porous media.
- Temperature, concentration, and microorganism profiles are increasing with increasing values of λ when no dispersion effect is present. However, in the presence of dispersion effect, the profiles increase for free (λ = 0) to pure mixed convection (λ = 0.5), then decrease for those values of λ, which indicate forced convection.
- The dispersion effect has a substantial impact on the rate of heat, mass, and motile microbe higher effects of dispersion, the rate of heat, mass, and motile microorganism transfer increases in a free-convection zone and drops in the forced convection region.
- The Biot number increases the rate of heat, mass, and motile microorganism transfer from free to forced convection with no influence on dispersion, and the flow transfer rates decrease with the influence of the dispersion effect.

Chapter 6

Dual solutions in mixed convection flow along non-isothermal inclined cylinder containing gyrotactic microorganism

This study seeks to propose a dual solution for mixed free and forced convection flow towards a non-isothermal permeable inclined cylinder holding a gyrotactic microbe. Two steps were performed to perform the numerical calculations. Through the aid of similarity transformations, the controlling partial differential equations were first condensed into a set of linked nonlinear ordinary differential equations, which were subsequently numerically resolved with the help of MATLAB bvp4c function. Beyond a critical point, dual solutions are seen for velocity, temperature, concentration, and the profile of the motile microorganisms as well as for heat, mass, and density of the transfer rate. The research reached an excellent conclusion by comparing the results obtained from the MATLAB and Maple algorithms in a few cases. This research can be applied to the development of bioconvection technology and cylindrical urine-fed microbial fuel cells in engineering, geothermal, and industrial fields.

6.1 Mathematical formulation

This study considered the laminar boundary layer flow of free forced convection over an inclined cylinder with a radius r_0 inserted in a permeable, saturated media containing gyrotactic microorganisms, given in **Fig. 6.1**. It is assumed that the mainstream velocity U(x) and cylindrical surface are kept at a constant temperature T_w , concentration of fluid C_w, and motile microorganism concentration n_w, whereas distant from cylinder's outside surface, the velocity, temperature, and concentrations are u_∞ , T_∞ , C_∞, and n_∞ , respectively. Coordinates in axial and radial space are considered to be x and r, respectively, where along the cylinder's axis, the vertical height of the x-axis is measured, and the axis r is measured perpendicular to axis x. The acceleration of gravitation, g, carries out downward motion, in contrast to the x-direction.

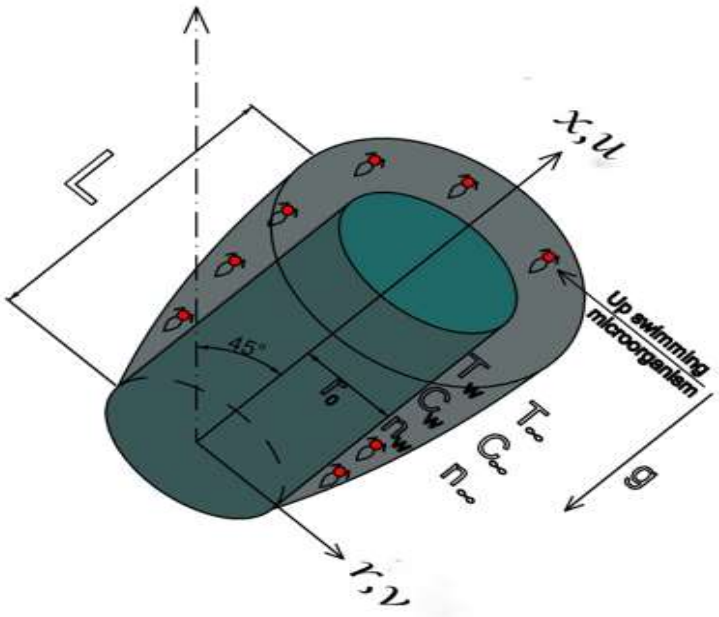

Fig. 6.1 Coordinates and the physical model

According to the models put forth by Alsenafi and Ferdows (2021), Sudhagar et al. (2019), and taking into account the hypotheses, physical phenomena, and Boussinesq approximations, the governing equations are as follows:

$$\frac{\partial(ru)}{\partial x}+\frac{\partial(rv)}{\partial r}=0 \tag{6.1}$$

$$\frac{\partial u}{\partial r}=\pm\frac{gK}{\nu}\left(\beta_T\frac{\partial T}{\partial r}+\beta_C\frac{\partial C}{\partial r}+\beta_n\frac{\partial n}{\partial r}\right)\cos\omega \tag{6.2}$$

$$u\frac{\partial T}{\partial x}+v\frac{\partial T}{\partial r}=\alpha\left(\frac{1}{r}\frac{\partial}{\partial r}\left(r\frac{\partial T}{\partial r}\right)\right) \tag{6.3}$$

$$u\frac{\partial C}{\partial x}+v\frac{\partial C}{\partial r}=D_m\left(\frac{1}{r}\frac{\partial}{\partial r}\left(r\frac{\partial C}{\partial r}\right)\right) \tag{6.4}$$

$$u\frac{\partial n}{\partial x}+v\frac{\partial n}{\partial r}+\frac{bW_c}{\nabla C}\left(\frac{\partial}{\partial r}\left(n\frac{\partial C}{\partial r}\right)\right)=D_n\left(\frac{1}{r}\frac{\partial}{\partial r}\left(r\frac{\partial n}{\partial r}\right)\right) \tag{6.5}$$

The boundary conditions take the following shape:

$$v=0,\ T=T_w(x)\ ,\ C=C_\infty(x)\ ,\ n=n_\infty(x),\qquad \text{at } r=r_0 \tag{6.6}$$

$$u\to U(x),\ T\to T_\infty,\ C\to C_\infty,\ n\to n_\infty\qquad \text{at } r=\infty \tag{6.7}$$

Conforming to Mahmood and Merkin (1988), we presume the following dimensionless quantities:

$$\eta=\frac{r^2-r_0^{\,2}}{2r_0L}\left(Pe^{\frac{1}{2}}+Ra^{\frac{1}{2}}\right),\ \psi=\alpha\ r_0\left(Pe^{\frac{1}{2}}+Ra^{\frac{1}{2}}\right)\frac{x}{L}f(\eta) \tag{6.8}$$

$$T=T_\infty+\frac{ax^{m+1}\nabla T}{L}\theta(\eta),C=C_\infty+\frac{bx^{m+1}\nabla C}{L}\varphi(\eta),n=n_\infty+\frac{cx^{m+1}\nabla n}{L}\chi(\eta) \tag{6.9}$$

The continuity equation is satisfied by stream function such that

$$u=\frac{1}{r}\frac{\partial\psi}{\partial r}\ \text{and}\ v=-\frac{1}{r}\frac{\partial\psi}{\partial x}$$

The following coupled differential equations are produced by applying transformations (6.8) and (6.9) to equations (6.1) and (6.7):

$$f''=(1-\lambda)^2(\theta'+N_1\phi'+N_2\chi')Cos\omega \tag{6.10}$$

$$(1+\gamma\eta)\theta''+\gamma\theta'+f\theta'-(m+1)f'\theta=0 \tag{6.11}$$

$$(1+\gamma\eta)\varphi''+\gamma\varphi'+Le.f\varphi'-(m+1)Le.f'\phi=0 \tag{6.12}$$

$$(1+\gamma\eta)\chi''+\gamma\chi'+Lb.f\chi'-Lb.(m+1)f'\chi-Pe((1+\gamma\eta)\phi'\chi'+(\chi+A)(\gamma\varphi'+(1+\gamma\eta)\phi''))=0 \tag{6.13}$$

The modified boundary conditions change into

$$\eta = 0, f = 0, \theta = 1, \varphi = 1, \chi = 1 \tag{6.14}$$

$$\eta \to \infty, f' \to \lambda^2, \theta \to 0, \varphi \to 0, \chi \to 0 \tag{6.15}$$

Where Mixed Convection Parameter $\lambda = \left(1 + \frac{Ra^{\frac{1}{2}}}{Pe^{\frac{1}{2}}}\right)^{-1}$, Raleigh Number $Ra = \frac{g\beta kLax^m \nabla T}{\upsilon\alpha}$, Peclet Number $Pe = \frac{u_\infty L}{\alpha}$, Curvature Parameter $\gamma = \frac{2L}{r_0(Pe^{\frac{1}{2}} + Ra^{\frac{1}{2}})}$, Bioconvection Peclet number $Pe = \frac{bW_c}{D_n}$, Bioconvection Lewis parameter $Lb = \frac{\alpha}{D_n}$, Lewis number $Le = \frac{\alpha}{D_m}$, Buoyancy parameters $N_1 = \frac{\beta_c \nabla C}{\beta_T \nabla T}$, $N_2 = \frac{\beta_n \nabla n}{\beta_T \nabla T}$, Microorganism concentration difference parameter $A = \frac{n_\infty}{n_w - n_\infty}$.

6.2 Solution methodology

Similarity transformations were used to convert the governing partial differential equations into ordinary differential equations and mathematically solved using the MATLAB bvp4c solver. In this method, using different initial guesses of $f, f', \theta, \theta', \phi, \phi', \chi, \chi'$, we can find the first and second solutions. Within the framework of the aforementioned bvp4c function, the governing equations (6.10)−(6.13) need to be modified into a first-order differential equation, letting $\eta = x$ and $y_1 = f, y_2 = f', y_3 = \theta, y_4 = \theta', y_5 = \phi, y_6 = \phi', y_7 = \chi, y_8 = \chi'$.

Here are the equivalent first order differential equations:

$$\frac{dy_1}{dx} = f' = y_2, \frac{dy_2}{dx} = f'' = (1-\lambda)^2 (y_4 + N_1 y_6 + N_2 y_8)$$

$$\frac{dy_3}{dx} = \theta' = y_2, \frac{dy_4}{dx} = \theta'' = \frac{(m+1)y_2 y_3 - \gamma y_4 - y_1 y_4}{(1+\gamma\eta)}$$

$$\frac{dy_5}{dx} = \varphi' = y_6, \frac{dy_6}{dx} = \varphi'' = \frac{(m+1)Ley_2 y_5 - \gamma y_6 - Ley_1 y_6}{(1+\gamma\eta)}$$

$$\frac{dy_7}{dx} = \chi' = y_8, = \frac{dy_8}{dx} = \chi'' = \frac{\begin{matrix}(m+1)Lby_2 y_7 - \gamma y_8 - Lby_1 y_8 + Pe\begin{pmatrix}(1+\gamma\eta)y_6 y_8 + (y_7 + A)(\gamma y_6 + \\ (1+\gamma\eta)\begin{pmatrix}-\gamma y_6 - \\ Ley_1 y_6 + Le(m+1)y_2 y_5\end{pmatrix}\end{pmatrix}\end{matrix}}{(1+\gamma\eta)}$$

The boundary conditions (6.14) − (6.15) are changed such that the right boundary is yq and the left boundary is yp, respectively.

$$yp(1) = 0, yq(2) - \lambda^2 = 0$$
$$yp(3) - 1 = 0, yq(3) = 0$$
$$yp(5) - 1 = 0, yq(5) = 0$$
$$yp(7) - 1 = 0, yq(7) = 0$$

To verify the findings, the differential equations were solved numerically using Maple through the use of the **dsolve** command, wherein asymptotic boundary conditions (6.14) – (6.15) were utilising in place of a value five for the similarity variable $\eta_{max} = 5$. The results obtained for both cases are listed in **Table 6.1**, demonstrates the precision and high consistency of the mathematical calculations.

Table 6.1 Effect of mixed convection parameter λ on $-\theta'(0)$ when

$$N_1 = 0.5, N_2 = 0.6, m = 0.2, \gamma = 0.1, \omega = \frac{\pi}{4}, Lb = 0.0, Le = 0.0, Pe = 0.0, A = 0.0$$

λ	$-\theta'(0)$ (MATLAB Bvp4c) First Solution	$-\theta'(0)$ (Maple) First Solution
0.0	1.4543	1.4550

0.3	1.0922	1.0929
0.5	0.9937	0.9941
0.8	1.1238	1.1239
1.0	1.3520	1.3520

For further confirmation, the present result for the unique case is validated in contrast to the findings of the studies by Gorla *et al*. (1996), Chamkha and Khaled (2000), and Nima (2020), as specified in **Table 6.2**.

Table 6.2 Comparison of $f'(0)$ for the values of

$N_1 = 0.0, N_2 = 0.0, m = 0.0, \gamma = 0.0, \omega = 0, Lb = 0.0, Le = 0.0, Pe = 0.0, A = 0.0, \lambda = 1$

	Present Result (First Solution)	Gorla *et al*. (1996)	Chamkha and Khaled (2000)	Nima (2020)
$f'(0)$	1.0000	1.0000	1.0000	1.0000

An investigation of stability as provided by Weidman *et al*. (2006), Sparrow (1977), and Postelnicu and Pop (2017) revealed that first solutions are stable and attainable on a practical level; In contrast, second solutions are unstable and consequently impractical. As their research is in a similar physical situation, we will not repeat the analysis in this paper. Every figure displays the dual solutions for all values of $\lambda_c \leq \lambda$, where λ_c is the critical value.

6.3 Numerical results and discussion

6.*3.1 Velocity profile:*

In **Fig. 6.2(a)** shows dual solution for the velocity profile $f'(\eta)$ against η for several values of the mixed convection parameter λ. The mixed convection parameter λ covers the entirety of the mixed convection regime (when λ = 0 to pure forced convection (when λ = 1). As

shown in **Fig. 6.2(b),** the velocity profile raises with growing values of curvature parameter γ**.** As the curvature parameter increased, the velocity profile dropped. For the higher values of curvature parameter, the radius of cylinder decreases. Because there is less friction between fluid particles and the surface area, the velocity profile exhibits a higher value. In **Figs. 6.2(a-b),** the first solution is stable when the velocity profile moves into the positive range, and the flow becomes unstable when the lower branch solution moves into the negative range, which is consistent with the onset of a disturbance. As a result, the second solution was unable to asymptotically achieve the far field boundary conditions. The velocity flow profiles indicated the existence of a dual solution when $\lambda > \lambda_C$.

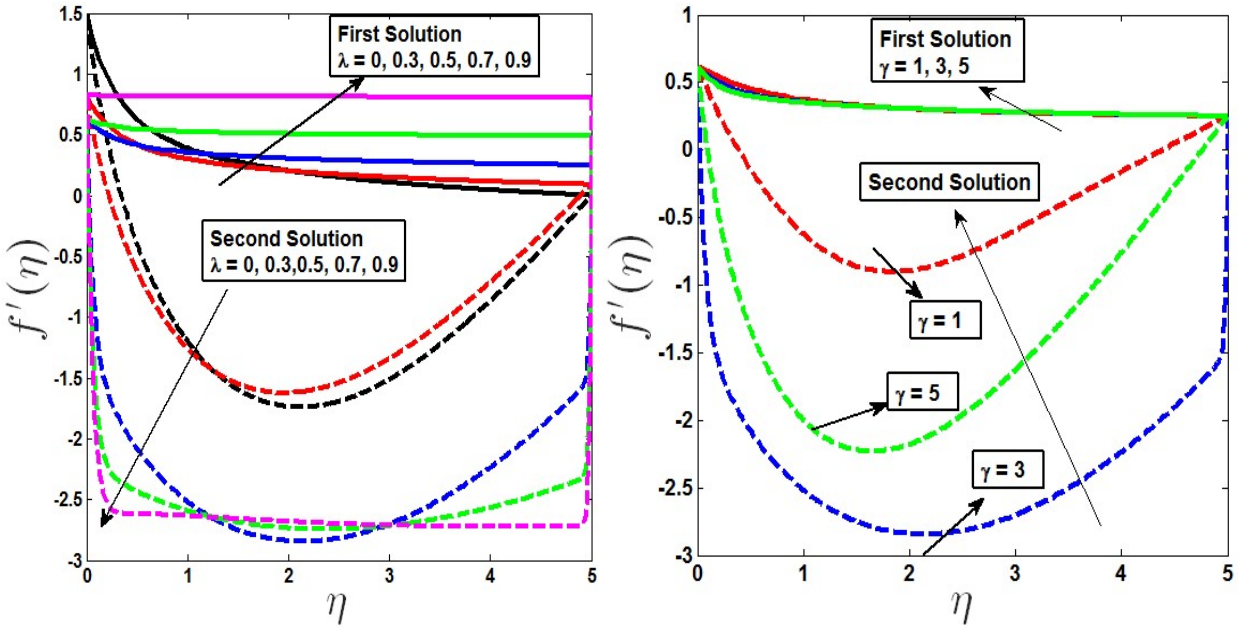

(a) **(b)**

Fig. 6.2 Velocity profile with the a) variation of λ b) variation of γ

6.3.2 Heat transfer rate and temperature profile:

A variant of the Nusselt number with λ for several variations in γ is shown in **Fig. 6.3(a)**. We can observe that dual solution exists for the temperature profile $\lambda > \lambda_c$, where $\lambda_c = 0.31,0.28,0.24$ when $\gamma = 0.3,0.4,0.5,$ respectively. Nusselt number diminishes from free

convection to regime of mixed convection, subsequently it gradually enhances to forced convective regime in light of rising values of curvature parameter λ. It is also observed that dual solution exists in free convective regime. Because the radius of the curve decreases as the curvature parameter increases, and the fluid particles' velocity increases. Therefore, average kinetic energy increase, causing the growth of temperature profile. So, increase in curvature enhances the rate of heat transfer from cylinder to the surface. **Figs. 6.3(a)** and **6.4(a)** show heat transmission rate and temperature profile increase for the higher values of λ for the first solution, although opposite phenomena are observed for second solution.

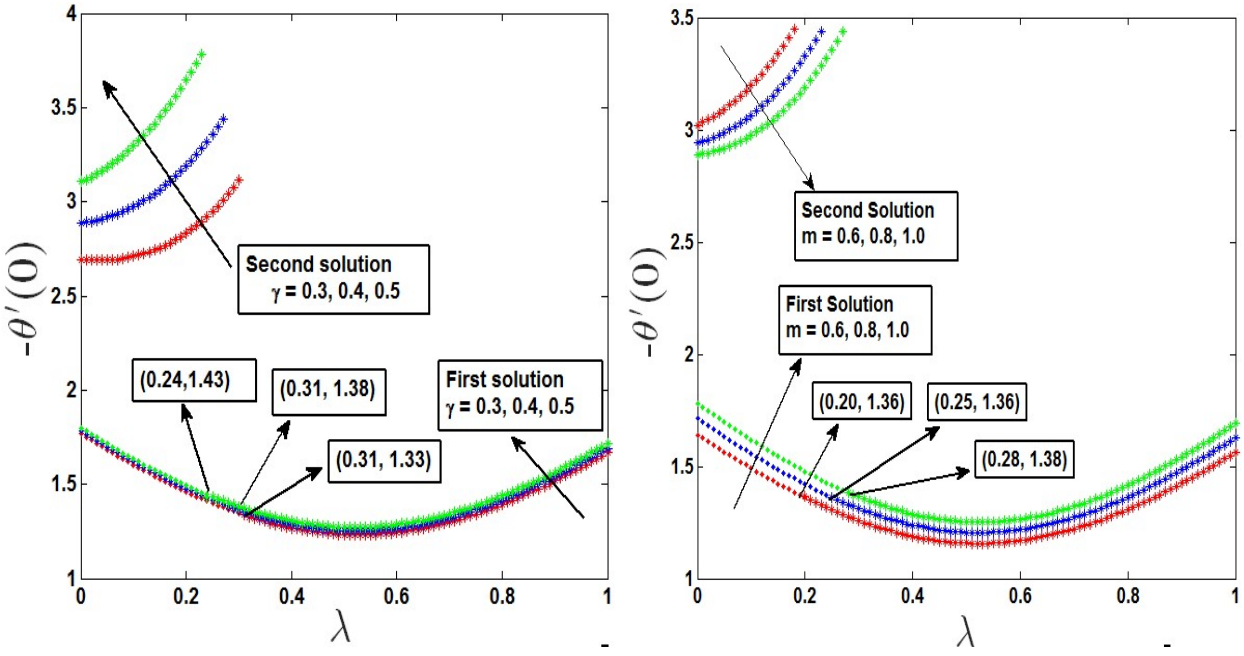

(a) **(b)**

Fig. 6.3 The influence of λ on heat transfer rate with the a) variation of γ b) variation of m

Fig. 6.3(b) shows variation of heat transmission rate with λ for the variations in power law exponent m. Decreasing power index m, as the fluid tends to thicken and increase the viscosity and thus increase the shear stress, the heat transfer rate decreases in the free convection dominated zone where influence of λ is not prominent. But in the forced convection region higher heat transfer rate is observed. Dual solution exists for $\lambda > \lambda_c$, where $\lambda_c = 0.20, 0.25, 0.28$ when $m = 0.6, 0.8, 1.0$ respectively. In light of **Fig. 6.4(b),** the temperature profile as well as the

thermal boundary layer thickness reduces with the increase of power law index m because fluid velocity increases for low viscosity reducing fluid temperature. In summary, raising the worth of m increases the heat transfer rate while decreasing the thermal boundary layer. Therefore, it is clearly stated that second solutions observed in **Figs. 6.3(b)** and **6.4(b)** are not physically realisable because stable solutions of equations (6.10-6.14) with respect to boundary conditions (6.15-6.15) do not exist for the second solutions.

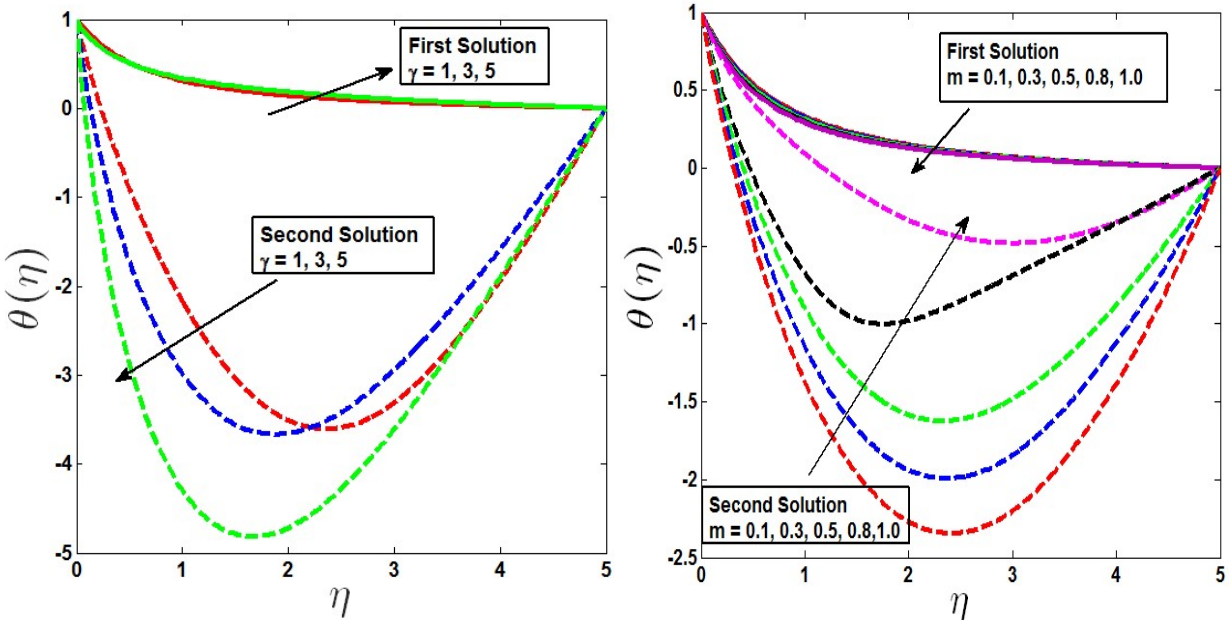

(a) **(b)**

Fig. 6.4 Temperature profile with the a) variation of γ b) variation of m

6.3.3 Mass transfer rate and concentration profile:

Fig. 6.5(a) shows the variant of Sherwood number with λ based on various values of γ**.** The fluid moves more quickly and the concentration gradient lessens as the curvature parameter's value rises. Larger values of the curvature parameter γ, which means more slender cylinder leads to higher mass transfer rates. For the concentration profile, the dual solution is seen at $\lambda > \lambda_c$, where $\lambda_c = 0.10, 0.17$ when $\gamma = 0.2, 0.5$ respectively. At this point, λ_c unique solution exists. Additionally, it is noted that the Sherwood number declines in free convection regime both for first and second solution, subsequently, it increases from mixed convective to forced convective regime considering the rising values of λ and γ for the first solution. **Fig. 6.6(a)** shows there

being a dual solution to concentration profile when $\lambda > \lambda_c$ for the values $\gamma = 0.1, 0.5, 1.0$ is shown. As the values of λ rise, the concentration profile does as well for the first solution and lowers for the second solution.

As shown in **Fig. 6.5(b),** effect of power law exponent m on mass transfer rate with the variation of λ provides that there is a dual solution for the variation of power law exponent m when $\lambda > \lambda_C$. For $m = 0.6, 0.8, 1.0$ we obtain the critical points $\lambda_C = 0.03, 0.07, 0.10$, where unique solutions exist. For the first solution mass transfer rate increases with m. **Fig. 6.6(b)** shows the decrease of boundary layer thickness of concentration profile for Lewis parameter Le. Unstable phenomena are observed for the second solutions.

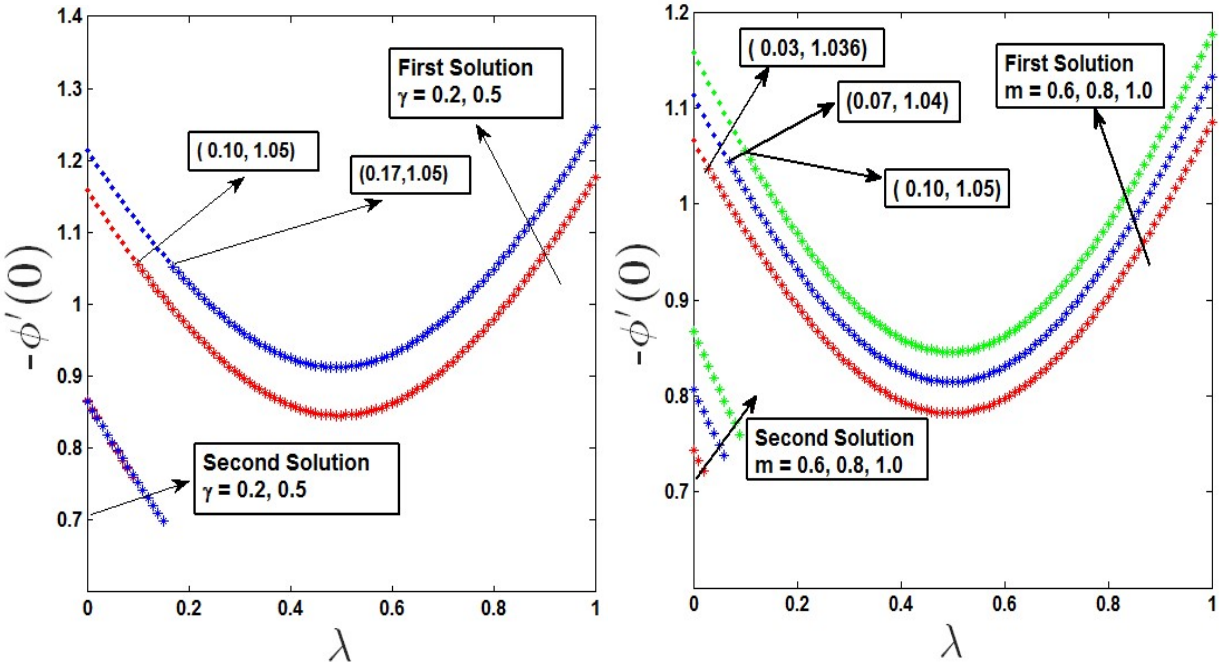

(a) **(b)**

Fig. 6.5 The influence of λ on mass transfer rate with the a) variation of γ b) variation of m

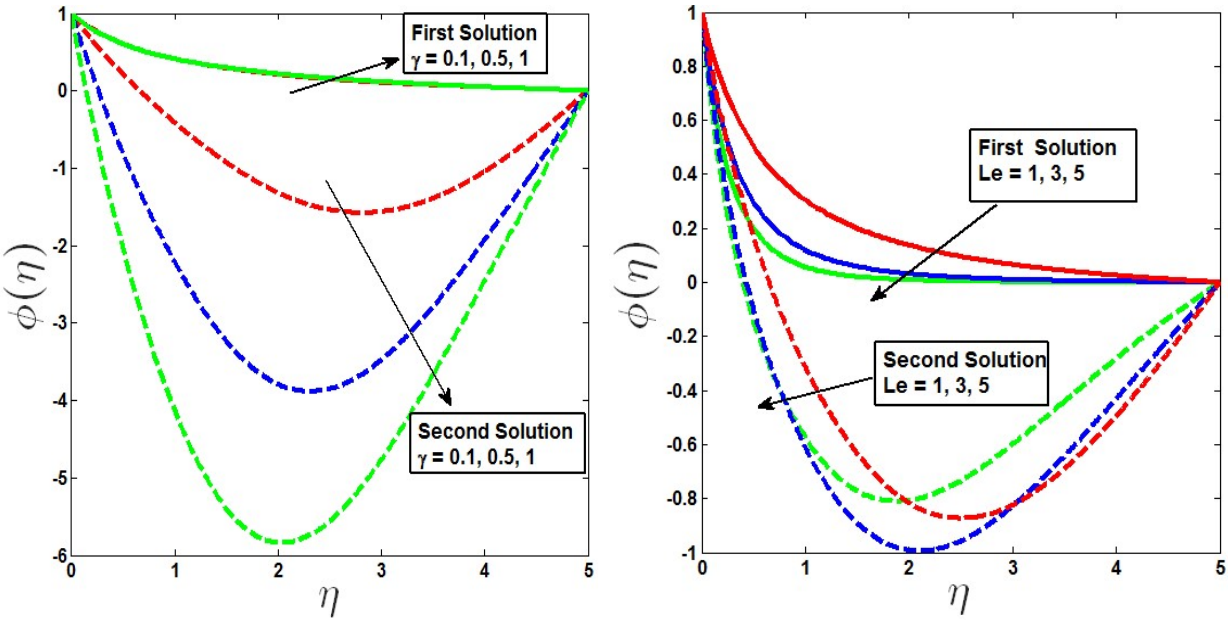

(a) **(b)**

Fig. 6.6 Concentration profile with the a) variation of γ b) variation of Le

6.3.4 Microorganism transfer rate and microorganism profiles:

Dual solutions for motile microorganism transfer rate with mixed convection parameter λ are noticed in **Figs. 6.7(a)** and **6.7(b).** The dual solutions are monitored for the microorganism profile $\lambda > \lambda_c$, where $\lambda_c = 0.28, 0.27, 0.26$ when $\gamma = 0.1, 0.2, 0.3$ and also when $m = 0.8, 0.9, 1.0$, $\lambda_c = 0.25, 0.26, 0.27$. Because of a higher density of moving microorganisms than the liquid, they often swim upward toward the cylinder wall's exterior, growing values of the curvature parameter accelerate the transmission of motile microorganisms. and decreases profile of the microorganism boundary layer thickness for the stable solutions, as shown in **Figs. 6.7(a)** and **6.8(a)**. Motile microorganism transfer rate also increases for power law exponent m, which is shown in **Fig. 6.7(b)**. A decrease in fluid velocity and an increase in the microorganism concentration gradient are caused by an increase in the power law exponent's value. This reflects on the increasing in the convective motile microorganism transfer rates shown in the first solution of **Fig. 6.7(b).**

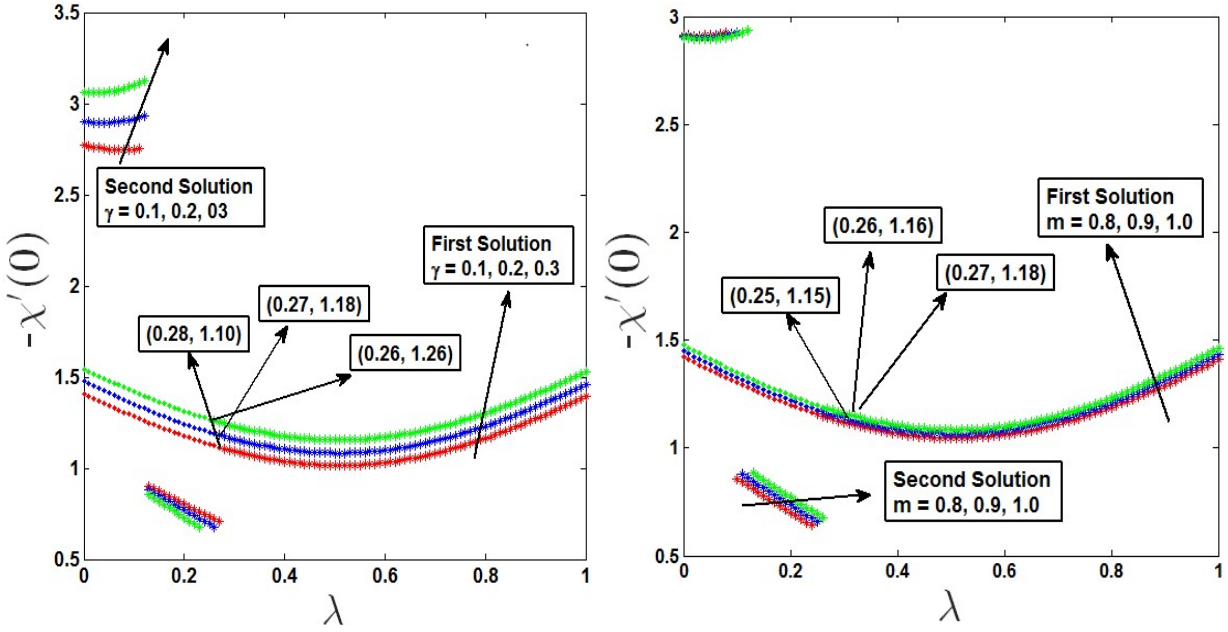

(a) **(b)**

Fig. 6.7 The influence of λ on microorganism transfer rate with the a) variation of γ b) variation of m

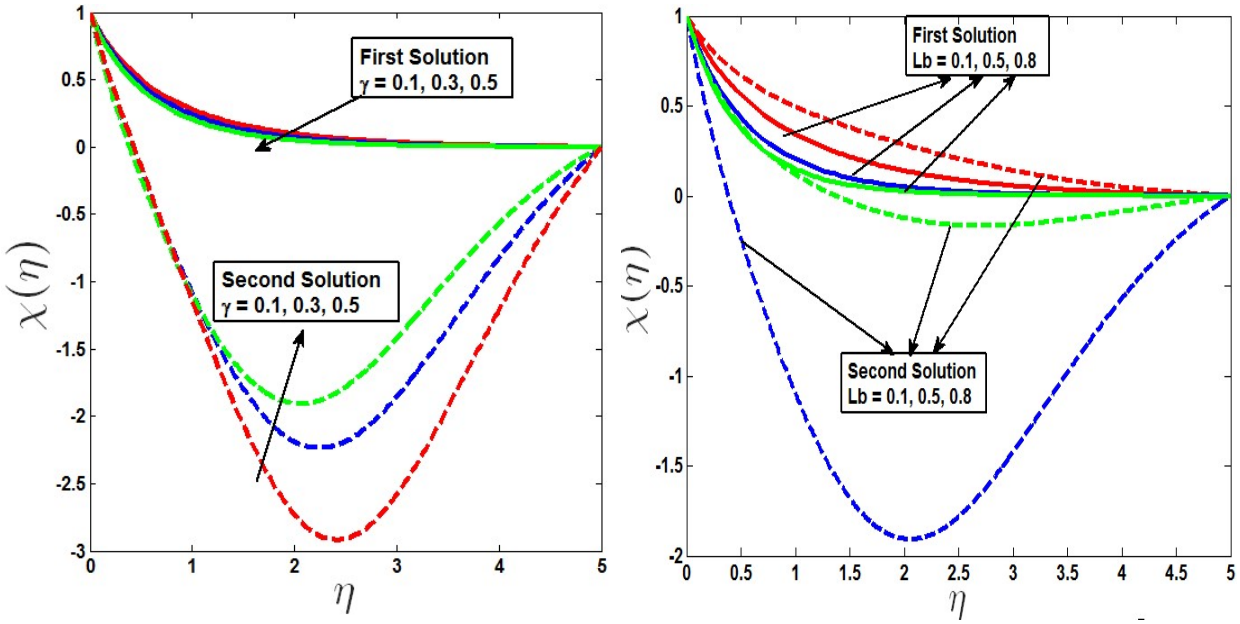

(a) **(b)**

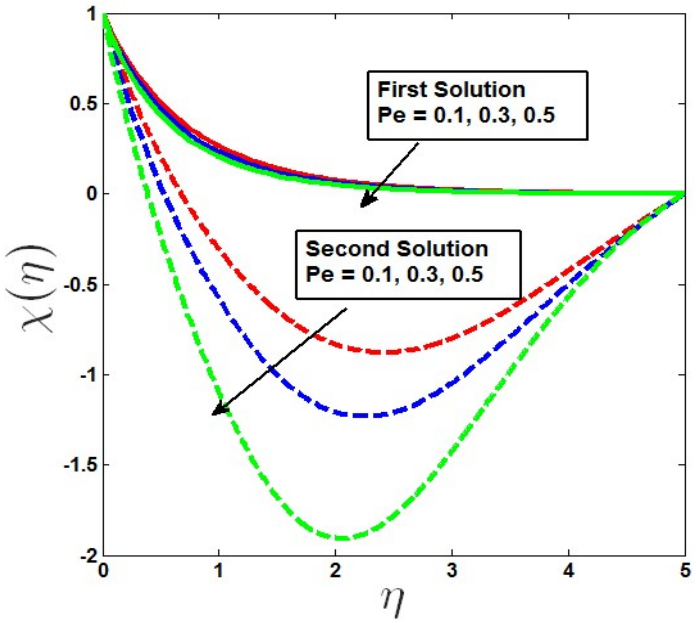

(c)

Fig. 6.8 Microorganism profile with the a) variation of γ b) variation of Le c) variation of Pe

Figs. 6.8(b) and **6.8(c)** demonstrate the presence of a dual microorganism profile when $\lambda > \lambda_c$ for the values Lb = 0.1, 0.5, 0.8 and Pe = 0.1, 0.3, 0.5. In both figures, we can observe that thickness of the microorganism profile boundary layer decreases with the growing values of Lb and Pe. Increase in the Lb causes a decrease in motile microorganism diffusivity, lowering the concentration of microorganisms as a result. By contrast, increase in bioconvection Peclet number causes expansion of the mobility of fluid, which leads to reduction of quantity of motile microorganism's thickness, hence microorganism's diffusivity and their concentration decreases. It is also observed as the microorganism profile went towards the positive range; the first solution is steady. Furthermore, the second solution is unstable as the profile turned negative.

6.3.5. Heat, mass and motile microorganism transfer rate for different inclination of cylinder:

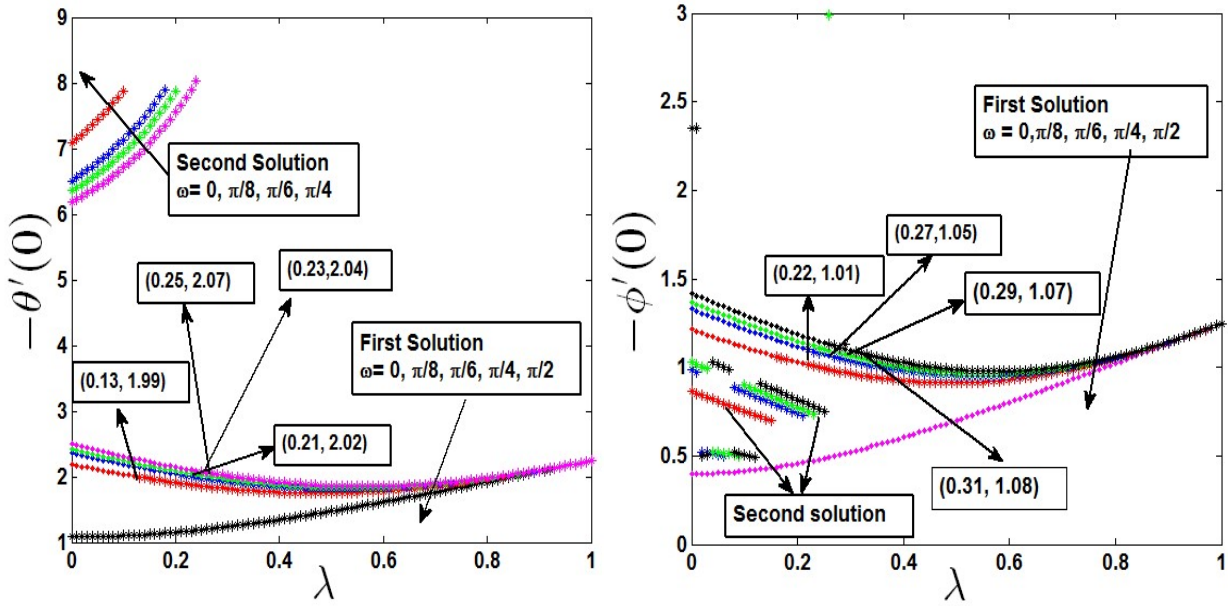

(a) **(b)**

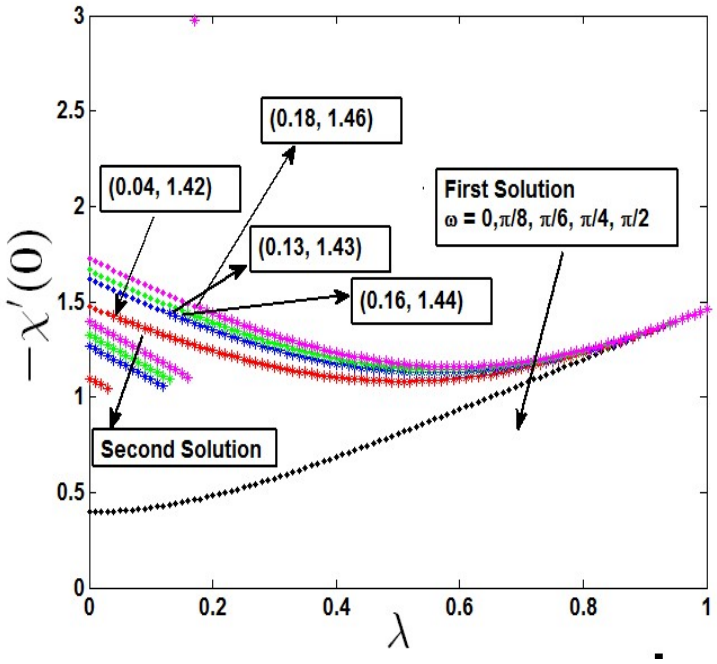

(c)

Fig. 6.9 Impact of different inclination of cylinder on a) heat transfer rate b) mass transfer rate c) motile microorganism transfer rate

Fig. 6.9 shows the heat, mass, and motile microbe transfer rates for various angles ($\omega = 0, \frac{\pi}{8}, \frac{\pi}{6}, \frac{\pi}{4}, \frac{\pi}{2}$) of cylinder inclination, where $\omega = \frac{\pi}{2}$ represents the horizontal cylinder, and $\omega = 0$ indicates the vertical cylinder. Whenever λ is nearer to zero (free convection regime), dual solutions are observed for different inclinations of the cylinder, whereas only one solution exists for the horizontal cylinder**. Table 6.3** shows the influence of curvature parameter γ for the different inclinations of cylinders in the forced convection region as only in forced convection zone stable solutions can be obtained in this study. Results also show heat, mass and microbe transfer rates are higher for slender vertical cylinders.

Table 6.3 Effect of curvature parameter γ on heat and mass transfer, and density of motile microorganism for the different angles of inclination of cylinder when $Le = 0.4, Lb = 0.4, Pe = 0.5, A = 0.2, kp = 10, N_1 = 0.8, N_2 = 0.6, m = 1, \lambda = 0.6$

ω	$-\theta'(0)$		$-\varphi'(0)$		$-\chi'(0)$	
	$\gamma = 0.2$	$\gamma = 0.5$	$\gamma = 0.2$	$\gamma = 0.5$	$\gamma = 0.2$	$\gamma = 0.5$
0	1.30789	1.36880	0.81937	0.88801	1.15853	1.38105
$\frac{\pi}{8}$	1.28737	1.34873	0.80844	0.87754	1.14325	1.36635
$\frac{\pi}{6}$	1.27155	1.33328	0.80003	0.86949	1.13148	1.35550
$\frac{\pi}{4}$	1.22706	1.28988	0.77641	0.84694	1.09840	1.32390
$\frac{\pi}{2}$	1.00571	1.07584	0.65999	0.73700	0.93462	1.16779

6.4 Summary

The steady flow of gyrotactic microorganisms in a mixed convection boundary layer through an inclined cylinder is analysed in this chapter. The outcomes show that multiple solutions exist in the free convection-dominated regime. The critical point separates the upper branch and lower branch solutions indicating stable and unstable solutions. The following is a summary of the major reviews:

- The variation in the Nusselt number indicates that a dual solution exists for the temperature profile $\lambda > \lambda_c$, where the critical values $\lambda_c = 0.31, 0.28, 0.24$ for the curvature parameter $\gamma = 0.3, 0.4, 0.5$, and the critical value $\lambda_c = 0.20, 0.25, 0.28$ for the exponent $m = 0.6, 0.8, 1.0$.
- The variation of Sherwood number shows the existence of dual solution in concentration profile, when $\lambda > \lambda_c = 0.10, 0.17$ for $\gamma = 0.2, 0.5$, and $\lambda_c = 0.03, 0.07, 0.10$ for the $m = 0.6, 0.8, 1.0$, respectively.
- Variations in the density of microorganisms show that the dual solution of the microorganism profile arises when $\lambda > \lambda_c = 0.25, 0.26, 0.27$ for $\gamma = 0.1, 0.2, 0.3$ and $\lambda_c = 0.25, 0.26, 0.27$ for the $m = 0.8, 0.9, 1.0$, respectively.

Chapter 7

Assisting and opposing mixed convective flow over a solid sphere at its bottom stagnation point with a constant surface heat, mass and mobile microorganism flux

The laminar mixed-convective flow approaching a lower level of stagnation of a solid sphere with constant heat, mass, and motile microbe flux containing gyrotactic microorganisms was investigated in this study. First, a non-dimensional set of equations employing dimensionality-free variables is created from the fundamental boundary layer equations, which are next utilised to address the reduced ordinary differential equations at the lowest stagnation point of the sphere computationally. A dual solution was discovered in a specific region of mixed convection when the rates of wall heat, mass, and microbe transfer were monitored for opposing as well as aiding flows.

7.1 Mathematical formulation

In this study, we considered the laminar mixed convection flow over a radially heated as well as cooled solid sphere with radius nested in medium with pores harbouring gyrotactic microorganisms. The coordinate framework and flow diagram displayed in **Fig. 7.1**, where the coordinates $\bar{x}, \bar{y}$ measure the distance measured perpendicular to the sphere's surface and along the sphere's exterior from the stagnation point, respectively, and $\bar{u}_e(\bar{x})$ is considered the external flow velocity.

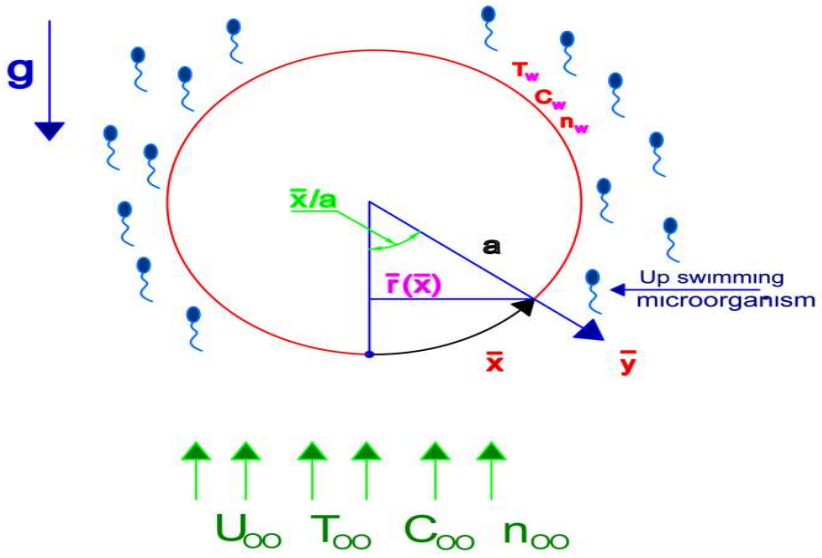

Fig 7.1 Coordinates and the physical model

According to the models proposed by Fauzi *et al*. (2014) and Tham *et al.* (2013), under the aforementioned assumptions and invoking the Boussinesq approximation, the governing partial differential equations describing the conservation of mass, momentum, energy, and microorganisms can be expressed in the following way:

$$\frac{\partial(\bar{r}\vec{u})}{\partial\bar{x}}+\frac{\partial(\bar{r}\vec{v})}{\partial\bar{y}}=0 \tag{7.1}$$

$$\frac{\partial\bar{u}}{\partial\bar{y}}=\pm\frac{gk\rho}{\mu}\left(\beta_T\frac{\partial T}{\partial\bar{y}}+\beta_C\frac{\partial C}{\partial\bar{y}}+\beta_n\frac{\partial n}{\partial\bar{y}}\right)Sin\left(\frac{\bar{x}}{a}\right) \tag{7.2}$$

$$\bar{u}\frac{\partial T}{\partial\bar{x}}+\bar{v}\frac{\partial T}{\partial\bar{y}}=\alpha\frac{\partial^2 T}{\partial\bar{y}^2} \tag{7.3}$$

$$\bar{u}\frac{\partial C}{\partial\bar{x}}+\bar{v}\frac{\partial C}{\partial\bar{y}}=D_m\frac{\partial^2 C}{\partial\bar{y}^2} \tag{7.4}$$

$$\bar{u}\frac{\partial n}{\partial\bar{x}}+\bar{v}\frac{\partial n}{\partial\bar{y}}+\frac{bW_c}{\nabla C}\left(\frac{\partial^2 C}{\partial\bar{y}^2}\right)=D_n\frac{\partial^2 n}{\partial\bar{y}^2} \tag{7.5}$$

Boundary condition can be expressed as follows:

$$\bar{v} = 0, \frac{\partial T}{\partial \bar{y}} = \frac{-q_w}{k}, \frac{\partial C}{\partial \bar{y}} = -\frac{-q_m}{D_m}, \frac{\partial n}{\partial \bar{y}} = -\frac{q_n}{D_n} \qquad \text{at } \bar{y} = 0 \tag{7.6}$$

$$\bar{u} = \bar{u}_e(\bar{x}), T \to T_\infty, C \to C_\infty, n \to n_\infty \qquad \text{at } \bar{y} \to \infty \tag{7.7}$$

where $\bar{r}(\bar{x}) = aSin(\frac{\bar{x}}{a})$ is the radial distance from the sphere's symmetric axis, and the local free-stream velocity is $\bar{u}_e(\bar{x}) = \frac{3}{2} u_\infty Sin(\frac{\bar{x}}{a})$. $\bar{x}, \bar{y},$ which correspond to velocities $\bar{u}$ and $\bar{v}$ respectively. In Equation (7.2), the addition sign (+) denotes the assisting flow and the negative (-) symbol denotes the opposing flow. $T_w > T_\infty$ is assumed for the heated sphere (assisting flow), and $T_w < T_\infty$ is assumed regarding a cooled sphere (opposing flow).

To solve dimensions-based governing equations (7.1)−(7.5) subject to boundary conditions (7.6)−(7.7), we nondimensionalise these equations by incorporating the non-dimensional factors listed below:

$$x = \frac{\bar{x}}{a}, y = Pe^{\frac{1}{2}} \frac{\bar{y}}{a}, u = \frac{\bar{u}}{u_\infty}, v = Pe^{\frac{1}{2}} \frac{\bar{v}}{u_\infty}$$

$$\theta = \frac{kPe^{\frac{1}{2}}(T - T_\infty)}{q_w a}, \phi = \frac{D_m Pe^{\frac{1}{2}}(C - C_\infty)}{q_m a}, \chi = \frac{D_n Pe^{\frac{1}{2}}(n - n_\infty)}{q_n a} \tag{7.8}$$

$$Ra = \frac{g\beta_T q_w a}{\nu\alpha}, Pe = \frac{u_\infty a}{\alpha}$$

Substituting (7.8) in (7.1)−(7.7) we can procure the following:

$$\frac{\partial u}{\partial x} + \frac{\partial v}{\partial y} = 0 \tag{7.9}$$

$$\frac{\partial u}{\partial y} = \pm\lambda^3 \left(\frac{\partial \theta}{\partial y} + N_1 \frac{\partial \phi}{\partial y} + N_2 \frac{\partial \chi}{\partial y} \right) Sinx \tag{7.10}$$

$$u\frac{\partial\theta}{\partial x}+v\frac{\partial\theta}{\partial y}=\frac{\partial^2\theta}{\partial y^2} \tag{7.11}$$

$$u\frac{\partial\phi}{\partial x}+v\frac{\partial\phi}{\partial y}=\frac{1}{Le}\frac{\partial^2\phi}{\partial y^2} \tag{7.12}$$

$$u\frac{\partial\chi}{\partial x}+v\frac{\partial\chi}{\partial y}+\frac{Pe}{Lb}\left((A+\chi)\frac{\partial\phi}{\partial y}\right)=\frac{1}{Lb}\frac{\partial^2\chi}{\partial y^2} \tag{7.13}$$

Boundary conditions become as follows:

$$v=0,\theta'=-1,\phi'=-1,\chi'=-1 \qquad \text{at } y=0$$

$$u\to u_e(x),\theta\to 0,\phi\to 0,\chi\to 0 \qquad \text{at } y\to\infty \tag{7.14}$$

where mixed convection parameter $\lambda=\frac{Ra^{\frac{1}{3}}}{Pe^{\frac{1}{2}}}$, Lewis number $Le=\frac{\alpha}{D_m}$, buoyancy parameters $N_1=\frac{\beta_c\nabla Cq_m k}{\beta_T\nabla Tq_w D_m}, N_2=\frac{\beta_n\nabla nq_n k}{\beta_T\nabla Tq_w D_n}$, bioconvection Lewis number $Lb=\frac{\alpha}{D_n}$, bioconvection Peclet number $Pe=\frac{bW_c}{D_n}$, and microorganism concentration difference parameter $A=\frac{n_\infty}{n_w-n_\infty}$.

Equations (7.9)−(7.13) with boundary conditions (7.14) admit a similarity solution of the following form:

$$\psi=xr(x)f(x,y),\theta=\theta(x,y),\phi=\phi(x,y),\chi=\chi(x,y) \tag{7.15}$$

Where ψ denotes the stream function, is specified as follows:

$$u=\frac{1}{r}\frac{\partial\psi}{\partial y},v=-\frac{1}{r}\frac{\partial\psi}{\partial x} \tag{7.16}$$

Substituting (7.15) – (7.16) into equations (7.9) – (7.14) we obtain

$$\frac{\partial^2 f}{\partial y^2}=\pm\lambda^3\left(\frac{\partial\theta}{\partial y}+N_1\frac{\partial\phi}{\partial y}+N_2\frac{\partial\chi}{\partial y}\right)\frac{Sinx}{x} \tag{7.17}$$

$$\frac{\partial^2\theta}{\partial y^2} + f\frac{\partial\theta}{\partial y} = x\left(\frac{\partial f}{\partial y}\frac{\partial\theta}{\partial x} - \frac{\partial f}{\partial x}\frac{\partial\theta}{\partial y}\right) \tag{7.18}$$

$$\frac{\partial^2\phi}{\partial y^2} + Le.f\frac{\partial\phi}{\partial y} = xLe\left(\frac{\partial f}{\partial y}\frac{\partial\phi}{\partial x} - \frac{\partial f}{\partial x}\frac{\partial\phi}{\partial y}\right) \tag{7.19}$$

$$\frac{1}{Lb}\frac{\partial^2\chi}{\partial y^2} + f\frac{\partial\chi}{\partial y} - \frac{Pe}{Lb}\frac{\partial}{\partial y}\left((A+\chi)\frac{\partial\phi}{\partial y}\right) = x\left(\frac{\partial f}{\partial y}\frac{\partial\chi}{\partial x} - \frac{\partial f}{\partial x}\frac{\partial\chi}{\partial y}\right) \tag{7.20}$$

Considering the boundary conditions

$$f = 0, \frac{\partial\theta}{\partial y} = -1, \frac{\partial\phi}{\partial y} = -1, \frac{\partial\chi}{\partial y} = -1 \qquad \text{at } y = 0$$

$$f' \to \frac{3}{2}\frac{Sinx}{x}, \theta \to 0, \phi \to 0, \chi \to 0 \qquad \text{at } y \to \infty \tag{7.21}$$

According to (Fauzi *et al*. (2014), Tham *et al*. (2013)) we can remark that at the sphere's lower stagnation point, that is, (x≈ 0). The following ordinary differential equations result from the reduction of equations (7.17) – (7.21):

$$f'' = \pm\lambda^3\left(\theta' + N_1\phi' + N_2\chi'\right) \tag{7.22}$$

$$\theta'' + f\theta' = 0 \tag{7.23}$$

$$\phi'' + Lef\phi' = 0 \tag{7.24}$$

$$\chi'' + Lbf\chi' - Pe\left(\phi'\chi' + (A+\chi)\phi''\right) = 0 \tag{7.25}$$

With the boundary conditions

$$f(0) = 0, \theta'(0) = -1, \phi'(0) = -1, \chi'(0) = -1 \qquad \text{at} \quad y = 0$$

$$f'(\infty) = \frac{3}{2}, \theta(\infty) = 0, \phi(\infty) = 0, \chi(\infty) = 0 \qquad \text{at } y \to \infty \tag{7.26}$$

Where prime represents differentiation with respect to y.

7.2 Solution methodology

By utilising non-dimensional variables, the governing equations in this work were first converted into a array of non-dimensional equations, and then finally becoming ordinary differential equations at the lower stagnation point of the sphere considering $x \approx 0$. Then nonlinear ordinary differential equations were mathematically solved using the MATLAB bvp4c solver. In the case of opposing flows using different initial guesses of $f, f', \theta, \theta', \phi, \phi', \chi, \chi'$, we can find two types of solutions. With regard to the aforementioned bvp4c function, the governing equations must be transformed into first-order differential equations. First Equations (7.11)−(7.14) can be rearranged as follows:

$$f'' = \pm\lambda^3\left(\theta' + N_1\phi' + N_2\chi'\right)$$
$$\theta'' = -f\theta'$$
$$\phi'' = -Lef\phi'$$
$$\chi'' = -Lbf\chi' + Pe\left(\phi'\chi' + (A+\chi)\phi''\right)$$

This equation must be changed into a first-order differential equation. For this let $\eta = x$ and

$$y_1 = f, y_2 = f'$$
$$y_3 = \theta, y_4 = \theta', y_5 = \phi,$$
$$y_6 = \phi', y_7 = \chi, y_8 = \chi'$$

First order differential equations that apply to these problems are:

$$\frac{dy_1}{dx} = f' = y_2$$
$$\frac{dy_2}{dx} = f'' = \pm\lambda^3\left(y_4 + y_6N_1 + y_8N_2\right)$$
$$\frac{dy_4}{dx} = \theta'' = -y_1y_4$$
$$\frac{dy_6}{dx} = \phi'' = -Ley_1y_6$$
$$\frac{dy_8}{dx} = \chi'' = -Lby_1y_8 + Pe\left(y_6y_8 + (A+y_7)(-Ley_1y_6)\right)$$

The boundary conditions are changed such that yp be the left edge and yq be the right edge.

$$yp(1) = 0, yq(2) - 3/2 = 0$$
$$yp(4) + 1 = 0, yq(3) = 0$$
$$yp(6) + 1 = 0, yq(5) = 0$$
$$yp(8) + 1 = 0, yq(7) = 0$$

To validate the results, with the assistance of the dsolve command, the differential equations were mathematically resolved applying Maple. The outcomes for both situations are provided in **Table 7.1.** This shows the accuracy and high agreement of the mathematical calculations.

Table 7.1 Effect of mixed convection parameter λ on $\theta_w(0)$ when $N_1 = 0.1, N_2 = 0.3, Lb = 1.0, Le = 1.0, Pe = 0.3, A = 0.2$

λ	$\theta_w(0)$ (MATLAB Bvp4c) First Solution	$\theta_w(0)$ (Maple) First Solution
0.0	1.023327	1.023326
0.3	1.015545	1.015545
0.5	0.989574	0.989574
0.8	0.911108	0.911108
1.0	0.843289	0.843289
2.0	0.549716	0.549716

For further confirmation, the present conclusion for the specific situation is compared to the findings of studies by Alsenafi and Ferdows (2021) and Chamkha and Khaled (2000), which are listed in Table 7.2.

Table 7.2 Comparison of $f'(0)$ for the values of $N_1 = 0.0, N_2 = 0.0, Lb = 0.0, Le = 0.0, Pe = 0.0, A = 0.0, \lambda = 0$			
	Present Result (First Solution)	Chamkha and Khaled (2000)	Alsenafi and Ferdows (2021)
$f'(0)$	1.0000	1.0000	1.0000

7.3 Numerical results and discussion

This section features several flow characteristics for assisting and opposing flows are analysed. For opposing flows, dual solutions were found for some specific parameters. These solutions are referred to as the first solution and the second solution, respectively, for opposing flows. The first solution in this study is shown by the solid line, whereas the second solution is shown by the dashed lines.

7.3.1. *Analysis of the velocity profile:*

Fig. 7.2(a) demonstrates that the velocity profile grows with the mixed convection value λ for assisting flow. Increased mixed convection parameter numerical values for aiding flow correspond to increased buoyancy forces during the flow and result in an increase in velocity profiles. An overshoot in velocity profiles can be noticed close to the surface due to rising mixed convection parameter, which corresponds to the pressure gradient scenario that is beneficial for the flow near the surface. In **Fig. 7.2(b)**, dual solution is noticed in the event of opposing flow, where for the first solution, the velocity profile falls as the mixed convection parameter increases. Opposite phenomena is seen with regard to the second solution. In **Figs. 7.3** and **7.4**, effects of buoyancy forces N_1, N_2 on velocity profile are shown. Buoyancy parameters N_1, N_2, which accounts for thermal and solutal buoyancy has sped up the flow in assisting flows, increasing the velocity profile. If there is opposing flows, velocity profile decreases, as shown in **Figs. 7.2(b) and 7.3(b)**. We can observe that in opposing flow cases, first solution is stable and

since the velocity profile changed to a negative value, the second solution is unstable. The velocity flow profiles show that the dual solution is present when $\lambda > \lambda_C$.

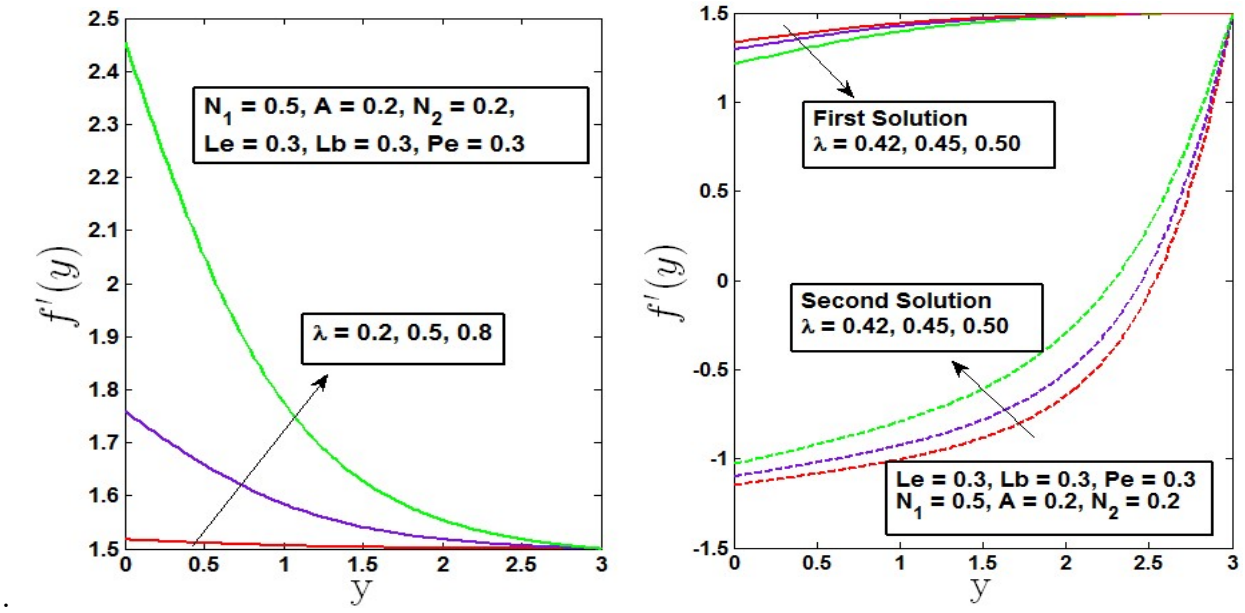

(a) **(b)**

Fig. 7.2 Velocity profile on varying values of λ a) assisting flow b) opposing flow

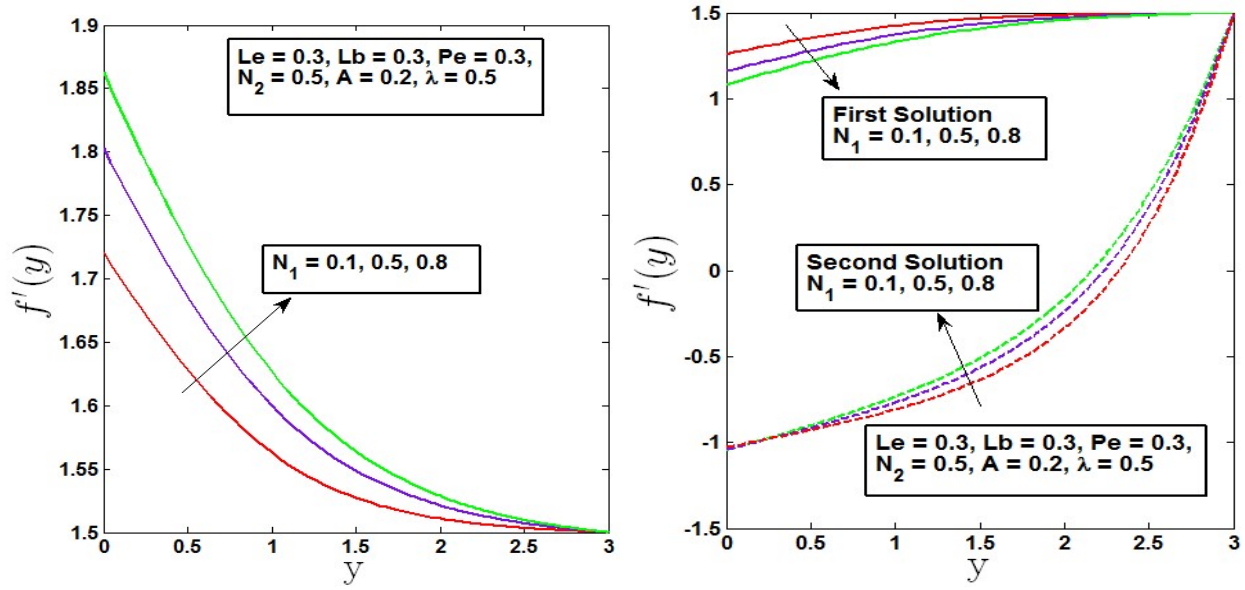

(a) **(b)**

Fig. 7.3 Velocity profile on varying values of N_1 a) assisting flow b) opposing flow

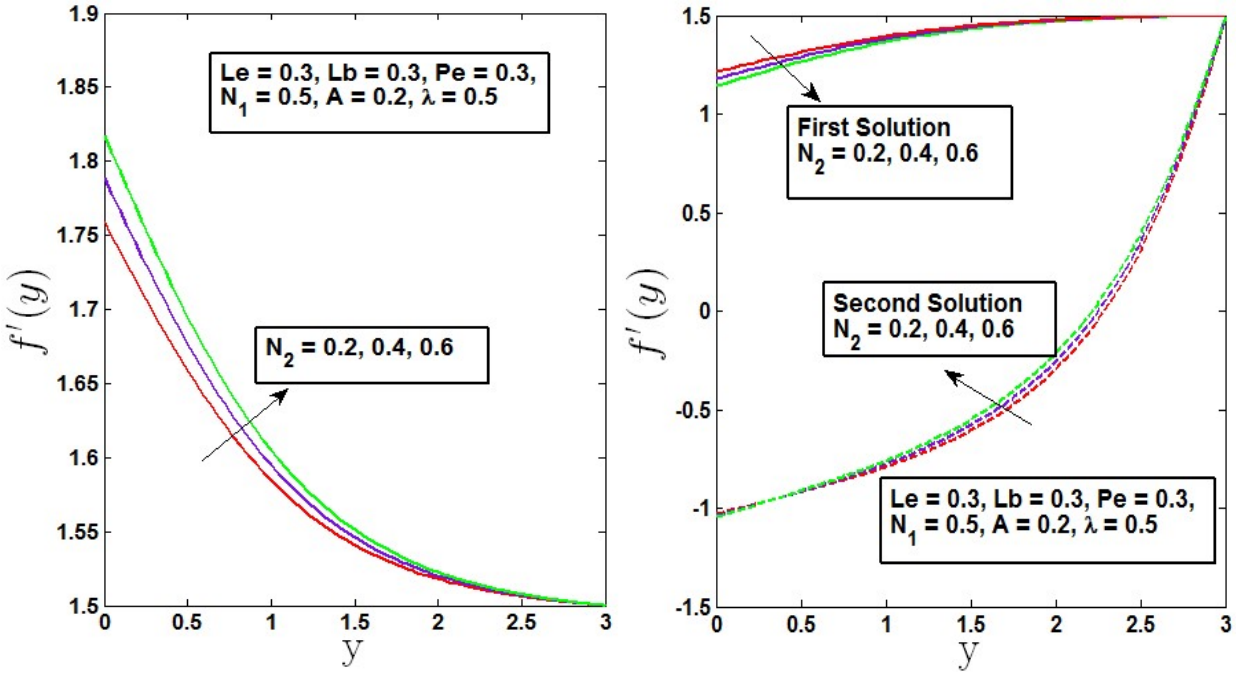

(a) **(b)**

Fig. 7.4 Velocity profile on varying values of N_2 a) assisting flow b) opposing flow

7.3.2. *Analysis of temperature profile:*

Fig. 7.4 shows the variant of wall temperature θ_w with λ for different values of N_1 is shown in. Increasing values of λ and N_1 raise the motion of the fluid results in higher heat transfer rate, as a result in case of assisting flow, a wall's temperature drops as values rise of λ and N_1 seen in **Fig. 7.5(a)**. So it is clearly observed that the temperature profile decreases within the range of $0 < \lambda < 1$. So for the values $\lambda = 0.2,0.5,0.8$ and also for growing values of N_1 decreasing temperature profile has been observed in **Fig. 7.6(a).** As shown in **Fig. 7.4 (b),** dual solution exists for the wall temperature in case of opposing flow. For $N_1 = 0.1,$ dual solution is present at the range $0.49 < \lambda < 0.65$, and for $N_1 = 0.3$, dual solution is present at the range $0.48 < \lambda < 0.65$. For $N_1 = 0.1$, $\lambda_C = 0.49,0.65$ and for $N_1 = 0.3$, $\lambda_C = 0.48,0.65$ are the critical values, where both solutions are connected and at this point distinct solution exist. Dual solution for temperature profile for different values of λ is shown in **Fig. 7.5(b)**. In **Figs. 7.5(b), 7.6(b), 7.7(b),** and **7.8(b).** We can see that the temperature profile rises when the values of λ, N_1, and N_2

rise for solution in case of opposing flows. When using the second solution, opposite effects are seen.

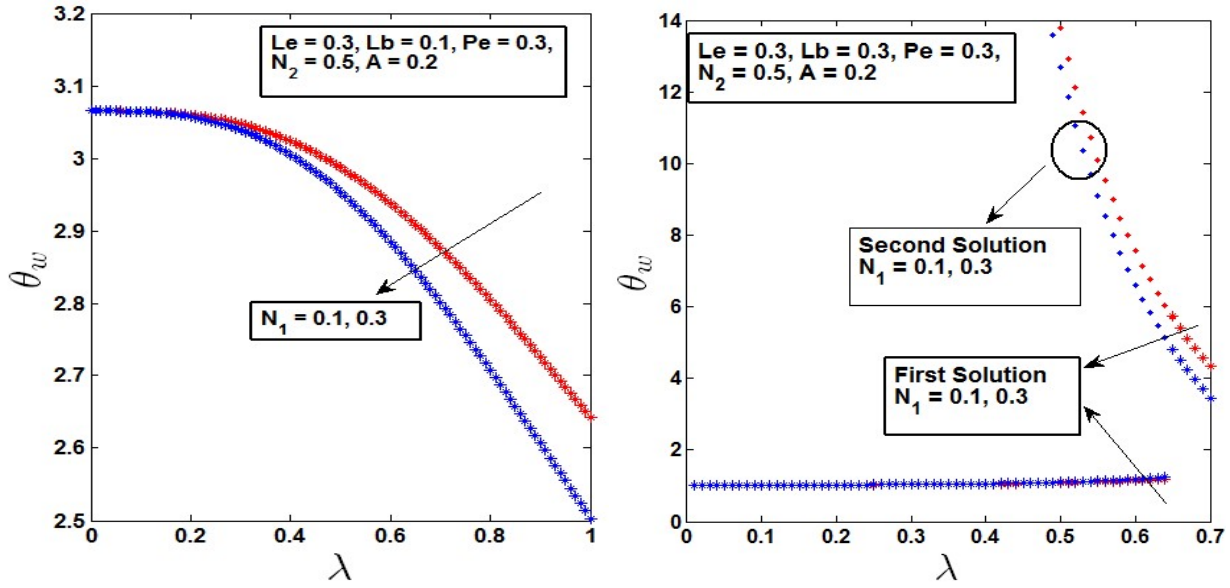

(a) **(b)**

Fig. 7.5 Wall temperature variation with λ a) assisting flow b) opposing flow

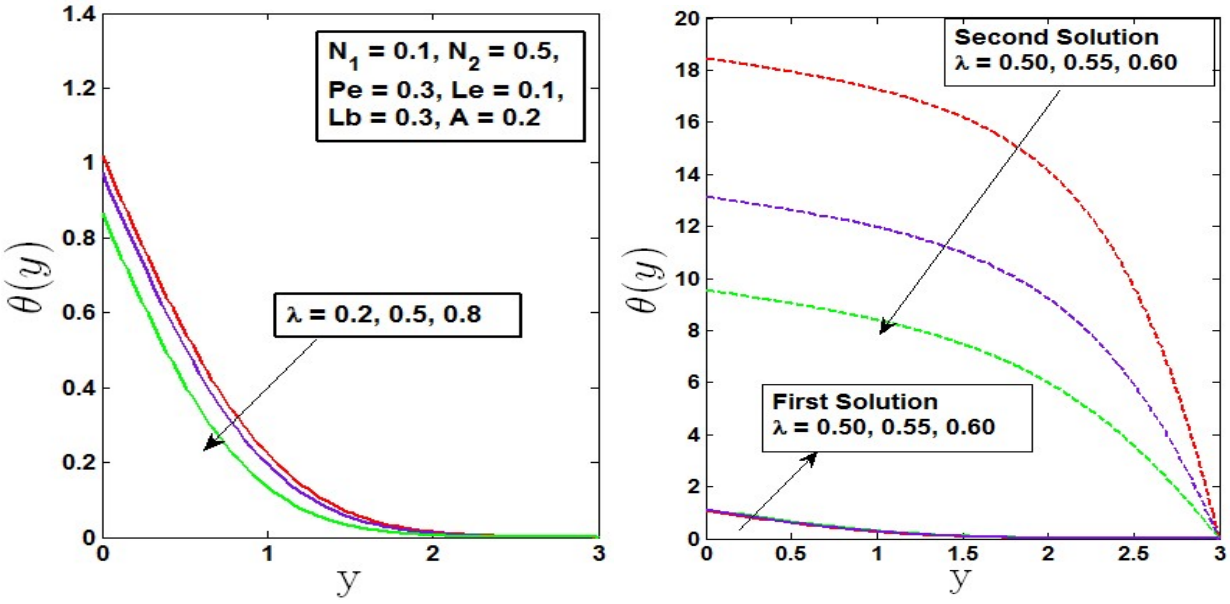

(a) **(b)**

Fig. 7.6 Temperature profile on varying values of λ a) assisting flow b) opposing flow

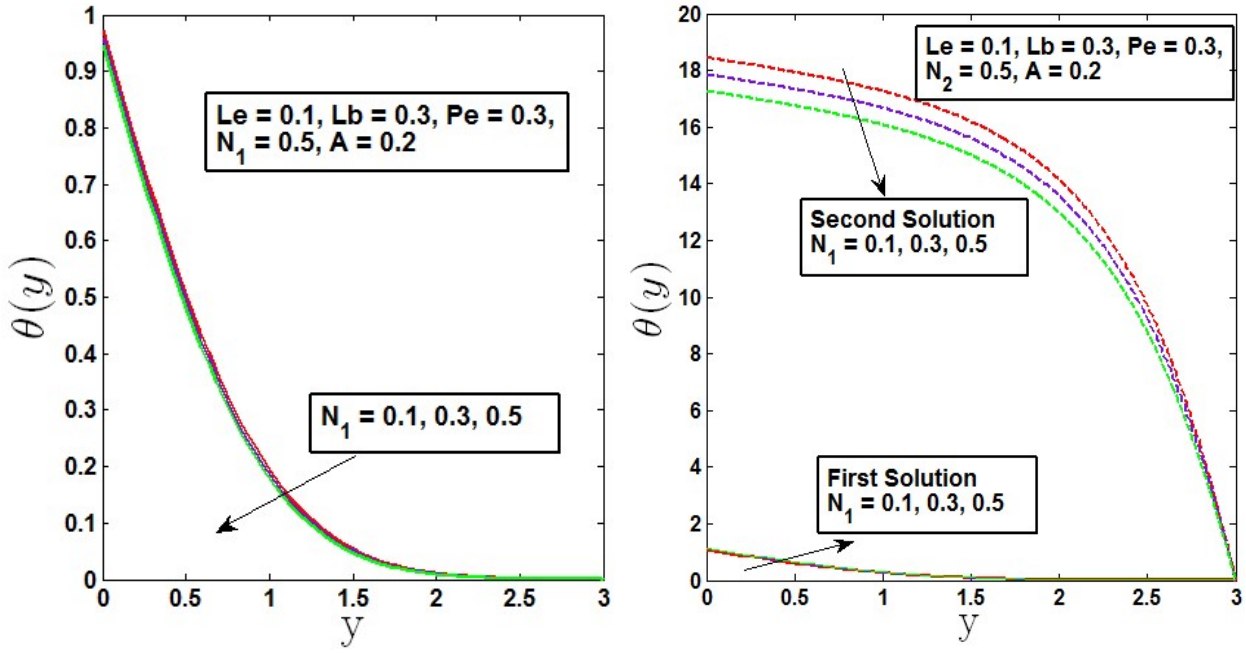

(a) **(b)**

Fig. 7.7 Temperature profile on varying values of N_1 a) assisting flow b) opposing flow

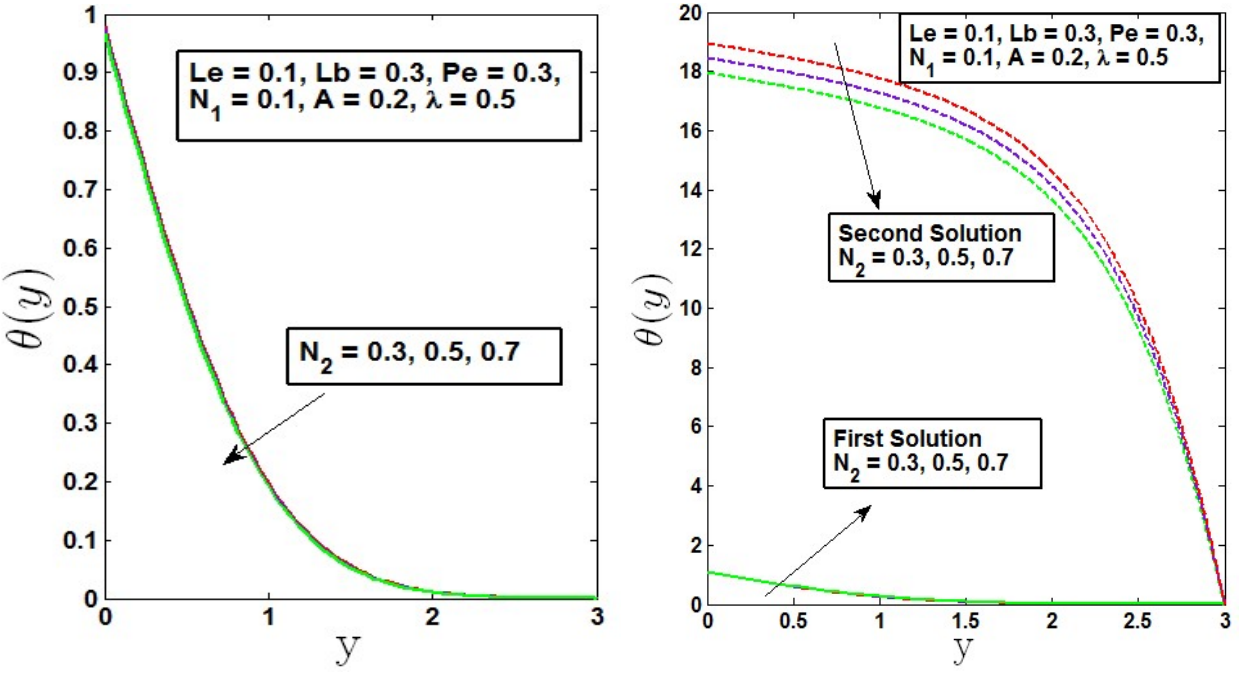

(a) **(b)**

Fig. 7.8 Temperature profile on varying values of N_2 a) assisting flow b) opposing flow

7.3.3. Analysis *of Concentration profile:*

Fig. 7.9 shows the variant of wall fluid concentration φ_w with λ for the values of Le, for aiding flow and also for opposing flow. With the growing values of λ and Le, In opposing flow, wall concentration rises, although when η≈ 0.57 suddenly, φ_w decreases for first solution in **Fig. 7.9(b).** Growing values of λ and Le, accelerates rate of mass transfer which lessen the quantity of fluid near wall lowers the concentration profile are seen in **Fig. 7.9(a)**. As shown in **Figs. 7.10(a)** and **7.11(a)**, concentration profile decreases with the increasing values of λ and Le for assisting flow. Bioconvection Lewis number and diffusion coefficient are inversely related; therefore, rise of Le results in fall of concentration profile. For opposing flow concentration profile raises with λ and drops with the growing values of Le for the first solution. In **Fig. 7.9(b)**, dual solution is observed for Le = 0.1 when 0.41< λ< 0.57, and for Le = 0.2 when 0.42< λ< 0.57. Therefore, in between the range of critical points dual solutions are observed in **Figs. 7.10(b)** and **7.11(b)**, where concentration profiles decline with growing values of mixed convection parameter and increase with Le for the second solution.

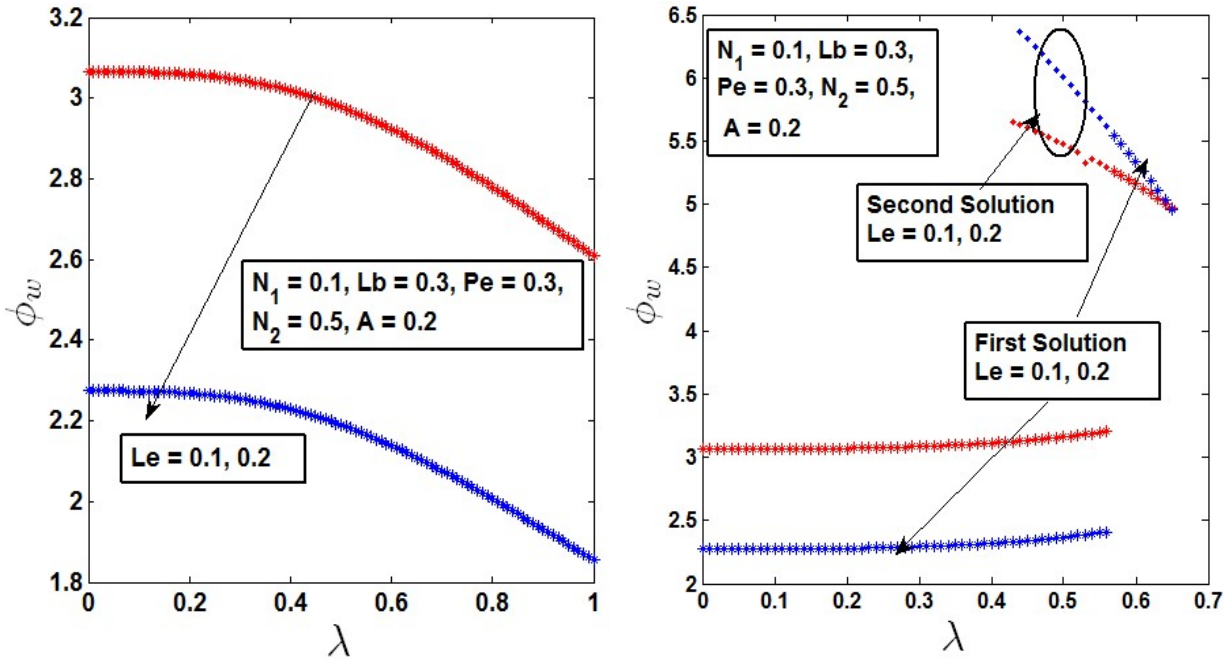

(a) **(b)**

Fig. 7.9 Variation of wall fluid concentration with λ a) assisting flow b) opposing flow

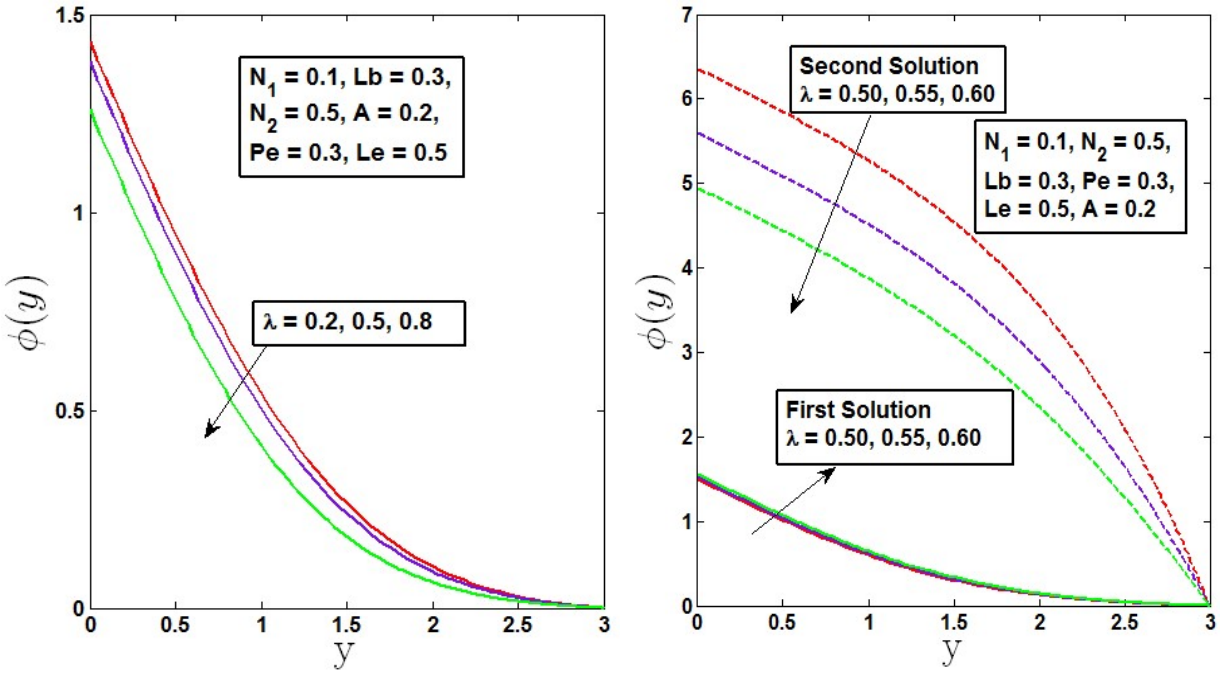

(a) **(b)**

Fig. 7.10 Concentration profile on varying values of λ a) assisting flow b) opposing flow

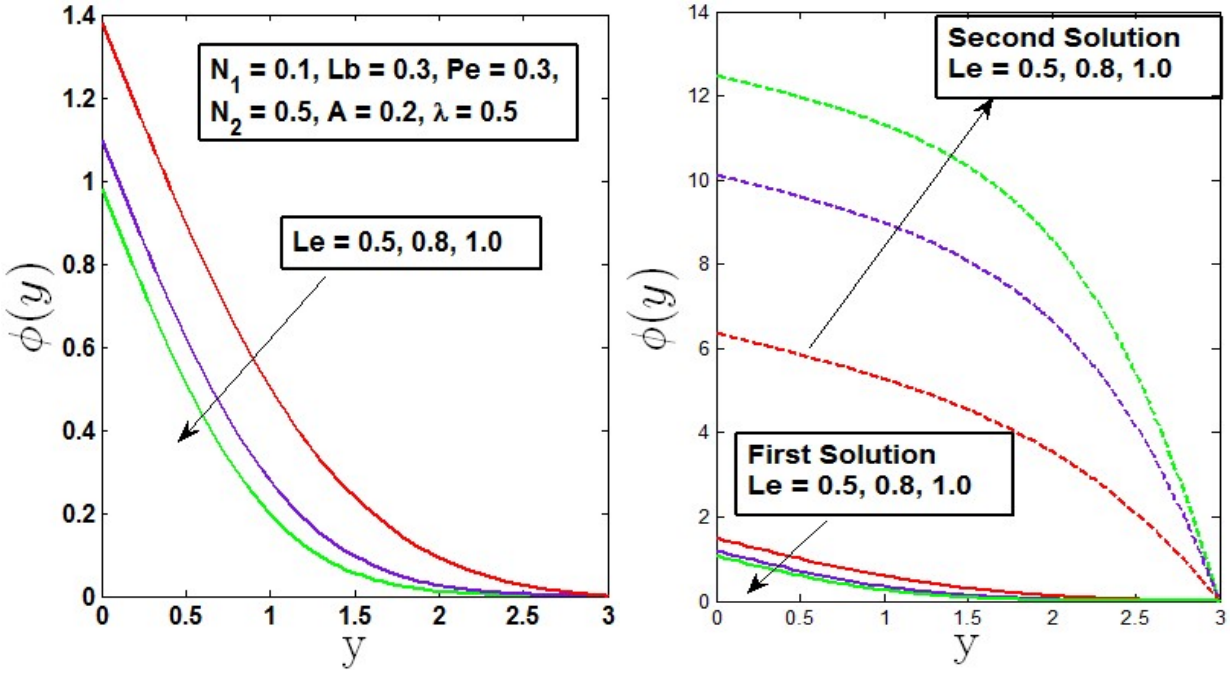

(a) **(b)**

Fig. 7.11 Concentration profile on varying values of *Le* a) assisting flow b) opposing flow

7.3.4. *Analysis of Microorganism profile*

In **Fig. 7.12,** impact of λ and bioconvection Peclet number on wall microorganism concentration φ_w are shown for assisting flow and opposing flow. The effect of the bioconvection Peclet number increases the swimming rate of the motile microorganisms, and this property causes the microorganisms' thickness to decrease near the surface. With the rising values of λ and Pe , For aiding flow, wall microbe concentration falls, while for opposing flow, it rises., although when η≈ 0.57 suddenly, χ_w decreases, which is similar to wall concentration. In opposing flow for 0.48< λ< 0.57, dual solution is observed in **Fig. 7.12(b)**.

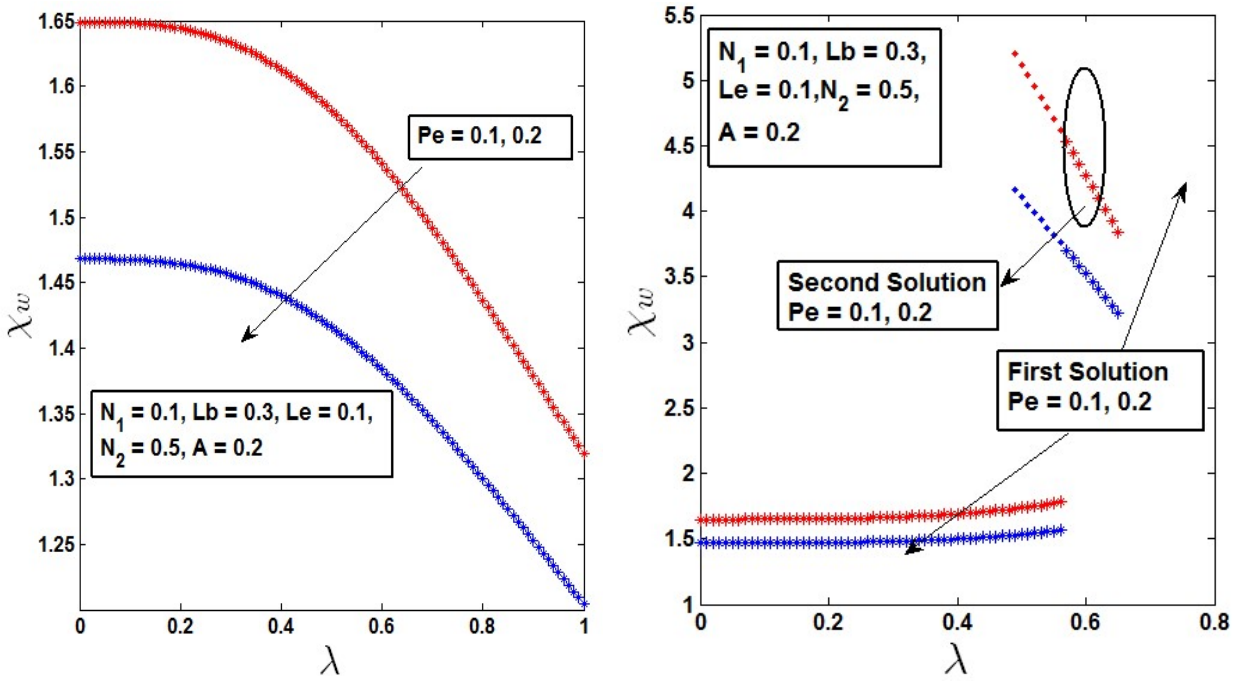

(a) **(b)**

Fig. 7.12 Variation of local wall microorganism concentration with λ a) assisting flow b) opposing flow

Fig. 7.13 shows that mixed convection parameter λ decreases for microorganism profile for aiding flow and increases for opposing flow. In case of opposing flow dual solution shows opposite phenomena. Bioconvection Lewis number decreases microorganism profile up to η≈ 0.7 after that it and increases in case of assisting flow. According to **Fig. 7.14(a),** as *Le*

increases, the viscous diffusion rate increases. As a result, the fluid speed at the surface reduces, which in turn results in a reduction in the density distribution of the motile microorganisms. On the other hand, in **Fig. 7.14(b),** Le reduces the microorganism profile in the first solution for opposing flow and raises it for the second solution. Reduced motile microorganism diffusivity leads to decreased bioconvection Lewis number Lb, which lowers the concentration of microorganisms in **Fig 7.15.** As the wall microorganism profile exhibits dual solution between $0.48 < \lambda < 0.57$ in regard to opposing flow, opposing microorganism profile phenomenon is seen considering $\lambda = 0.5$ for expanding values of Lb as shown in **Fig. 7.15(b)**. Two different types of solutions are shown in **Fig. 7.15(b)**, where the second solution is not asymptotically stable.

By contrast, increase in bioconvection Peclet number increases the mobility of fluid, causing reduction in quantity of motile microorganism's thickness, hence microorganism's diffusivity and their concentration decreases. The convection of motile microorganism shown in **Fig. 7.16** reduces for greater increase in the bioconvection Peclet number Pe for the both assisting and opposing flow. **Fig. 7.16(b)** display dual solutions beyond the critical points. So, it is evident that mixed convection only exhibits an unstable solution for opposing flow in a particular region. Only stable solutions can be produced in cases where there is an aiding flow.

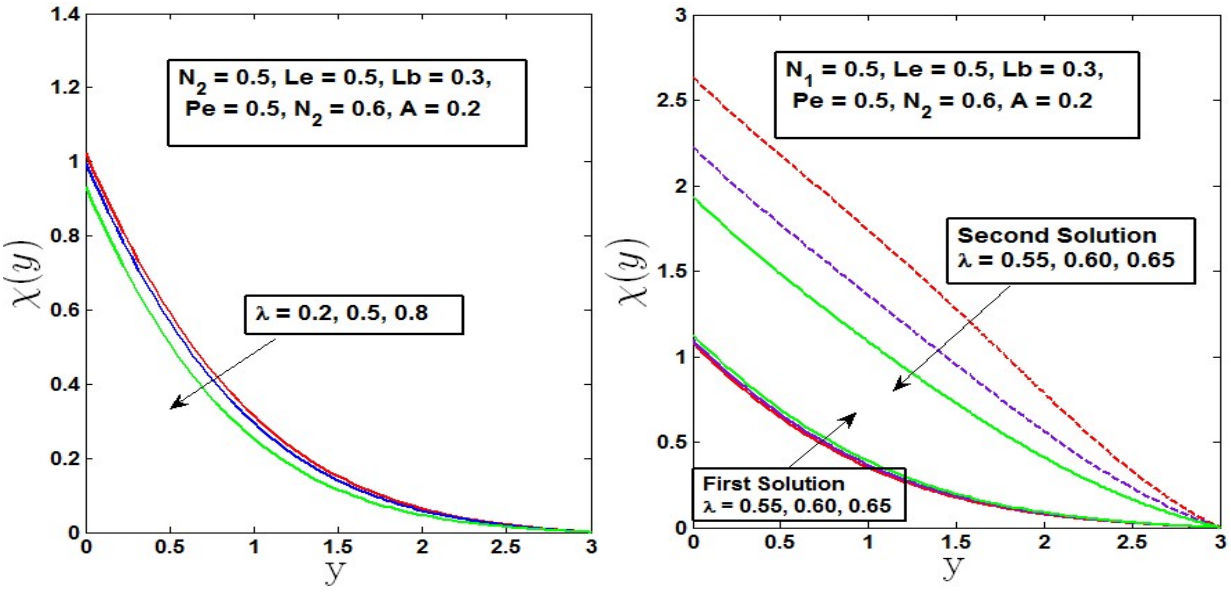

(a) **(b)**

Fig. 7.13 Microorganism profile on varying values of λ a) assisting flow b) opposing flow

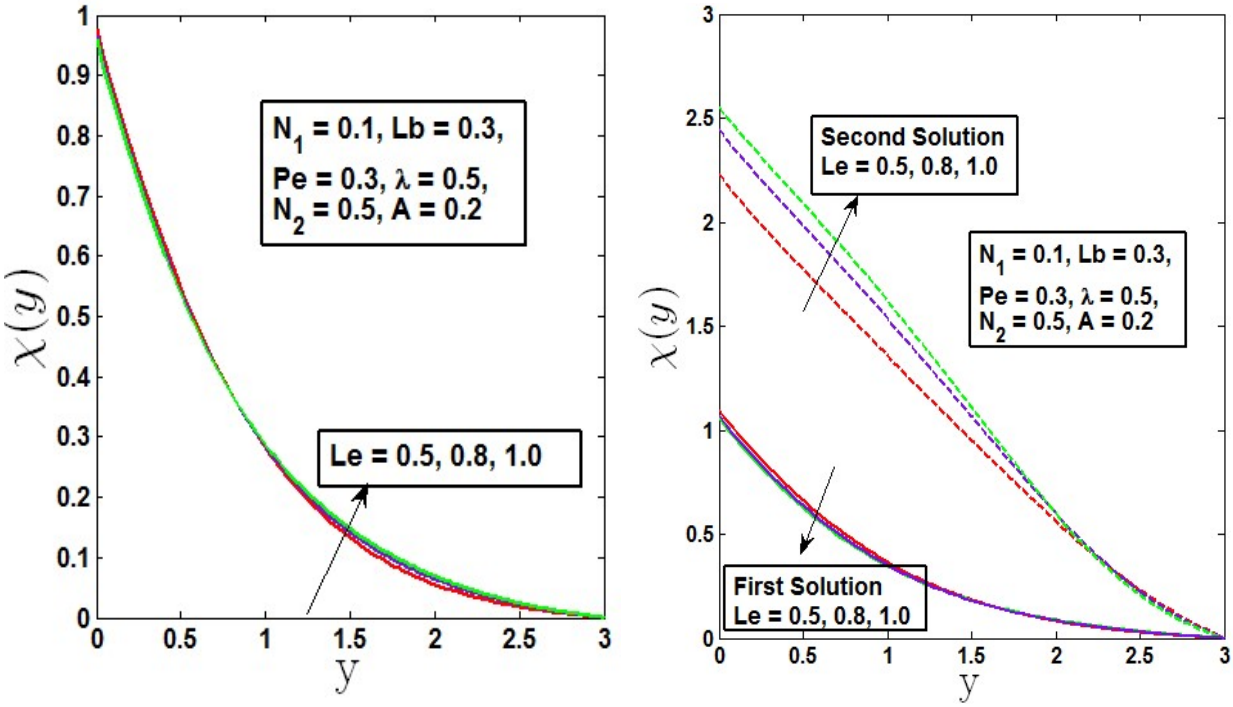

(a) **(b)**

Fig. 7.14 Microorganism profile on varying values of *Le* a) assisting flow b) opposing flow

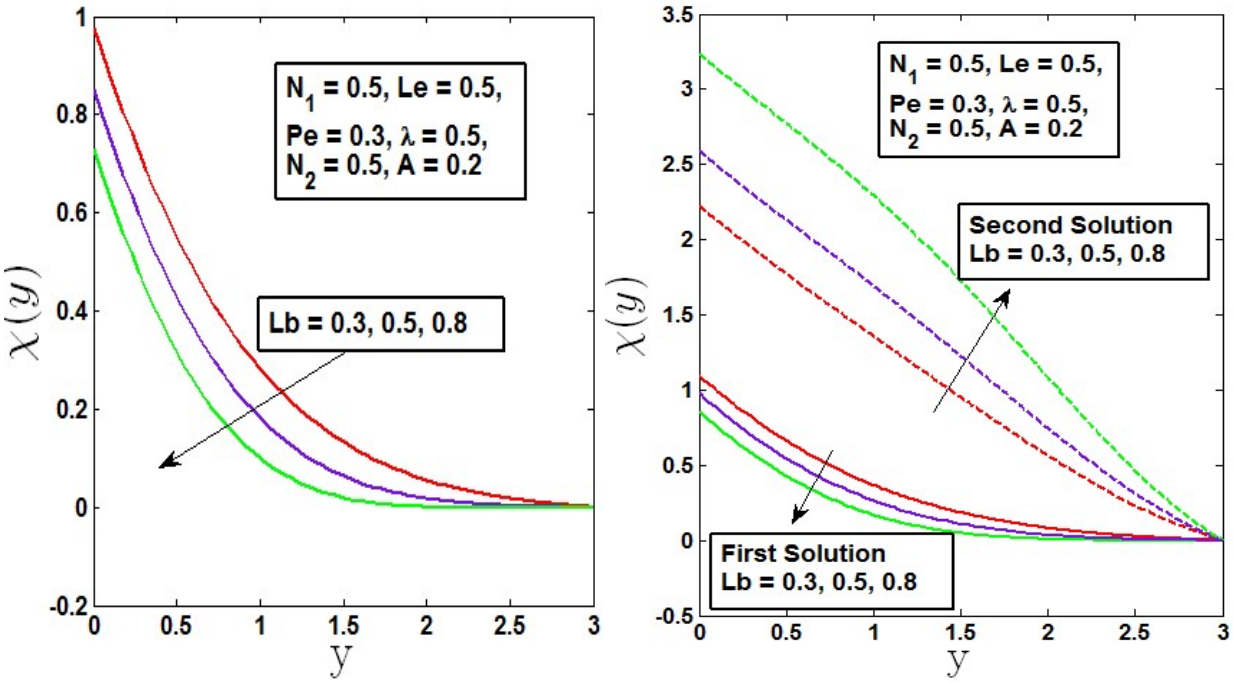

(a) **(b)**

Fig. 7.15 Microorganism profile on varying values of *Lb* a) assisting flow b) opposing flow

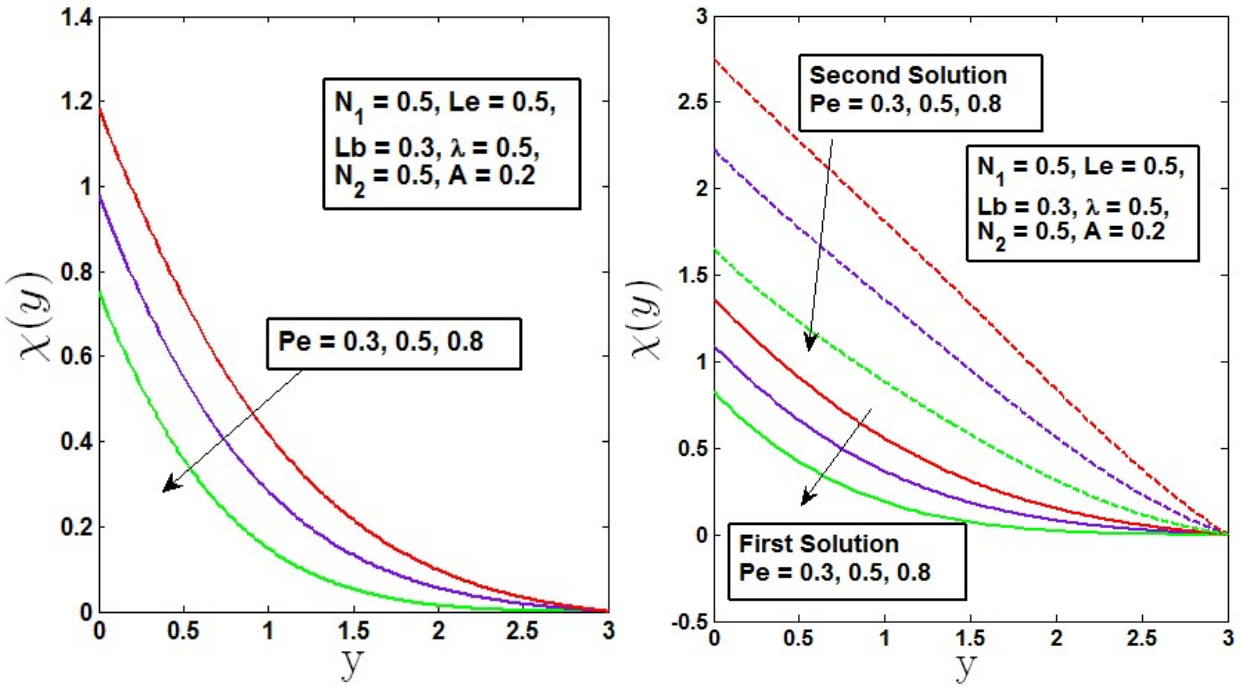

(a) **(b)**

Fig. 7.16 Microorganism profile on varying values of Pe a) assisting flow b) opposing flow

The physical quantities of primary concern in practical applications are heat, mass, and motile microbe transmission, which can be expressed in the following non-dimensional manner:

$$\theta_w(x) = \theta(x,0), \phi_w(x) = \phi(x,0), \chi_w(x) = \chi(x,0)$$

7.4 Summary

Analysis of aiding and opposing flows is done for the steady combined convective boundary layer flow containing gyrotactic microorganisms close to the lower stagnation point of a solid sphere with constant heat, mass, and motile microorganism flux. For opposing flows, it was discovered that there were two possible solutions. Following is an overview of the major reviews:

- For assisting, the flow velocity profile increases with an increase in the values of the mixed convection parameter λ and the buoyancy parameters N_1, N_2 and it decreases when

it comes to opposing flow, where dual solutions are also observed for a specific range of mixed convection parameters.

- The assisting flow wall temperature decreased with the variation in λ with increasing values of N_1. Consequently, temperature profile also decreased with λ, N_1 and N_2. Opposite phenomena were observed when it comes to opposing flows. Wall temperature variation with λ shows dual solution at the range $0.49 < \lambda < 0.65$ when N_1 = 0.1, and for N_1 = 0.3 dual solution resides at the range $0.48 < \lambda < 0.65$. Therefore, the temperature profiles also show a dual solution for this specific range of λ when it comes to opposing flow.
- The wall fluid concentration and concentration profiles become less pronounced with rising levels of λ and Le for assisting flow. Dual solution exists for opposing flow at the range $0.41 < \lambda < 0.57$ when Le = 0.1 and for Le = 0.2 at the range $0.42 < \lambda < 0.57$.
- The wall Microorganism concentration decreases with increasing values of λ and the bioconvection Peclet number Pe in the case of assisting flow. Therefore, the mixed convection parameter λ, Lewis number Le, biconvection Peclet number Pe, and bioconvection Lewis number Lb decreased the boundary layer thickness of the microorganism profile. For opposing flow dual solution exists for microorganism profile at the range $0.48 < \lambda < 0.57$ when Pe = 0.1, 0.2.

Chapter 8

Conclusion

8.1 Summary of the findings

This dissertation presents the study of free forced convective stable incompressible fluid flows over various geometries that contain gyrotactic microorganisms. The Darcy model and Oberbeck Boussinesq approximation assumptions were used to developing governing equations that account for the principle of momentum conservation, heat energy, mass, and motile microorganisms. In Chapter 2, An examination of the flow of a free-forced convective boundary layer from a vertical plate buried in a permeable Darcian medium has been conducted theoretically and computationally as a biomathematical model of near-wall PEM fuel cell transport phenomenon. In Chapter 3, the bioconvection process has been observed with heat generation effects and variable fluid properties such as variable permeability, variable porosity, variable effective thermal diffusivity, variable effective solute diffusivity, and variable effective diffusivity of microorganisms. Chapter 4 deals with the steady mixed convective flow of a non-Newtonian fluid containing gyrotactic microorganisms in the presence of non-Darcy and melting phenomena. In Chapter 5, gyrotactic mixed convective non-Darcy flow was observed accompanied by dispersion's effects and the presence of convective boundary circumstances. Dual solutions have been observed for non-isothermal inclined cylinders with the gyrotactic microorganism-saturated free forced convective flow in Chapter 6. Over a certain area of the sphere, a two-dimensional steady mixed-convection flow considering constant heat, mass and motile microorganism flux was investigated in Chapter 7. The following significant outcomes are noticed in this dissertation:

- The effects of buoyancy parameters Nb, bioconvection Rayleigh number Rb, Lewis number Le, bioconvection Lewis number Lb and bioconvection Peclet number Pe in the forced convection regime are more pronounced than in pure free convection regime.
- The density of motile microorganisms increases with bioconvection Lewis number Lb, Lewis number Le, and bioconvection Peclet number Pe, implying improved performance in the near wall zone of the fuel cell.
- Temperature, concentration and microorganism profiles decrease with mixed convection parameter λ which means for pure free convection to pure forced convection. And all the profiles decrease mostly for variable permeability and non-porous cases.
- Lewis number Le reduces concentration and microbe profile in the presence of varying permeability, while the profiles rise for non-Newtonian fluid.
- Bioconvection Lewis parameter Lb and bioconvection Peclet number Pe decrease microorganism profile especially for variable permeability and absence of porous media. On the other hand, for the influence of non-Newtonian fluid mostly for pseudoplastic fluid, Lb and Pe raise the microorganism profile.
- Particularly for medium with variable permeability and without porous structure, bioconvection Lewis number Lb and bioconvection Peclet number Pe reduce the microorganism profile. However, Lb and Pe cause the microbe profile to increase due to the action of non-Newtonian fluid, particularly pseudoplastic fluid.
- Nusselt number, Sherwood number and motile microorganism density number increase with buoyancy parameters N_1, N_2 in the presence of variable permeability comparing to Uniform permeability.
- The non-Darcy parameter F and melting parameter causes a drop in the Nusselt number, Sherwood number, and motile microbe density number, primarily for dilatant fluid.
- Nusselt number, Sherwood number and motile microorganism density number increase with mixed convection parameter λ mostly for pseudoplastic fluid.
- The impact of thermal, solute, and microbiological dispersion exhibits stimulating behaviour in forced convection when compared to free and mixed convection. Therefore, under the forced convection regime, the flow transfer rate with the influence of the Biot numbers diminishes as the dispersion impact grows.

- Dual solution phenomena can be observed in the free convective regime while observing heat, mass and motile microorganism transfer rate over non isothermal inclined cylinder beyond a critical point and results indicate that first solution is stable (physically realizable) and second solution is unstable which is not physically realizable.
- Velocity, temperature and concentration profiles increase with curvature parameter γ but microorganism profile decrease with γ.
- Dual solution exists for vertical and inclined cylinder but for the horizontal cylinder only dual solution exists.
- When opposing flow is present at the lower stagnation flow over a solid sphere, dual solutions can be obtained in a particular range of the mixed convection parameter, whereas aiding flow only exhibits stable solutions.

8.2 Future recommendations

In the future, this research could be expanded to include more in–depth analyses, considering the following concepts:

- The scope of this study can be increased by considering hybrid nanofluids.
- Because the first study is limited to Newtonian fluids, future research can analyse microstructural working fluids using the Erigen micropolar model to assess the efficacy of PEM fuel cell devices.
- For stretching/shrinking sheets, exponential stretching sheets, and stretching cylinders, all models could be solved.
- The study is only applicable to two-dimensional steady incompressible fluid flows; following that, three-dimensional unsteady incompressible viscous flows can be included.

Bibliography

Abd El-Aziz, M., & Saleem, S. (2019). Numerical simulation of entropy generation for power-law liquid flow over a permeable exponential stretched surface with variable heat source and heat flux. *Entropy*, *21*(5), 484.

Abdou, M. M. M. (2017). Effects of MHD and Joule heating on free convective boundary layer with a variable plate temperature in a porous medium. *Applied Mathematical Sciences*, *11*(36), 1765-1777.

Abu-Hamdeh, N. H., Oztop, H. F., & Alnefaie, K. A. (2020). A computational study on mixed convection in a porous media filled and partially heated lid-driven cavity with an open side. *Alexandria Engineering Journal*, *59*(3), 1735-1750.

Aghbari, A., Ali Agha, H., & Sadaoui, D. (2019). Soret-Dufour effect on mixed convection past a vertical plate in non-Darcy porous medium saturated with Buongiorno nanofluid in the presence of thermal dispersion. *Journal of Mechanics*, *35*(6), 851-862.

Ahmad, S., & Pop, I. (2010). Mixed convection boundary layer flow from a vertical flat plate embedded in a porous medium filled with nanofluids. *International Communications in Heat and Mass Transfer*, *37*(8), 987-991.

Ahmad, S., & Pop, I. (2014). Melting effect on mixed convection boundary layer flow about a vertical surface embedded in a porous medium: opposing flows case. *Transport in porous media*, *102*(3), 317-323.

Ahmad, S., Ashraf, M., & Ali, K. (2020). Bioconvection due to gyrotactic microbes in a nanofluid flow through a porous medium. *Heliyon*, *6*(12), e05832.

Ahmad, S., Younis, J., Ali, K., Rizwan, M., Ashraf, M., & Abd El Salam, M. A. (2022). Impact of swimming gyrotactic microorganisms and viscous dissipation on nanoparticles flow through a permeable medium: a numerical assessment. *Journal of Nanomaterials*, *2022*, 1-11.

Ahmed, S. E., Mansour, M. A., Hussein, A. K., Mallikarjuna, B., Almeshaal, M. A., & Kolsi, L. (2019). MHD mixed convection in an inclined cavity containing adiabatic obstacle and filled with Cu–water nanofluid in the presence of the heat generation and partial slip. *Journal of Thermal Analysis and Calorimetry*, *138*(2), 1443-1460.

Ahmed, Z., Al-Qahtani, A., Nadeem, S., & Saleem, S. (2019). Computational study of MHD nanofluid flow possessing micro-rotational inertia over a curved surface with variable thermophysical properties. *Processes*, *7*(6), 387.

Aldoss, T. K., Al-Nimr, M. A., Jarrah, M. A., & Al-Sha'er, B. J. (1995). Magnetohydrodynamic mixed convection from a vertical plate embedded in a porous medium. *Numerical Heat Transfer, Part A: Applications*, *28*(5), 635-645.

Ali, M. E. (1995). On thermal boundary layer on a power-law stretched surface with suction or injection. *International Journal of Heat and Fluid Flow*, *16*(4), 280-290.

Alkasasbeh, H. T., Salleh, M. Z., Tahar, R. M., & Nazar, R. (2014, April). Numerical solutions of free convection boundary layer flow on a solid sphere with convective boundary conditions. In *Journal of Physics: Conference Series* (Vol. 495, No. 1, pp. 012025).

Alkasasbeh, H. T., Salleh, M. Z., Tahar, R. M., Nazar, R., & Pop, I. (2014). Free convection boundary layer flow on a solid sphere with convective boundary conditions in a micropolar fluid. *World Applied Sciences Journal*, *32*(9), 1942-1951.

Alloui, Z., Nguyen, T. H., & Bilgen, E. (2007). Numerical investigation of thermo-bioconvection in a suspension of gravitactic microorganisms. *International journal of heat and mass transfer*, *50*(7-8), 1435-1441.

Alsenafi, A., & Ferdows, M. (2021). Dual solution for double-diffusive mixed convection opposing flow through a vertical cylinder saturated in a Darcy porous media containing gyrotactic microorganisms. *Scientific Reports*, *11*(1), 19918.

Aman, F., & Ishak, A. (2012). Mixed convection boundary layer flow towards a vertical plate with a convective surface boundary condition. *Mathematical Problems in*

Engineering, *2012*, 453457.

Amanulla, C. H., Saleem, S., Wakif, A., & AlQarni, M. M. (2019). MHD Prandtl fluid flow past an isothermal permeable sphere with slip effects. *Case Studies in Thermal Engineering*, *14*, 100447.

Avramenko, A. A., & Kuznetsov, A. V. (2010). The onset of bio-thermal convection in a suspension of gyrotactic microorganisms in a fluid layer with an inclined temperature gradient. *International Journal of Numerical Methods for Heat & Fluid Flow*, *20*(1), 111-129.

Aziz, L. A., Kasim, A. R. M., Salleh, M. Z., & Shafie, S. (2019). Mixed Convection Boundary Layer Flow on a Solid Sphere in a Viscoelastic Micropolar Fluid. In *Proceedings of the Third International Conference on Computing, Mathematics and Statistics (iCMS2017)* (pp. 111-117). Springer, Singapore.

Bachok, N., Ishak, A., & Pop, I. (2013). Mixed convection boundary layer flow over a moving vertical flat plate in an external fluid flow with viscous dissipation effect. *Plos one*, *8*(4), e60766.

Bakar, N. A., & Roslan, R. (2020). Mixed Convection in a Lid-Driven Horizontal Cavity in the Presence of Internal Heat Generation or Absorption. *Journal of Advanced Research in Numerical Heat Transfer*, *3*(1), 1-11.

Bansod, V. (2003). The Darcy model for boundary layer flows in a horizontal porous medium induced by combined buoyancy forces. *Journal of Porous Media*, *6*(4).

Basir, M. F., Uddin, M. J., Md. Ismail, A. I., & Bég, O. A. (2016). Nanofluid slip flow over a stretching cylinder with Schmidt and Péclet number effects. *AIP Advances*, *6*(5), 055316.

Basha, H. T., & Sivaraj, R. (2021). Numerical simulation of blood nanofluid flow over three different geometries by means of gyrotactic microorganisms: applications to the flow in a circulatory system. *Proceedings of the Institution of Mechanical Engineers, Part C:*

Journal of Mechanical Engineering Science, *235*(2), 441-460.

Beg, O. A., Espinoza, D. E., Kadir, A., Shamshuddin, M. D., & Sohail, A. (2018). Experimental study of improved rheology and lubricity of drilling fluids enhanced with nano-particles. *Applied Nanoscience*, *8*(5), 1069-1090.

Beg, O. A., Zueco, J., Takhar, H. S., Bég, T. A., & Sajid, A. (2009). Transient nonlinear optically-thick radiative–convective double-diffusive boundary layers in a Darcian porous medium adjacent to an impulsively started surface: Network simulation solutions. *Communications in Nonlinear Science and Numerical Simulation*, *14*(11), 3856-3866.

Beg, O. A., Vasu, B., Sochi, T., & Prasad, V. R. (2013). Keller box and smoothed particle hydrodynamic numerical simulation of two-phase transport in blood purification auto-transfusion dialysis hybrid device with Stokes and Darcy number effects. *Journal of Advanced Biotechnology and Bioengineering*, *1*(2), 80-100.

Beg, O. A., Ali, N., Zaman, A., Beg, T. A., & Sohail, A. (2016). Computational modelling of heat transfer in annular porous medium solar energy absorber with a P1-radiative differential approximation. *J. Taiwan Inst. Chem. Eng*, *66*, 258-268.

Beg, O. A., Gorla, R. S. R., Prasad, V. R., Vasu, B., & Prashad, R. D. (2011, August). Computational study of mixed thermal convection nanofluid flow in a porous medium. In *12th UK National Heat Transfer Conference, 30th August-1st September*.

Beg, O. A., Prasad, V. R., & Vasu, B. (2013). Numerical study of mixed bioconvection in porous media saturated with nanofluid containing oxytactic microorganisms. *Journal of Mechanics in Medicine and Biology*, *13*(4), 1350067.

Beg, O. A., Takhar, H. S., Zueco, J., Sajid, A., & Bhargava, R. (2008). Transient Couette flow in a rotating non-Darcian porous medium parallel plate configuration: network simulation method solutions. *Acta Mechanica*, *200*(3), 129-144.

Beg, O. A., Uddin, M. J., Bég, T., & Gorla, R. R. (2016). Numerical simulation of self-similar thermal convection from a spinning cone in anisotropic porous medium. *Journal of*

Hydrodynamics, Ser. B, *28*(2), 184-194.

Beg, O. A. (2018). Nonlinear multiphysical laminar nanofluid bioconvection flows: Models and computation. *In: Sohail A, Li Z (eds) Computational approaches in biomedical nano-engineering*, chapter 5. Wiley, 113-145.

Beg, O. A., Zueco, J., & Takhar, H. S. (2008). Laminar free convection from a continuously-moving vertical surface in thermally-stratified non-Darcian high-porosity medium: network numerical study. *International Communications in Heat and Mass Transfer*, *35*(7), 810-816.

Beg, O. A., Bakier, A. Y., & Prasad, V. R. (2009). Numerical study of free convection magnetohydrodynamic heat and mass transfer from a stretching surface to a saturated porous medium with Soret and Dufour effects. *Computational Materials Science*, *46*(1), 57-65.

Bejan, A. (2013). *Convection heat transfer*. John wiley & sons.

Benenati, R. F., & Brosilow, C. B. (1962). Void fraction distribution in beds of spheres. *AIChE Journal*, *8*(3), 359-361.

Berg, H. C. (1975). Chemotaxis in bacteria. *Annual review of biophysics and bioengineering*, *4*(1), 119-136.

Bhargava, R., Takhar, H. S., Rawat, S., Beg, T. A., & Bég, O. A. (2007). Finite element solutions for non-Newtonian pulsatile flow in a non-Darcian porous medium conduit. *Nonlinear analysis: modelling and control*, *12*(3), 317-327.

Bradean, R., Promislow, K., & Wetton, B. (2002). Transport phenomena in the porous cathode of a proton exchange membrane fuel cell. *Numerical Heat Transfer: Part A: Applications*, *42*(1-2), 121-138.

Butler, C. S., & Nerenberg, R. (2010). Performance and microbial ecology of air-cathode microbial fuel cells with layered electrode assemblies. *Applied microbiology and biotechnology*, *86*(5), 1399-1408.

Chamkha, A. J., & Khaled, A. R. (2000). Hydromagnetic simultaneous heat and mass transfer by mixed convection from a vertical plate embedded in a stratified porous medium with thermal dispersion effects. *Heat and Mass Transfer*, *36*(1), 63-70.

Chandrasekhara, B. C., Namboodiri, P. M. S., & Hanumanthappa, A. R. (1984). Similarity solutions for buoyancy induced flows in a saturated porous medium adjacent to impermeable horizontal surfaces. *Wärme-und Stoffübertragung*, *18*(1), 17-23.

Chandrasekhara, B. C. (1985). Mixed convection in the presence of horizontal impermeable surfaces in saturated porous media with variable permeability. *Wärme-und Stoffübertragung*, *19*(3), 195-201.

Chandrasekhara, B. C., & Vortmeyer, D. (1979). Flow model for velocity distribution in fixed porous beds under isothermal conditions. *Wärme-und Stoffübertragung*, *12*(2), 105-111.

Cheng, P., & Minkowycz, W. J. (1977). Free convection about a vertical flat plate embedded in a porous medium with application to heat transfer from a dike. *Journal of Geophysical Research*, *82*(14), 2040-2044.

Cheng, P. (1977). Combined free and forced convection flow about inclined surfaces in porous media. *Int. J. Heat Mass Transfer*, *20*, 807-814.

Cheng, C. Y. (2012). Soret and Dufour effects on mixed convection heat and mass transfer from a vertical wedge in a porous medium with constant wall temperature and concentration. *Transport in porous media*, *94*(1), 123-132.

Cheng, W. T., & Lin, C. H. (2007). Melting effect on mixed convective heat transfer with aiding and opposing external flows from the vertical plate in a liquid-saturated porous medium. *International journal of heat and mass transfer*, *50*(15-16), 3026-3034.

Chiang, T., Ossin, A., & Tien, C. L. (1964). Laminar free convection from a sphere. *ASME Journal of Heat and Mass Transfer, 86*(4), 537-542.

Choi, I. G. (1982). The effect of variable properties of air on the boundary layer for a moving continuous cylinder. *International Journal of Heat and Mass Transfer*, *25*(5), 597-602.

Chowdhury, M. S., Zheng, W., Kumari, S., Heyman, J., Zhang, X., Dey, P. & Haag, R. (2019). Dendronized fluorosurfactant for highly stable water-in-fluorinated oil emulsions with minimal inter-droplet transfer of small molecules. *Nature communications*, *10*(1), 1-10.

Deng, H., Chen, Z., & Zhao, F. (2012). Energy from plants and microorganisms: progress in plant–microbial fuel cells. *ChemSusChem*, *5*(6), 1006-1011.

Dhanai, R., Rana, P., & Kumar, L. (2016). MHD mixed convection nanofluid flow and heat transfer over an inclined cylinder due to velocity and thermal slip effects: Buongiorno's model. *Powder Technology*, *288*, 140-150.

Dinesh, P. A., Nalinakshi, N., & Sandeep, N. (2015). Double diffusive mixed convection in a couple stress fluids with variable fluid properties. *Adv Phys Theor Appl*, *41*, 30-42.

Dinesh, M. G. R. (2018). Double diffusive convection and internal heat generation with Soret and Dufour effects over an accelerating surface with variable viscosity and permeability. *Adv Phys Theor Appl, 69,* 7-25.

El-Amin, M. F. (2004). Double dispersion effects on natural convection heat and mass transfer in non-Darcy porous medium. *Applied Mathematics and Computation*, *156*(1), 1-17.

Epstein, M., & Cho, D. H. (1976). Melting heat transfer in steady laminar flow over a flat plate. *J. Heat Transfer*, *98*(3), 531-533.

Fauzi, N. F., Ahmad, S., & Pop, I. (2014, July). Mixed convection boundary layer flow at the lower stagnation point of a sphere embedded in a porous medium in presence of heat source/sink: Constant heat flux case. In *AIP Conference Proceedings* (Vol. 1605, No. 1, pp. 470-475).

Ferdows, M., & Liu, D. (2017). Similarity solutions on mixed convection heat transfer from a horizontal surface saturated in a porous medium with internal heat generation. *International Journal of Applied Mechanics and Engineering*, *22*(1), 253-258.

Ferdows, M., Murtaza, M. G., & Shamshuddin, M. D. (2019). Effect of internal heat generation

on free convective power-law variable temperature past a vertical plate considering exponential variable viscosity and thermal conductivity. *Journal of the Egyptian Mathematical Society*, *27*(1), 1-11.

Fischer, F. (2018). Photoelectrode, photovoltaic and photosynthetic microbial fuel cells. *Renewable and Sustainable Energy Reviews*, *90*, 16-27.

Fojt, L., Strašák, L., Vetterl, V., & Šmarda, J. (2004). Comparison of the low-frequency magnetic field effects on bacteria Escherichia coli, Leclercia adecarboxylata and Staphylococcus aureus. *Bioelectrochemistry*, *63*(1-2), 337-341.

Gaffar, S. A., Prasad, V. R., Reddy, E. K., & Beg, O. A. (2015). Thermal radiation and heat generation/absorption effects on viscoelastic double-diffusive convection from an isothermal sphere in porous media. *Ain Shams Engineering Journal*, *6*(3), 1009-1030.

Gangadhar, K., Edukondala Nayak, R., & Venkata Subba Rao, M. (2022). Buoyancy effect on mixed convection boundary layer flow of Casson fluid over a non linear stretched sheet using the spectral relaxation method. *International Journal of Ambient Energy*, *43*(1), 1994-2002.

Gibanov, N. S., Sheremet, M. A., Ismael, M. A., & Chamkha, A. J. (2017). Mixed convection in a ventilated cavity filled with a triangular porous layer. *Transport in Porous Media*, *120*(1), 1-21.

Golafshan, B., & Rahimi, A. B. (2019). Effects of radiation on mixed convection stagnation-point flow of MHD third-grade nanofluid over a vertical stretching sheet. *Journal of Thermal Analysis and Calorimetry*, *135*(1), 533-549.

Gorla, R. S. R., Bakier, A. Y., & Byrd, L. (1996). Effects of thermal dispersion and stratification on combined convection on a vertical surface embedded in a porous medium. *Transport in Porous Media*, *25*(3), 275-282.

Hady, F. M., Mohamed, R. A., Mahdy, A., & Abo Zaid, O. A. (2016). Non-Darcy natural convection boundary layer flow over a vertical cone in porous media saturated with a nanofluid containing gyrotactic microorganisms with a convective boundary

condition. *Journal of Nanofluids*, *5*(5), 765-773.

Han, S., Zhang, Q., Zhang, X., Liu, X., Lu, L., Wei, J. & Zheng, G. (2019). A digital microfluidic diluter-based microalgal motion biosensor for marine pollution monitoring. *Biosensors and Bioelectronics*, *143*, 111597.

Hayat, T., Haider, F., & Alsaedi, A. (2020). Darcy-Forchheimer flow with nonlinear mixed convection. *Applied Mathematics and Mechanics*, *41*(11), 1685-1696.

Hemmat Esfe, M., Saedodin, S., Hasani Malekshah, E., Babaie, A., & Rostamian, H. (2019). Mixed convection inside lid-driven cavities filled with nanofluids. *Journal of Thermal Analysis and Calorimetry*, *135*(1), 813-859.

Hill, N. A., & Pedley, T. J. (2005). Bioconvection. *Fluid Dynamics Research*, *37*(1-2), 1-20.

Hsieh, J. C., Chen, T. S., & Armaly, B. F. (1993). Nonsimilarity solutions for mixed convection from vertical surfaces in porous media: variable surface temperature or heat flux. *International Journal of Heat and Mass Transfer*, *36*(6), 1485-1493.

Huang, M. J., & Chen, C. K. (1985). Effects of surface mass transfer on free convection flow over vertical cylinder embedded in a saturated porous medium. *ASME Journal of Energy Resources Technology*. *107*, 394-396.

Ibrahim, F. S., & Hassanien, I. A. (2000). Influence of variable permeability on combined convection along a nonisothermal wedge in a saturated porous medium. *Transport in porous media*, *39*(1), 57-71.

Ibrahim, F. S., Abdel-Gaid, S. M., & Gorla, R. S. R. (2000). Non-Darcy mixed convection flow along a vertical plate embedded in a non-Newtonian fluid saturated porous medium with surface mass transfer. *International Journal of Numerical Methods for Heat & Fluid Flow*, *10*(4), 397- 408.

Jafarpur, K., & Yovanovich, M. M. (1992). Laminar free convective heat transfer from isothermal spheres: a new analytical method. *International Journal of Heat and Mass Transfer*, *35*(9), 2195-2201.

Jeng, K. T., Lee, S. F., Tsai, G. F., & Wang, C. H. (2004). Oxygen mass transfer in PEM fuel cell gas diffusion layers. *Journal of Power sources*, *138*(1-2), 41-50.

Kada, B., Hussain, I., Pasha, A. A., Khan, W. A., Tabrez, M., Juhany, K. A., ... & Othman, R. (2023). Significance of gyrotactic microorganism and bioconvection analysis for radiative Williamson fluid flow with ferromagnetic nanoparticles. *Thermal Science and Engineering Progress*, *39*, 101732.

Kafoussias, N. G., & Williams, E. W. (1993). An improved approximation technique to obtain numerical solution of a class of two-point boundary value similarity problems in fluid mechanics. *International journal for numerical methods in fluids*, *17*(2), 145-162.

Kairi, R. R. (2011). Viscosity and dispersion effects on natural convection from a vertical cone in a non-Newtonian fluid saturated porous medium. *Thermal Science*, *15*(2), 307-316.

Kameswaran, P. K., Hemalatha, K., & Madhavi, M. V. D. N. S. (2016). Melting effect on convective heat transfer from a vertical plate embedded in a non-Darcy porous medium with variable permeability. *Advanced Powder Technology*, *27*(2), 417-425.

Khan, W. A., Rashad, A. M., Abdou, M. M. M., & Tlili, I. (2019). Natural bioconvection flow of a nanofluid containing gyrotactic microorganisms about a truncated cone. *European Journal of Mechanics-B/Fluids*, *75*, 133-142.

Khan, W. A., & Makinde, O. D. (2014). MHD nanofluid bioconvection due to gyrotactic microorganisms over a convectively heat stretching sheet. *International Journal of Thermal Sciences*, *81*, 118-124.

Khan, W. A., Uddin, M., & Ismail, A. I. (2013). Free convection of non-Newtonian nanofluids in porous media with gyrotactic microorganisms. *Transport in porous media*, *97*(2), 241-252.

Khashi'ie, N. S., Arifin, N. M., & Pop, I. (2020). Non-Darcy mixed convection of hybrid nanofluid with thermal dispersion along a vertical plate embedded in a porous medium. *International Communications in Heat and Mass Transfer*, *118*, 104866.

Kim, M., Doo, J. H., Park, Y. G., Yoon, H. S., & Ha, M. Y. (2014). Natural convection in a square enclosure with a circular cylinder according to the bottom wall temperature variation. *Journal of Mechanical Science and Technology*, *28*(12), 5013-5025.

Kohno, M., Yamazaki, M., Kimura, I., & Wada, M. (2000). Effect of static magnetic fields on bacteria: Streptococcus mutans, Staphylococcus aureus, and Escherichia coli. *Pathophysiology*, *7*(2), 143-148.

Krishnamurthy, M. R., Prasannakumara, B. C., Gireesha, B. J., & Gorla, R. S. R. (2016). Effect of chemical reaction on MHD boundary layer flow and melting heat transfer of Williamson nanofluid in porous medium. *Engineering Science and Technology, an International Journal*, *19*(1), 53-61.

Kulikovsky, A. A. (2009). Optimal effective diffusion coefficient of oxygen in the cathode catalyst layer of polymer electrode membrane fuel cells. *Electrochemical and solid-state letters*, *12*(4), B53-B56.

Kumari, M., & Nath, G. (2010). Natural convection on a horizontal cone in a porous medium with non-uniform wall temperature/concentration or heat/mass flux and suction/injection. *Transport in porous media*, *84*(2), 275-284.

Kumari, M., & Gorla, R. S. R. (1997). Combined convection along a non-isothermal wedge in a porous medium. *Heat and Mass Transfer*, *32*(5), 393-398.

Kumari, P., Nigam, M., Kumar, S., Kumar, V., Raturi, S., Pargaei, M., & Kumar, B. R. (2019). Magnetic field effect on non-darcy mixed convection from a horizontal plate in a nanofluid-saturated porous medium. *Journal of Porous Media*, *22*(5), 599-610.

Kuznetsov, A. V. (2006). The onset of thermo-bioconvection in a shallow fluid saturated porous layer heated from below in a suspension of oxytactic microorganisms. *European Journal of Mechanics-B/Fluids*, *25*(2), 223-233.

Kuznetsov, A. V. (2011). Bio-thermal convection induced by two different species of microorganisms. *International Communications in Heat and Mass Transfer*, *38*(5), 548-

553.

Kuznetsov, A. V. (2010). The onset of nanofluid bioconvection in a suspension containing both nanoparticles and gyrotactic microorganisms. *International Communications in Heat and Mass Transfer*, *37*(10), 1421-1425.

Kuznetsov, A. V., & Avramenko, A. A. (2004). Effect of small particles on this stability of bioconvection in a suspension of gyrotactic microorganisms in a layer of finite depth. *International communications in heat and mass transfer*, *31*(1), 1-10.

Lai, F. C., & Kulacki, F. A. (1990). The effect of variable viscosity on convective heat transfer along a vertical surface in a saturated porous medium. *International Journal of Heat and Mass Transfer*, *33*(5), 1028-1031.

Lai, F. C., Kulacki, F. A., & Prasad, V. (1991). Mixed convection in saturated porous media. In *Convective heat and mass transfer in porous media* (pp. 225-287). Springer, Dordrecht.

Latiff, N. A. A., Yahya, E., Ismail, A. I. M., Amirsom, A., & Basir, F. (2017, August). The effect of velocity slip and multiple convective boundary conditions in a Darcian porous media with microorganism past a vertical stretching/shrinking sheet. In *AIP Conference Proceedings* (Vol. 1870, No. 1, pp. 040052).

Latiff, N. A. A., Uddin, M. J., Bég, O. A., & Ismail, A. I. (2016). Unsteady forced bioconvection slip flow of a micropolar nanofluid from a stretching/shrinking sheet. *Proceedings of the Institution of Mechanical Engineers, Part N: Journal of Nanomaterials, Nanoengineering and Nanosystems*, *230*(4), 177-187.

Lee, Y. Y., Kim, T. G., & Cho, K. S. (2015). Effects of proton exchange membrane on the performance and microbial community composition of air-cathode microbial fuel cells. *Journal of Biotechnology*, *211*, 130-137.

Liu, F., Darjani, S., Akhmetkhanova, N., Maldarelli, C., Banerjee, S., & Pauchard, V. (2017). Mixture effect on the dilatation rheology of asphaltenes-laden

interfaces. *Langmuir*, *33*(8), 1927-1942.

Li, S., Ali, F., Zaib, A., Loganathan, K., Eldin, S. M., & Ijaz Khan, M. (2023). Bioconvection effect in the Carreau nanofluid with Cattaneo–Christov heat flux using stagnation point flow in the entropy generation: Micromachines level study. *Open Physics*, *21*(1), 20220228.

Loganathan, P., & Eswari, B. (2017). Natural convective flow over moving vertical cylinder with temperature oscillations in the presence of porous medium. *Global Journal of Pure and Applied Mathematics*, *13*(2), 839-855.

Mabood, F., Khan, W. A., & Ismail, A. I. M. (2014, December). Analytical modelling of free convection of non-Newtonian nanofluids flow in porous media with gyrotactic microorganisms using OHAM. In *AIP Conference Proceedings* (Vol. 1635, No. 1, pp. 131-137).

Magyari, E., Pop, I., & Postelnicu, A. (2007). Effect of the source term on steady free convection boundary layer flows over an vertical plate in a porous medium. Part I. *Transport in porous media*, *67*(1), 49-67.

Mahat, R., Rawi, N. A., Shafie, S., & Kasim, A. R. M. (2019). Mixed convection boundary layer flow of viscoelastic nanofluid past a horizontal circular cylinder with convective boundary condition. *Int. J. Mech. Eng. Robot. Res*, *8*(1), 87-91.

Mahdy, A. (2013). Mixed convection in non-Newtonian fluids along a vertical plate in a liquid-saturated porous medium with melting effect. *Journal of Engineering Physics and Thermophysics*, *86*, 1117-1126.

Mahdy, A., & Nabwey, H. A. (2020). Microorganisms time-mixed convection nanofluid flow by the stagnation domain of an impulsively rotating sphere due to Newtonian heating. *Results in Physics*, *19*, 103347.

Mahdy, A. (2021). Unsteady Mixed Bioconvection Flow of Eyring–Powell Nanofluid with Motile Gyrotactic Microorganisms Past Stretching Surface. *BioNanoScience*, *11*(2),

295-305.

Mahmood, T., & Merkin, J. H. (1988). Mixed convection on a vertical circular cylinder. *Zeitschrift für angewandte Mathematik und Physik*, *39*(2), 186-203.

Makinde, O. D., & Aziz, A. (2011). Mixed convection from a convectively heated vertical plate to a fluid with internal heat generation. *Journal of Heat Transfer*, *133*(12), 122501.

Maleque, K. (2020). Similarity requirements for mixed convective boundary layer flow over vertical curvilinear porous surfaces with heat generation/absorption. *International Journal of Aerospace Engineering*, *2020*, 7486971.

Marpu, D. R., & Satyamurty, V. V. (1989). Influence of variable fluid density on free convection in rectangular porous media, *11*(4), 214-220.

Mathur, P., & Jha, A. (2017). Hydromagnetic free Convection from a Moving Permeable Vertical Surface through Porous medium with Heat Source and first order Chemical Reaction, *International Journal of Mathematics Trends and Technology*, *48*(2), 120-127.

Mealey, L., & Merkin, J. H. (2008). Free convection boundary layers on a vertical surface in a heat-generating porous medium. *IMA journal of applied mathematics*, *73*(1), 231-253.

Meena, O. P. (2021). Mixed convection flow over a vertical cone with double dispersion and chemical reaction effects. *Heat Transfer*, *50*(5), 4516-4534.

Merkin, J. H. (1969). The effect of buoyancy forces on the boundary-layer flow over a semi-infinite vertical flat plate in a uniform free stream. *Journal of Fluid Mechanics*, *35*(3), 439-450.

Merkin, J. H. (1972). Free convection with blowing and suction. *International journal of heat and mass transfer*, *15*(5), 989-999.

Merkin, J. H. (2008). Free convective boundary-layer flow in a heat-generating porous medium: similarity solutions. *The Quarterly Journal of Mechanics & Applied*

Mathematics, *61*(2), 205-218.

Merkin, J. H., Pop, I., & Ahmad, S. (2015). Note on the melting effect on mixed convection boundary-layer flow over a vertical flat surface embedded in a porous medium. *International Journal of Heat and Mass Transfer*, *84*, 786-790.

Mkhatshwa, M. P., Motsa, S. S., Ayano, M. S., & Sibanda, P. (2020). MHD mixed convective nanofluid flow about a vertical slender cylinder using overlapping multi-domain spectral collocation approach. *Case Studies in Thermal Engineering*, *18*, 100598.

Mondal, H., De, P., Goqo, S., & Sibanda, P. (2020). A numerical study of nanofluid flow over a porous vertical plate with internal heat generation and nonlinear thermal radiation. *Journal of Porous Media*, *23*(6), 517-529.

Mozaffari, S., Li, W., Dixit, M., Seifert, S., Lee, B., Kovarik, L., & Karim, A. M. (2019). The role of nanoparticle size and ligand coverage in size focusing of colloidal metal nanoparticles. *Nanoscale Advances*, *1*(10), 4052-4066.

Munoz-Cobo, J. L., Corberán, J. M., & Chiva, S. (2003). Explicit formulas for laminar natural convection heat transfer along vertical cylinders with power-law wall temperature distribution. *Heat and mass transfer*, *39*(3), 215-222.

Nakayama, A., & Koyama, H. A. (1987). General similarity transformation for free, forced and mixed convection in Darcy and non-Darcy porous media. *J. Heat Transfer*, *109*, 1041-1045.

Nakayama, A. (1995). *PC-aided numerical heat transfer and convective flow*. CRC press.

Nalinakshi, N., Dinesh, P. A., & Chandrashekar, D. V. (2013). Effects of variable fluid properties and MHD on mixed convection heat transfer from a vertical heated plate embedded in a sparsely packed porous medium. *IOSR Journal of Mathematics*, *7*(1), 20-31.

Nasser, I., & Duwairi, H. M. (2016). Thermal dispersion effects on convection heat transfer in porous media with viscous dissipation. *International Journal of Heat and*

Technology, *34*(2), 207-212.

Nazar, R., Amin, N., & Pop, I. (2002). Mixed convection boundary layer flow from a sphere with a constant surface heat flux in a micropolar fluid. *Journal of Energy Heat and Mass Transfer*, *24*(3), 195-212.

Nield, D. A., & Bejan, A. (2006). *Convection in porous media* (Vol. 3). New York: Springer.

Nield, D. A., & Bejan, A. (2013). *Convection in porous media* (Vol. 4). New York: Springer.

Nima, N. I., Ferdows, M., & Ardekani, M. M. (2020). Effects of cross diffusion and radiation on magneto mixed convective stagnation flow from a vertical surface in porous media with gyrotactic microorganisms: Similarity and numerical analysis. *Special Topics & Reviews in Porous Media: An International Journal*, *11*(3), 203-219.

Niu, J., Fu, C., & Tan, W. (2012). Slip-flow and heat transfer of a non-Newtonian nanofluid in a microtube. *Plos one*, *7*(5), e37274.

Ogunseye, H. A., Salawu, S. O., Tijani, Y. O., Riliwan, M., & Sibanda, P. (2019). Dynamical analysis of hydromagnetic Brownian and thermophoresis effects of squeezing Eyring–Powell nanofluid flow with variable thermal conductivity and chemical reaction. *Multidiscipline Modeling in Materials and Structures*, *15*(6), 1100-1120.

Olanrewaju, P. O., Arulogun, O. T., & Adebimpe, K. (2012). Internal heat generation effect on thermal boundary layer with a convective surface boundary condition. *American journal of fluid Dynamics*, *2*(1), 1-4.

Pantokratoras, A. (2007). Non-Darcian forced convection heat transfer over a flat plate in a porous medium with variable viscosity and variable Prandtl number. *Journal of Porous Media*, *10*(2), 201-208.

Pantokratoras, A. (2005). Forced and mixed convection boundary layer flow along a flat plate with variable viscosity and variable Prandtl number: new results. *Heat and Mass Transfer*, *41*(12), 1085-1094.

Patil, P. M., Momoniat, E., & Roy, S. (2014). Influence of convective boundary condition on

double diffusive mixed convection from a permeable vertical surface. *International Journal of Heat and Mass Transfer*, *70*, 313-321.

Plumb, O. A. (1983). The effect of thermal dispersion on heat transfer in packed bed boundary layers. In *ASME/JSME Thermal Engineering Joint Conference* (Vol. 2, pp. 17-21).

Pop, I., & Ingham, D. B. (2001). *Convective heat transfer: mathematical and computational modelling of viscous fluids and porous media*. Elsevier, Amsterdam, 668.

Pop, I., Gorla, R. S. R., & Rashidi, M. (1992). The effect of variable viscosity on flow and heat transfer to a continuous moving flat plate. *International journal of engineering science*, *30*(1), 1-6.

Postelnicu, A., & Pop, I. (2011). Falkner–Skan boundary layer flow of a power-law fluid past a stretching wedge. *Applied Mathematics and Computation*, *217*(9), 4359-4368.

Pranitha, J., Suman, G. V., & Srinivasacharya, D. (2015). Effects of double dispersion on mixed convection in a power-law fluid saturated porous medium with variable properties using Lie scaling group transformations. *Procedia Engineering*, *127*, 362-369.

Prasad, P. D., Saleem, S., Varma, S. V. K., & Raju, C. S. K. (2019). Three dimensional slip flow of a chemically reacting Casson fluid flowing over a porous slender sheet with a non-uniform heat source or sink. *Journal of the Korean Physical Society*, *74*(9), 855-864.

Qasim, M., Afridi, M. I., Wakif, A., & Saleem, S. (2019). Influence of variable transport properties on nonlinear radioactive Jeffrey fluid flow over a disk: utilization of generalized differential quadrature method. *Arabian Journal for Science and Engineering*, *44*(6), 5987-5996.

Raees, A., Xu, H., Sun, Q., & Pop, I. (2015). Mixed convection in gravity-driven nano-liquid film containing both nanoparticles and gyrotactic microorganisms, *Applied Mathematics and Mechanics, 36*, 163-178.

Rahman, M. M., Merkin, J. H., & Pop, I. (2015). Mixed convection boundary-layer flow past a vertical flat plate with a convective boundary condition. *Acta Mechanica*, *226*(8), 2441-2460.

Rajput, J. S., & Upadhyay, V. (2018). Hydromagnetic mixed convection flow through horizontal channel, analysis with viscous dissipation, joule heating, variable viscosity and thermal conductivity. *Int J Math Trends Technol.*, *55*(7), 463-481.

RamReddy, C., & Kairi, R. R. (2015). The effect of melting on mixed convection heat and mass transfer in non-Newtonian nanofluid saturated in porous medium. *Frontiers in Heat and Mass Transfer (FHMT)*, *6*(1), 1-7.

RamReddy, C., Naveen, P., & Srinivasacharya, D. (2018). Nonlinear convective flow of non-Newtonian fluid over an inclined plate with convective surface condition: a Darcy–Forchheimer model. *International Journal of Applied and Computational Mathematics*, *4*(1), 1-18.

Rana, P., Bhargava, R., & Bég, O. A. (2012). Numerical solution for mixed convection boundary layer flow of a nanofluid along an inclined plate embedded in a porous medium. *Computers & Mathematics with Applications*, *64*(9), 2816-2832.

Rashad, A. M., & Nabwey, H. A. (2019). Gyrotactic mixed bioconvection flow of a nanofluid past a circular cylinder with convective boundary condition. *Journal of the Taiwan Institute of Chemical Engineers*, *99*, 9-17.

Rashidi, M. M., Bég, O. A., & Rahimzadeh, N. (2012). A generalized differential transform method for combined free and forced convection flow about inclined surfaces in porous media. *Chemical Engineering Communications*, *199*(2), 257-282.

Rihan, Y. A. (2020). Mixed convection heat transfer from a short vertical cylinder placed in a cross flow. *ERJ. Engineering Research Journal*, *43*(3), 195-197.

Rosali, H., Ishak, A., Nazar, R., & Pop, I. (2016). Mixed convection boundary layer flow past a vertical cone embedded in a porous medium subjected to a convective boundary

condition. *Propulsion and Power Research*, *5*(2), 118-122.

Salawu, S. O., & Dada, M. S. (2018). Lie Group Analysis of Soret and Dufour effects on radiative inclined magnetic pressure-driven flow past a Darcy-Forchheimer medium. *Journal of the Serbian Society for Computational Mechanics*, *12*(1), 108-125.

Salawu, S. O., Hassan, A. R., Abolarinwa, A., & Oladejo, N. K. (2019). Thermal stability and entropy generation of unsteady reactive hydromagnetic Powell-Eyring fluid with variable electrical and thermal conductivities. *Alexandria Engineering Journal*, *58*(2), 519-529.

Salawu, S. O., & Ogunseye, H. A. (2020). Entropy generation of a radiative hydromagnetic Powell-Eyring chemical reaction nanofluid with variable conductivity and electric field loading. *Results in Engineering*, *5*, 100072.

Saleem, S., Rafiq, H., Al-Qahtani, A., El-Aziz, M. A., Malik, M. Y., & Animasaun, I. L. (2019). Magneto Jeffrey nanofluid bioconvection over a rotating vertical cone due to gyrotactic microorganism. *Mathematical Problems in Engineering*, *2019*, 3478037.

Saleem, S., & Abd El-Aziz, M. (2019). Entropy generation and convective heat transfer of radiated non-Newtonian power-law fluid past an exponentially moving surface under slip effects. *The European Physical Journal Plus*, *134*(4), 184.

Schwartz, C. E., & Smith, J. M. (1953). Flow distribution in packed beds. *Industrial & Engineering Chemistry*, *45*(6), 1209-1218.

Selimefendigil, F., & Öztop, H. F. (2017). Mixed convection in a partially heated triangular cavity filled with nanofluid having a partially flexible wall and internal heat generation. *Journal of the Taiwan Institute of Chemical Engineers*, *70*, 168-178.

Sewucipto, S., & Yuwono, T. (2021). The Influence of Upstream Installation of D-53 Type Cylinder on the Performance of Savonius Turbine. *Journal of Advanced Research in Experimental Fluid Mechanics and Heat Transfer*, *3*(1), 36-47.

Shamshuddin, M. D., Mishra, S. R., Kadir, A., & Bég, O. A. (2019). Unsteady chemo-

tribological squeezing flow of magnetized bioconvection lubricants: numerical study. *Journal of Nanofluids*, *8*(2), 407-419.

Shaw, S., Sibanda, P., Sutradhar, A., & Murthy, P. V. S. N. (2014). Magnetohydrodynamics and soret effects on bioconvection in a porous medium saturated with a nanofluid containing gyrotactic microorganisms. *Journal of heat transfer*, *136*(5), 052601.

Sheikholeslami, M., Saleem, S., Shafee, A., Li, Z., Hayat, T., Alsaedi, A., & Khan, M. I. (2019). Mesoscopic investigation for alumina nanofluid heat transfer in permeable medium influenced by Lorentz forces. *Computer Methods in Applied Mechanics and Engineering*, *349*, 839-858.

Shitanda, I., Yoshida, Y., & Tatsuma, T. (2007). Microimaging of algal bioconvection by scanning electrochemical microscopy. *Analytical chemistry*, *79*(11), 4237-4240.

Sobha, V. V., Vasudeva, R. Y., Ramakrishna, K., & Latha, K. H. (2010). Non-Darcy mixed convection with thermal dispersion in a saturated porous medium. *Journal of heat transfer*, *132*(1), 014501.

Singh, P. K. (2012). Effects of variable fluid proper ties and viscous dissipation on mixed convection fluid flow past a vertical plate in porous medium. *International Journal of Scientific & Engineering Research*, *3*(7), 1-10.

Sobamowo, M. G., & Akinshilo, A. T. (2017). Analysis of flow, heat transfer and entropy generation in a pipe conveying fourth grade fluid with temperature dependent viscosities and internal heat generation. *Journal of Molecular Liquids*, *241*, 188-198.

Sobha, V. V., Vasudeva, R. Y., Ramakrishna, K., & Latha, K. H. (2010). Non-Darcy mixed convection with thermal dispersion in a saturated porous medium. *Journal of heat transfer*, *132*(1), 014501.

Sparrow, E. M., Patankar, S. V., & Ramadhyani, S. (1977). Analysis of melting in the presence of natural convection in the melt region. *ASME Journal of Heat and Mass Transfer, 99*(4), 520-526.

Srinivasacharya, D., Mallikarjuna, B., & Bhuvanavijaya, R. (2016). Effects of thermophoresis and variable properties on mixed convection along a vertical wavy surface in a fluid saturated porous medium. *Alexandria Engineering Journal*, *55*(2), 1243-1253.

Srinivasacharya, D., & Reddy, G. S. (2015). Mixed convection on a vertical plate in a power-law fluid saturated porous medium with cross diffusion effects. *Procedia Engineering*, *127*, 591-597.

Srinivasacharya, D., & Surender, O. (2014). Non-Darcy mixed convection in a doubly stratified porous medium with Soret-Dufour effects. *International Journal of Engineering Mathematics*, *2014*, 126218.

Srinivasacharya, D., & Reddy, G. S. (2012). Double diffusive natural convection in power-law fluid saturated porous medium with Soret and Dufour effects. *Journal of the Brazilian Society of Mechanical Sciences and Engineering*, *34*, 525-530.

Srinivasacharya, D., & Reddy, G. S. (2015). Mixed convection on a vertical plate in a power-law fluid saturated porous medium with cross diffusion effects. *Procedia Engineering*, *127*, 591-597.

Srinivasacharya, D., & Surender, O. (2015). Effect of double stratification on mixed convection boundary layer flow of a nanofluid past a vertical plate in a porous medium. *Applied Nanoscience*, *5*(1), 29-38.

Srivastava, V., & Bég, D. T. O. A. (2016). Numerical study of oxygen diffusion from capillaries to tissues with external force effects. *J. Mechanics in Medicine and Biology*, *17*, 1750027-1.

Strašák, L., Vetterl, V., & Šmarda, J. (2002). Effects of low-frequency magnetic fields on bacteria Escherichia coli. *Bioelectrochemistry*, *55*(1-2), 161-164.

Sudhagar, P., Kameswaran, P. K., & Kumar, B. R. (2019). Gyrotactic microorganism effects on mixed convective nanofluid flow past a vertical cylinder. *Journal of Thermal Science and Engineering Applications*, *11*(4), 041018.

Swalmeh, M. Z., Alkasasbeh, H. T., Hussanan, A., & Mamat, M. (2019). Numerical investigation of heat transfer enhancement with Ag-GO water and kerosene oil based micropolar nanofluid over a solid sphere. *Journal of Advanced Research in Fluid Mechanics and Thermal Sciences*, *59*(2), 269-282.

Tashtoush, B., & Duwairi, H. M. (2005). Transient mixed convection with internal heat generation and oscillating plate temperature. *Acta mechanica*, *174*(3), 185-199.

Tham, L., Nazar, R., & Pop, I. (2013, April). Numerical solutions of mixed convection flow on a solid sphere embedded in a porous medium filled by a nanofluid containing gyrotactic microorganisms. In *AIP Conference Proceedings* (Vol. 1522, No. 1, pp. 604-613).

Tripathi, D., & Beg, O. A. (2012). A numerical study of oscillating peristaltic flow of generalized Maxwell viscoelastic fluids through a porous medium. *Transport in porous media*, *95*(2), 337-348.

Tsai, R., & Huang, J. S. (2009). Numerical study of Soret and Dufour effects on heat and mass transfer from natural convection flow over a vertical porous medium with variable wall heat fluxes. *Computational Materials Science*, *47*(1), 23-30.

Tsai, T. H., Liou, D. S., Kuo, L. S., & Chen, P. H. (2009). Rapid mixing between ferro-nanofluid and water in a semi-active Y-type micromixer. *Sensors and Actuators A: Physical*, *153*(2), 267-273.

Uddin, M. J., Khan, W. A., & Ismail, A. M. (2013). Free convective flow of non-Newtonian nanofluids in porous media with gyrotactic microorganism. *Journal of Thermophysics and Heat transfer*, *27*(2), 326-333.

Uddin, M. J., Alginahi, Y., Beg, O. A., & Kabir, M. N. (2016). Numerical solutions for gyrotactic bioconvection in nanofluid-saturated porous media with Stefan blowing and multiple slip effects. *Computers & Mathematics with Applications*, *72*(10), 2562-2581.

Uddin, M. J., Khan, W. A., Qureshi, S. R., & Beg, O. A. (2017). Bioconvection nanofluid slip flow past a wavy surface with applications in nano-biofuel cells. *Chinese Journal of*

Physics, *55*(5), 2048-2063.

Vadász, P. (Ed.). (2008). Emerging topics in heat and mass transfer in porous media: From bioengineering and microelectronics to nanotechnology. Springer Science & Business Media, New York. USA: Springer, *22*.

Vajravelu, K. (1980). Effects of variable properties and internal heat generation on natural convection at a heated vertical plate in air. *Numerical Heat Transfer*, *3*(3), 345-356.

Wager, H. W. T. (1910). The effect of gravity upon the movements and aggregation of Euglena viridis, Ehrb., and other micro-organisms. *Proceedings of the Royal Society of London. Series B, Containing Papers of a Biological Character*, *83*(562), 94-96.

Wang, D. B., Song, T. S., Guo, T., Zeng, Q., & Xie, J. (2014). Electricity generation from sediment microbial fuel cells with algae-assisted cathodes. *International journal of hydrogen energy*, *39*(25), 13224-13230.

Wang, T. Y., & Kleinstreuer, C. (1988). Local skin friction and heat transfer in combined free-forced convection from a cylinder or sphere to a power-law fluid. *International journal of heat and fluid flow*, *9*(2), 182-187.

Wang, Y., & Qin, G. (2019). Accurate numerical simulation for non-Darcy double-diffusive mixed convection in a double lid-driven porous cavity using SEM. *Numerical Heat Transfer, Part A: Applications*, *75*(9), 598-615.

Waqas, H., Khan, S. U., Shehzad, S. A., Imran, M., & Tlili, I. (2020). Activation energy and bioconvection aspects in generalized second-grade nanofluid over a Riga plate: a theoretical model. *Applied Nanoscience*, *10*(12), 4445-4458.

Waqas, H., Manzoor, U., Shah, Z., Arif, M., & Shutaywi, M. (2021). Magneto-burgers nanofluid stratified flow with swimming motile microorganisms and dual variables conductivity configured by a stretching cylinder/plate. *Mathematical Problems in Engineering*, *2021*, 8817435.

Waqas, H., Oreijah, M., Guedri, K., Khan, S. U., Yang, S., Yasmin, S., ... & Galal, A. M.

(2022). Gyrotactic motile microorganisms impact on pseudoplastic nanofluid flow over a moving Riga surface with exponential heat flux. *Crystals*, *12*(9), 1308.

Weidman, P. D., Kubitschek, D. G., & Davis, A. M. J. (2006). The effect of transpiration on self-similar boundary layer flow over moving surfaces. *International journal of engineering science*, *44*(11-12), 730-737.

Wu, Y. C., Wang, Z. J., Zheng, Y., Xiao, Y., Yang, Z. H., & Zhao, F. (2014). Light intensity affects the performance of photo microbial fuel cells with Desmodesmus sp. A8 as cathodic microorganism. *Applied energy*, *116*, 86-90.

Xu, H., & Pop, I. (2014). Fully developed mixed convection flow in a horizontal channel filled by a nanofluid containing both nanoparticles and gyrotactic microorganisms. *European Journal of Mechanics-B/Fluids*, *46*, 37-45.

Yang, R., Gong, Z., Zhang, X., & Que, L. (2019). Single-walled carbon nanotubes (SWCNTs) and poly (3, 4-ethylenedioxythiophene) nanocomposite microwire-based electronic biosensor fabricated by microlithography and layer-by-layer nanoassembly. *Journal of Nanoscience and Nanotechnology*, *19*(12), 7591-7595.

Zaib, A., Rashidi, M. M., & Chamkha, A. J. (2018). Flow of nanofluid containing gyrotactic microorganisms over static wedge in darcy-brinkman porous medium with convective boundary condition. *Journal of Porous Media*, *21*(10), 911-928.

Zainal, N. A., Nazar, R., Naganthran, K., & Pop, I. (2020). MHD mixed convection stagnation point flow of a hybrid nanofluid past a vertical flat plate with convective boundary condition. *Chinese Journal of Physics*, *66*, 630-644.

Zhang, Q., Zhang, X., Zhang, X., Jiang, L., Yin, J., Zhang, P., & Zheng, G. (2019). A feedback-controlling digital microfluidic fluorimetric sensor device for simple and rapid detection of mercury (II) in costal seawater. *Marine pollution bulletin*, *144*, 20-27.

Zhao, J. (2021). Finite volume method for mixed convection boundary layer flow of viscoelastic fluid with spatial fractional derivatives over a flat plate. *Computational and*

Applied Mathematics, *40*(1), 1-17.